EFFECTS OF LARGE FIRES ON BOREAL FORESTS OF CHINA—Historical Reconstruction and Future Prediction through Landscape Modeling

---

A Dissertation

presented to

the Faculty of the Graduate School

at the University of Missouri-Columbia

In Partial Fulfillment

of the Requirements for the Degree

Doctor of Philosophy

---

by

Wenru Xu

Dr. Hong S. He, Dissertation Supervisor

December 2020

The undersigned, appointed by the Associate Vice Chancellor of the Office of Research and Graduate Studies, have examined the dissertation entitled

EFFECTS OF LARGE FIRES ON BOREAL FORESTS OF CHINA

— Historical Reconstruction and Future Prediction through Landscape Modeling

presented by Wenru Xu,

a candidate for the degree of Doctor of Philosophy,

and hereby certify that, in their opinion, it is worthy of acceptance.

Dr. Hong S. He

Dr. Grant P. Elliott

Dr. David R. Larsen

Dr. Michael C. Stambaugh

ACKNOWLEDGEMENTS

First I would like to give my sincere thanks to my advisor Dr. Hong S. He for introducing me to the world of science, for guiding me in proceeding research and overcoming difficulties in the research, and for enhancing my abilities in critical thinking and paper writing. His support and advice were indispensable during my Ph.D. study. I would also like to thank my committee members, Dr. David R. Larsen, Dr. Michael C. Stambaugh, and Dr. Grant P. Elliott for their time and effort in attending numerous meetings with me and helping improve my research.

I would also like to express my appreciation to Dr. Zhiliang Zhu, Dr. Todd J. Hawbaker, and Dr. Paul D. Henne for their precious time in reviewing my papers and giving recommendations, encouragement, and feedback to my research. I would also acknowledge the financial support from the National Biologic Carbon Sequestration Assessment Program under the U.S. Geological Survey Climate and Land Use Mission Area, and the University of Missouri GIS Mission Enhancement Program.

My thanks also goes to the members I met in the GIS Spatial Analysis Lab: Wenjuan Wang, Jacob Fraser, Shengwu Duan and his wife Lu Huang, Yuanyuan Fu, Wenchi Jin, Michael Sunde, and Saaruj Khadka as well as Dr. Benjamin O. Knapp and Dr. John Kabrick for being supportive and making my experience in the forestry department more enjoyable. I would like to extend my thanks to Dr. William Dijak. He is always kindly and generously grants me his time for advice and especially technical support.

Finally, I want to say thank you to my parents for all their love and unconditional support throughout my life.

TABLE OF CONTENTS

ACKNOWLEDGEMENTS ii

LIST OF FIGURES vii

LIST OF TABLES xi

ABSTRACT xiii

CHAPTER I. INTRODUCTION 1

1. Research background 1

2. Research objectives 3

3. Chapter outlines 3

Literature cited 6

CHAPTER II. Estimating burn severity and carbon emissions from a historic megafire in boreal forests of China 10

1. Introduction 10

2. Materials and Methods 14

2.1. Study area 14

2.2. Data Sets 14

2.3. Quantification of burn severity 16

2.4. Calculation of aboveground biomass consumption and carbon emission 17

3. Results 19

4. Discussion 21

4.1. Estimation of carbon emissions from the Black Dragon fire 21

4.2. Implications for understanding megafire impacts on fire emissions 23

5. Conclusions 25

Figures 26

Tables 30

Literature cited 35

CHAPTER III. Spatially explicit reconstruction of post-megafire forest recovery through landscape modeling 46

1. Introduction 46

2. Data and methods 50

2.1. Study area 50

2.2. General approach 51

2.3. Forest inventory data 52

2.4 Remote sensing data 53

2.5. Pre-fire forest conditions 54

2.6 Landscape model parameterization 55

2.7 Black Dragon fire and its implementation in LANDIS PRO 57

2.8 Model calibration and results validation 58

2.9. Post-fire tree planting simulation 60

3. Results 60

3.1. Results validation 60

3.2. The Black Dragon fire effects and post-fire forest recovery trajectories 62

4. Discussion 63

Figures 66

Tables 77

Literature cited 80

CHAPTER IV. Large fires or small fires, will they differ in affecting shifts in species composition and distribution under climate warming? 93

1. Introduction 93

2. Materials and methods 97

2.1 Study area 97

2.2 Model simulation and parameterization 97

2.3 Climate scenarios 99

2.4 Fire scenarios 100

2.5 Simulation design and model validation 100

2.6 Data analysis 101

3. Results 102

3.1 Model validation 102

3.2 Shifts in species composition and distribution 102

4. Discussion 104

Figures 107

Tables 113

Literature cited 114

CHAPTER V. CONCLUSIONS 125

VITA 128

LIST OF FIGURES

Figure 2-1. Location of the Black Dragon fire and the normalized burn ratio (NBR) value from Landsat Thematic Mapper data..... 26

Figure 2-2. The location of the forest inventory data; Inventory data A includes 1426 natural succession forest inventory polygons with mean stand DBH, height, age, tree species composition (volume proportion), and stand volume density from 1997 to 2001; Inventory data B includes 612 plots with tree species and diameter at breast height (DBH >5 cm) for each tree from 2010 to 2015..... 27

Figure 2-3. a) validation of pre-fire aboveground total biomass (single factor ANOVA p=0.78) and b) pre-fire species biomass composition (single factor ANOVA p>0.05 for each species). Error bars are marked as ± standard deviation..... 27

Figure 2-4. Maps of (a) total aboveground biomass and species-level biomass (b, Dahurian larch; c, white birch; d, aspen; e, Mongolian Scots pine) before the Black Dragon fire (1987)..... 28

Figure 2-5. Map of burn severity classification produced from the normalized burn ratio thresholds. 29

Figure 2-6. Maps of aboveground biomass consumption due to the Black Dragon fire in 1987..... 30

Fig. 3-1. The location of study area and the Black Dragon fire with Landsat 5 derived normalized burn ratio (NBR) values. The boundaries of the 10 forest bureaus are shown with thin black lines..... 67

Fig. 3-2. The framework of reconstructing historical forest conditions and post-megafire recovery trajectories of density and basal area at species level. (a) Calibrating tree species parameters to constrain tree species growth strategies. (b) Calibrating fire parameters to constrain fire-caused mortality. (c) The outcome of the calibration and validation processes is the time-series post-fire forest conditions at species level. 68

Fig. 3-3. The distribution map of forest inventory plots. 69

Fig. 3-4. Maps of total tree density and species-level density before the Black Dragon fire. 70

Fig. 3-5. Maps of total aboveground biomass and species-level biomass before the Black Dragon fire. 71

Fig. 3-6. Study area with a) 7 ecoregions divided by Xu et al. (1998), b) 8 land cover types, and c) 11 soil types. 72

Fig. 3-7. Scatterplots of simulated versus forest inventory density (a) and basal area (b) of eight species at the landscape scale in 2015 (n=21). The black line is the regression line and the grey shaded area represents 95% confidence intervals. RMSD: root mean squared deviation..... 73

Fig. 3-8. Comparison of simulated tree species density (a) and basal area (b) with inventory data by burn severities of the Black Dragon fire at 2015. Error bars are marked as ± 1 standard deviation (n= 584, 366, and 355 for low, moderate, and high severity area, respectively). 74

Fig. 3-9. Post-fire 28-year coniferous (a) and broadleaf (b) density in high burned area as a function of Euclidean distance to 1987 live-tree edge (trees mortality rate < 90%)

after the Black Dragon fire. The black lines are simulated means and grey lines are ± 1 standard error (SE). The points are observed values from field inventory data..... 75

Fig. 3-10. Tree species recovery trajectories over time for each burn severity following the 1987 Black Dragon fire: the trajectories of conifer species recovery in density (a), basal area (c), and biomass (e), and broadleaf species recovery in density (b), basal area (d), and biomass (f) from 1985 to 2015. 75

Fig. 3-11. Spatial pattern of post-fire coniferous and broadleaf recovery in basal area (a), density (b), and aboveground biomass (c) from 1987 to 2015 in the burned area of the Black Dragon fire. 76

Fig. 3-12. Tracking changes in species composition. (a) Trajectories of conifer proportion in basal area for each burn severity from 1985 to 2015. (b) Map of conifer proportion in basal area in 2015. Red line denotes perimeter of Black Dragon fire.... 77

Fig. 4-1. The location of the study area with 10 forest bureaus and a seed buffer zone. I only buffered the boundaries in China because they include the transition between temperate forests and boreal forests. 108

Fig. 4-2 Comparison of simulated basal area (a) and tree species density (b) with inventory data by ecoregions in 2015 109

Fig. 4-3. Comparison between simulated and observed values for total burned area (a), post-fire density (b) and basal area (c). The observed burned area represents the mean burned area/5 years from historic fire spanning 1965-2009. Error bars of simulated post-fire density and basal area are marked as ± 1 standard deviation (n= 100 for each timestep). 110

Fig. 4-4. Bray-Curtis dissimilarity indices for simulated forest communities projected under climate warming, large fires and small fires scenarios compared with those simulated under baseline climate at the same timestep by temperate zones. 111

Fig. 4-5. Predicted differences in important value for boreal, pioneer, and temperate tree species between climate warming vs base climate, small fires vs climate warming, and large fires vs climate warming scenarios in 2100. 112

LIST OF TABLES

Table 2-1. Investigated items and evaluation criterion of composite burn index (CBI). 30

Table 2-2. Normalized burn ratio (NBR) thresholds, tree mortality, and foliage consumption by burn severity class. 30

Table 2-3. Combustion efficiency (CE) and tree species biomass distribution of different components. 30

Table 2-4. Carbon fraction (fc) of organs by tree species (mg g^{-1}) 31

Table 2-5. Carbon emission factors for each species, in g per kg carbon of dry biomass burned. 31

Table 2-6. Estimates of consumed and remaining aboveground biomass and combustion efficiency (CE) in different burn severity classes. 32

Table 2-7. Emissions of CO_2, CO, CH_4 and NMHC (kg) during the Black Dragon fire. 32

Table 2-8. Combustion efficiency comparison (CBI: composite burn index, dNBR difference normalized burn ratio, NBR: normalized burn ratio). 33

Table 2-9. Fire and carbon emissions comparison. 34

Table 3-1. The acquired date, orbit number, and burning cover of Landsat. 77

Table 3-2. Individual tree species biological traits used in LANDIS PRO in the boreal forests of China. 78

Table 3-3. Individual tree species biological traits used in the ecosystem model LINKAGES 3.0 in the boreal forests of China. 79

Table 4-1. Changes (%) of tree species important values under climate warming, large fires, and small fires scenarios relative to baseline climate scenario by the year 2100. 113

EFFECTS OF LARGE FIRES ON BOREAL FORESTS OF CHINA

—Historical Reconstruction and Future Prediction through Landscape Modeling

Wenru Xu

Under the supervision of Professor Hong S. H

ABSTRACT

Boreal forests of China store about 350 Tg tree biomass carbon, which is approximately 24–31% of the total forest carbon storage in China, and thus, play an important role in maintain national carbon balance. Long-term fire exclusion and climate warming have foster larger and more severe fires. On 1987 May 6, a catastrophic fire, known as the Black Dragon Fire, occurred in this region, and burned 1.3 million ha. This fire is among the top five of such megafires ever recorded in the world, resulting in high degree of tree mortality and reset forest succession stage for most burned stands. Forests have grown back since, with much more homogeneous age classes and composition, which post new ecological risks and challenges. It is predicted that the warming will continue in the next century, and thus uncertainties exist in future fire regimes and vegetation response under novel climate.

Chapter II estimate the burn severity and carbon emissions from the Black Dragon fire. I combined field and remote sensing data to map four burn severity classes and calculated combustion efficiency in terms of the biomass immediately consumed in the

fire. Results of this chapter showed that 1.30 million hectares burned and 52% of that area burned with high severity. The emitted carbon dioxide equivalents (CO_2e), accounted for approximately 10% of total fossil fuel emissions from China in 1987, along with CO (2% - 3% of annual anthropogenic CO emissions from China) and non-methane hydrocarbons (NMHC) contributing to the atmospheric pollutants. This study provides an important basis for carbon emission estimation and understanding the impacts of megafires.

Chapter III developed a novel framework to spatially reconstruct the post-fire time-series of forest conditions after the 1987 Black Dragon fire of China by integrating a forest landscape model (LANDIS) with remote sensing and inventory data. I derived pre-fire (1985) forest composition and the megafire perimeter and severity using remote sensing and inventory data. I simulated the megafire and the post-megafire forest recovery from 1985-2015 using the LANDIS model. I calibrated the model and validated the simulation results using inventory data. I demonstrated that the framework was effective in reconstructing the post-fire stand dynamics and that it is applicable to other types of disturbances.

Chapter IV investigated the effects of future fire regimes on boreal forests of China under a warming climate. I simulated species composition and distribution changes to the year 2100 using a coupled forest dynamic model (LANDIS PRO) and ecosystem process model (LINKAGES). I focused on two possible fire regimes (frequent small fires and infrequent large fires). Results of this chapter showed that climate warming and fires strongly affected tree species composition and distribution in the boreal forests of China. Climate warming promoted transitions from boreal species to pioneer and temperate

species. Fire effects acted in the same direction as climate change effects on species occurrences, thereby catalyzing climate-induced transitions. Frequent small fires exerted stronger effects on the species composition shifts than infrequent large fires. The combined effects of climate warming and fire on the shifts in species composition will accumulate through time and space and can induce a complete transition of forest type, and alter forest dynamics and functions.

CHAPTER I. INTRODUCTION

1. Research background

Boreal forests cover in excess of 1.2 billion hectares, retain about 32% of the world's forest carbon stocks, and play an important role in maintaining global carbon balance (Melillo et al. 1993). Fires have been well recognized as a primary disturbance affecting the dynamics of forest structure, composition, and carbon storage across the boreal forest region (Lecomte et al. 2006; Bowman et al. 2009; Rogers et al. 2015). Over the past decades, fire suppression and fire exclusion in the Chinese boreal forest region has been carried out and resulted in an increase in hazardous fuels. Coupled with climate warming, the hazardous fuels can foster larger and more severe fires (Chang et al. 2007; Stephen et al. 2014). Large fires (or also called megafires) that burned extensive areas with high intensity can cause abrupt changes to the ecosystem by killing live trees and combusting a great amount of woody biomass carbon into atmosphere (Bradstock et al. 2008; Kean et al. 2009). Despite the increased megafires and their profound impact on the boreal forests, few have assessed the megafire effects on forest landscape and regional carbon balance. Thus, accurate assessments of megafires effects are needed to better understand the role of megafires in national and global carbon balance and forest dynamics, and provide insight into how boreal ecosystems would respond to changing fire regimes.

Assessing megafire effects on boreal forests is challenging because they have long-lasting impacts on forest ecosystems. Megafires can create large burn patches that could delay vegetation recovery processes by limiting the reach of seed dispersal (Kean et al. 2009; Johnstone et al. 2016). They produce ecological legacies that endure for decades to

centuries as forests recover following fires (Hicke et al.2013; Kashian et al. 2013; Turner et al. 2019). Precise information on extent and severity of the fire as well as on post-fire forest conditions is required to quantify the legacy effects of megafires over a large spatial extent and long time periods (i.e., decades to centuries). Spatial reconstructions of historical forest landscapes can capture spatial heterogeneity of the burn severity, and species regeneration strategies that determine forests recover and thus provide baseline information for anticipating future landscapes (Seidl et al. 2014; Thrippleton et al. 2014).

Quantifying megafire effects on boreal forests involves uncertainty in future fire regime and vegetation response under the warming climate. Both the fire occurrence probability and burned area have been projected to increase in the next century due to climate warming, extreme weather, increased anthropogenic ignitions, and fuel accumulation from fire exclusion policies (Arno et al. 2000; Flannigan et al. 2009; Liu et al. 2012; Stephens et al. 2014). However, there is considerable debate over the future fire regime. Even if the fire return interval and the total area burned are similar, the predicted fire regimes in a region can be from many small fires to a few large fires (Cui et al. 2008; Thonicke et al. 2010). Large and small fires are distinctively different in creating and regulating burn patterns (Romme et al. 1998; Bradstock 2008; Keane et al. 2008; Miller et al. 2012), which may lead to different tree species responses and post-fire succession trajectories especially under warming climate.

Boreal forests of China are at the southern range of Siberia boreal forest biome. They are a fire prone system historically characterized with small but low intensity fires (Chang et al. 2008). Due to decades of fire suppression and fire exclusion, forest fuel built up rapidly. These boreal forests have experienced considerable temperature increases over

the past decades, and are predicted to warm further over the 21st century (IPCC, 2013). The 1987 Black Dragon fire, which occurred in this region, stood out as fifth largest fire among all recorded megafires (the top four megafires are: the 1997/1998 Kalimantan Complex in Indonesia, the 2008 Ghanzi Fire in Botswana, the 1963 Paraná Forest Fire in Brazil, and the 1950 Chinchaga Fire in Canada) since the early 1800s and ranked first if the area burned in Russia is included (Leistikow et al. 2000; Williams et al. 2011; Ferreira-Leite et al. 2015).The fire burned 1.3 million ha over 28 days and resulted in over 200 deaths and 4 billion Yuan of losses at that time. In addition to the significant social and economic losses, the fire resulted in a high degree of tree mortality, emitted a large amount of carbon, and reset forest succession for most burned stands. Forests have grown back since, with much more homogeneous age classes and composition, which post new ecological risks and challenges.

2. Research objectives

The objectives of this research were to (1) assess the burn severity and carbon emission of the Black Dragon fire combining satellite and forest inventory data, (2) spatially reconstruct the post-fire time-series of forest conditions from 1987 to 2015 integrating forest landscape model (LANDIS) with remote sensing and inventory data, and (3) investigate how the boreal forests are influenced by future fires under warming climate in the next 100 years. The following three chapters in this dissertation each addresses one of these objectives.

3. Chapter outlines

Chapter II presents a study on the immediate effects of the megafires on the boreal forest ecosystem (i.e. the biomass immediately consumed in the fire and carbon emissions).

I integrated Landsat data, recent forest inventory data and the established correlation between remotely sensed indices and the composite burn index to (1) spatially reconstruct historical burn severity patterns for the megafire; (2) estimate aboveground forest-type specific combustion efficiency using tree mortality levels and consumed foliage estimated for each burn severity class; and (3) calculate aboveground forest biomass consumption and carbon emissions using the estimates of combustion efficiency.

Chapter III proposes a framework for integrating a forest landscape model (LANDIS) with remote sensing and inventory data to spatially reconstruct the post-fire time-series of forest conditions (i.e., forest composition, structure, and aboveground biomass) after the 1987 Black Dragon fire. I derived pre-fire (1985) forest composition and the megafire perimeter and severity using remote sensing and inventory data. I simulated the megafire and the post-megafire forest recovery from 1985-2015 using the LANDIS model and calibrated model parameters using inventory data. I evaluated whether the reconstructed forest conditions could realistically capture the post-fire recovery (e.g., density and basal area) at the level of individual tree species under different burn severities.

In Chapter IV, I predicted forest dynamics in response to climate change and future fire regime over a large region by using a hybrid forest ecosystem model LINKAGES (v3.0) and a forest landscape model LANDIS PRO (7.0). I choose to focus on two kinds of fire regimes (frequent small fires and infrequent large fires) under a warming climate and included the current climate as a baseline climate scenario, the current fire as a baseline fire scenario. By comparing and contrasting results of these different scenarios, I addressed the following research questions: 1) how fires interact with climate warming to affect the species composition and distribution, 2) whether the climate-induced composition and

distribution shifts will respond differently between small and large fires, and 3) to what extent could the small or large fires enhance or hinder the shifts in species composition and distribution under a warming climate?

Literature cited

Arno SF, Parsons DJ, Keane, R.E. (2000) Mixed-severity fire regimes in the northern Rocky Mountains: consequences of fire exclusion and options for the future. In *Proceedings of the wilderness science in a time of change conference* **5**, 225-232.

Bowman DM, Balch JK, Artaxo P, Bond WJ, Carlson JM, Cochrane MA, D'Antonio CM, DeFries RS, Doyle JC, Harrison SP, Johnston FH et al. (2009) Fire in the Earth System. *Science* **324**, 481-484.

Bradstock RA (2008) Effects of large fires on biodiversity in southeastern Australia: disaster or template for diversity? *International Journal of Wildland Fire* **17**, 809–22

Chang Y, He HS, Hu Y, Bu R, Li X (2008) Historic and current fire regimes in the Great Xing'an Mountains, northeastern China: Implications for long-term forest management. *Forest Ecology and Management* **254**, 445-453.

Chang Y, He HS, Bishop I, Hu Y, Bu R, Xu C, Li X (2007) Long-term forest landscape responses to fire exclusion in the Great Xing'an Mountains, China. *International Journal of Wildland Fire* **16**, 34-44.

Cui W, Perera AH (2008) What do we know about forest fire size distribution, and why is this knowledge useful for forest management?. *International Journal of Wildland Fire* **17**, 234-244.

Ferreira-Leite F, Bento-Gonçalves A, Vieira A, da Vinha L (2015) Mega-fires around the world: A literature review. In 'Wildland Fires: A Worldwide Reality'. (Eds Bento-Gonçalves A, Vieira A) pp. 15-34 (Nova Science Publishers: New York).

Flannigan MD, Krawchuk MA, deGroot WJ, Wotton BM, Gowman LM (2009) Implications of changing climate for global wildland fire. *International Journal of Wildland Fire*, **18**(5) 483- 507.

Hicke JA, Meddens AJ H, Allen CD, Kolden CA (2013) Carbon stocks of trees killed by bark beetles and wildfire in the western United States. *Environmental Research Letters* **8**, 35032.

IPCC (2013) Summary for policymakers. In: Climate Change 2013: The Physical Science Basis. Contribution of Working Group I to the Fifth Assessment Report of the Intergovern-mental Panel on Climate Change (eds Stocker TF, Qin D, Plattener GK et al.), 4–19. Cambridge University Press, Cambridge, UK and New York, NY, USA.

Johnstone JF, et al. (2016) Changing disturbance regimes, ecological memory, and forest resilience. *Frontiers in Ecology and the Environment* **14**, 369-378.

Kashian DM, Turner MG, Romme WH, Lorimer CG (2005) Variability and convergence in stand structural development on a fire-dominanted subalpine landscape. *Ecology* **86,** 643–654.

Keane RE, Agee JK, Fule P, Keeley JE, Key C, Kitchen SG, Miller R, Schulte LA (2008) Ecological effects of large fires on US landscapes: benefit or catastrophe? *International Journal of Wildland Fire* **17**, 696-712.

Lecomte N, Simard M, Fenton N, Bergeron Y (2006) Fire severity and long-term ecosystem biomass dynamics in coniferous boreal forests of eastern Canada. *Ecosystems* **9**, 1215-1230.

Leistikow BN, Martin DC, Milano CE (2000) Fire injuries, disasters, and costs from cigarettes and cigarette lights: a global overview. *Preventive medicine* **31**, 91-99.

Liu ZH, Yang J, Chang Y, Weisberg PJ, He HS (2012) Spatial patterns and drivers of fire occurrence and its future trend under climate change in a boreal forest of Northeast China. *Global Change Biology* **18**, 2041-2056.

Melillo JM, McGuire AD, Kicklighter DW, Moore B, Vorosmarty CJ, Schloss AL (1993) Global climate change and terrestrial net primary production. *Nature* **363**, 234–240

Miller JD, Skinner CN, Safford HD, Knapp EE and Ramirez CM (2012) Trends and causes of severity, size, and number of fires in northwestern California, USA. *Ecological Applications* **22**, 184-203.

Rogers BM, Soja AJ, Goulden ML, Randerson JT (2015). Influence of tree species on continental differences in boreal fires and climate feedbacks. *Nature Geoscience* **8**, pp.228-234.

Romme WH, Everham EH, Frelich LE, Moritz MA, Sparks RE (1998) Are large, infrequent disturbances qualitatively different from small, frequent disturbances? *Ecosystems* **1**, 524–534.

Seidl R, Rammer W, Spies TA (2014) Disturbance legacies increase the resilience of forest ecosystem structure, composition, and functioning. *Ecological Applications* **24**, 2063-2077.

Stephens SL, Burrows N, Buyantuyev A, Gray RW, Keane RE, Kubian R, Liu S, Seijo F, Shu L, Tolhurst KG (2014) Temperate and boreal forest mega-fires: characteristics and challenges. *Frontiers in Ecology and the Environment* **12**, 115-122.

Thonicke K, Spessa A, Prentice IC, Harrison SP, Dong L, Carmona-Moreno C (2010) The influence of vegetation, fire spread and fire behaviour on biomass burning and trace gas emissions: results from a process-based model. *Biogeosciences* **7**, 1991–2011.

Thrippleton T, Dolos K, Perry GLW, Groeneveld J, Reineking B (2014) Simulating long-term vegetation dynamics using a forest landscape model: the post-Taupo succession on Mt Hauhungatahi, North Island, New Zealand. *New Zealand Journal of Ecology* **38**, 26-U43.

Turner MG, Whitby TG, Tinker DB, Romme WH (2016) Twenty-four years after the Yellowstone Fires: Are postfire lodgepole pine stands converging in structure and function? *Ecology* **97**, 1260-1273.

Williams J, Albright D, Hoffmann AA, Eritsov A, Moore P, Mendes de Morais J, Leonard M, San Miguel-Ayanz J, Xanthopoulos G, Van Lierop P (2011) Findings and implications from a coarse-scale global assessment of recent selected mega-fires. International Wildland Fire Conference (5th, 9-13 May 2011, Sun City, South Africa). FAO.

CHAPTER II. Estimating burn severity and carbon emissions from a historic megafire in boreal forests of China

1. Introduction

Natural and anthropogenic forest fires, especially megafires (large and uncontrolled forest fire events, burning large areas >10,000 ha) emit a great amount of carbon (Van der Werf et al. 2010; Ito 2011). Carbon dioxide (CO_2) is predominant among the emissions, along with other carbon-containing trace gases including carbon monoxide (CO), methane (CH_4) and non-methane hydrocarbons (NMHC), resulting in perturbations in air quality and the carbon cycle (Urbanski er al. 2008). Forest fires (extent, frequency aand severity) are predicted to increase under warmer and dryer conditions, earlier snowmelt and longer fire seasons (Flannigan et al. 2009; Liu et al. 2012), contributing to the increase in carbon emissions from forest fires. Thus, accurate estimation of carbon emissions from forest fires is important to understand carbon balance and atmospheric chemistry.

Boreal forests of China store about 350 Tg tree biomass carbon, which is approximately 24–31% of the total forest carbon storage in China, and thus, play an important role in maintaining national carbon balance (Fang et al. 2001; Fu et al. 2013). The Black Dragon fire occurred in 1987, reduced forest cover by 15% in the boreal forests of China (Luo et al. 2002), and coincided with another 13 million ha burned in Russia (Cahoon et al. 1994). This megafire was noteworthy due to its size, rapid spread, and variable severities. The fire in China ranks fifth among all recorded megafires (the

top four megafires are: the 1997/1998 Kalimantan Complex in Indonesia, the 2008 Ghanzi Fire in Botswana, the 1963 Paraná Forest Fire in Brazil, and the 1950 Chinchaga Fire in Canada) since the early 1800s and ranked first if the area burned in Russia is included (Leistikow et al. 2000; Williams et al. 2011; Ferreira-Leite et al. 2015). Given the scale and catastrophic impacts, quantitative assessment of carbon emissions of the 1987 Black Dragon fire helps to better understand the role of extreme megafires in national and global carbon balance and atmospheric chemistry, especially for complying with the Paris Agreement on greenhouse gas reduction (UNFCCC, 2015).

Carbon emissions from forest fires are commonly calculated as the product of burned area, pre-fire biomass, combustion efficiency (the proportion of biomass consumed during burning), and emission factors (Seiler and Crutzen 1980). Each of the above components contribute to uncertainties in emission estimates (French et al. 2004). Burned area and pre-fire biomass density can be estimated and constrained with satellite imagery (Palacios-Orueta et al. 2005; Giglio et al. 2013). There are, however, few studies on combustion efficiency, particularly in boreal forests of Asia (Van Leeuwen et al. 2014). Field estimates of combustion efficiency are generally based on pre- and post-fire biomass sampling, which is costly, cumbersome, and spatially limited. As a result, many studies assume an average combustion efficiency, either by major vegetation type or over the entire burned area (e.g. Cahoon et al. 1994; Yi and Bao 2016). Uncertainties in combustion efficiency estimates due to spatial variability of fuel consumption within burned areas can lead to large errors in carbon emission estimates (French et al. 2004; De Santis et al. 2010). This is especially important for megafires given their spatial variability in fire severity. Burn severity quantifies the degree of vegetation change due to

fire and thus can be and has been used as an estimate of combustion efficiency (Boby et al. 2010; De Santis et al. 2010). Remote sensing indices are generally used in conjunction with field-based indices such as the composite burn index (CBI) to estimate burn severity (Key and Benson 2005; Kasischke et al. 2008). However, it is challenging to use CBI values to evaluate the burn severity of the historical fires that occurred decades ago because forest inventories immediately after fire are often not available. Relationships between remotely sensed indices and burn severity have been established in many ecosystems and regions and can be extrapolated to similar fires (Miller and Thode 2007; Escuin et al. 2008; Schepers et al. 2014). For example, Epting et al. (2005) demonstrated that normalized burn ratio (NBR) was highly correlated with the field-based CBI in forested burned sites of Alaska; Allen and Sorbel (2008) found strong linear relationship between a differenced normalized burn ratio (dNBR) and CBI (R^2 ranged from 0.45 to 0.88). In addition, spatial patterns of forest age structure developed after fires encapsulate disturbance and recovery history and can be used to verify and improve the established relationships, making spatially reconstructed burn severity sound (Naficy 2017). The well-established relationship between spectral indices and severity facilitates the estimation of biomass combustion and thus carbon emission in relation to heterogeneity in burned severity from historical megafires.

There have been many efforts to estimate carbon emissions from fires. Andreae and Merlet (2001) estimated global carbon emissions for important species emitted by the various types of biomass burning in the late 1990s. Using a combination of satellite derived datasets, Ito and Penner (2004) developed a monthly fire emissions inventory for the year 2000. The Global Fire Emissions Database (GFED, Van Der Werf et al., 2006,

2010, 2017) is a widely applied global biomass burning emissions dataset. GFED4s includes 8-day and monthly emissions of selected trace gas and particulate emissions from burning globally at horizontal resolutions as fine as 0.25° for 1997–2016 (Van Der Werf et al. 2017). The Fire Inventory from NCAR (FINN) includes daily 1 km resolution global carbon and particle emission estimates from open biomass burning (Wiedinmyer et al. 2011). The Global Fire Assimilation System (GFAS) provides daily emissions from biomass burning on a global 0.5° ×0.5° grid from 2003 to 2010 (Kaiser et al. 2012). All of these studies used relatively coarse resolution (e.g. 1.1 km of AVHRR, 250 m, 500 m and 1 km of MODIS) and generalized forest types (e.g. boreal forest, temperate forest, tropical forest, peat, and agriculture), and did not account for fine-scale variability in combustion efficiency that determines fire emissions and impacts. Thus, the uncertainty associated with fire emissions remains. For example, the GFED4s may overestimate tree mortality by overlooking remaining trees from the fire using coarse resolution and thus overestimate carbon emissions. Landsat data provide a high-resolution alternative at a spatial scale comparable with on-the-ground tree mortality data (30 m; Kennedy et al. (2014)). Landsat also has an extensive historical archive in some parts of the world (Wulder et al. 2016), and Landsat data have been used extensively to monitor disturbances and land-cover change around the world (Wulder et al. 2012).

In this chapter, I integrated Landsat data, recent forest inventory data and the established correlation between remotely sensed indices and CBI to assess the impact of the Black Dragon fire on aboveground forest carbon. The objectives were (1) to spatially reconstruct historical burn severity patterns for the megafire; (2) to estimate aboveground forest-type specific combustion efficiency using tree mortality levels and consumed

foliage estimated for each burn severity class; and (3) to calculate aboveground forest biomass consumption and carbon emissions using the estimates of combustion efficiency.

2. Materials and Methods

2.1. Study area

The Great Hinggan Mountain forests compose more than 30% of the total forest area in China, represent a major portion of forest carbon stocks in China, and are also within a fire-prone boreal forest region. Surface fire is historically the dominant fire type, occasionally mixed with stand-replacing fire in the high elevation regions (Xu et al. 1997). However, fire exclusion has altered fire regimes in this area. Since the 1980s, fires have been infrequent, but more intense than historically (Chang et al. 2008).

The Black Dragon fire ignited on May 6, 1987, within the Great Hinggan Mountains (Figure 2-1). The fire burned within four Forest Bureaus (Xilinji, Tuqiang, Amuer, and Tahe) over 28 days and resulted in over 200 deaths and 4 billion Yuan of losses at that time. In addition to the significant social and economic losses, the fire resulted in a high degree of tree mortality, reset forest succession for most burned stands, emitted a large amount of carbon, and caused the most forest fire damage in the history of China. The timing of the Black Dragon fire coincides with the start of the megafire era (Williams 2013).

2.2. Data Sets

2.2.1 Landsat data and Pre-Processing

Landsat Thematic Mapper (TM) and Enhanced Thematic Mapper plus (ETM+) data provide the longest consistent source of relatively high spatial and spectral resolution data, with 30-m spatial resolution, an 8 - to 16 - day repeat cycle, and a long-time span (1984-2018). Landsat data are responsive to relative changes in aboveground biomass

because of fire and can be used to discriminate fire occurrence and severity (Epting et al. 2005). In this chapter, nine pre- and post-fire Landsat images from the U.S. Geological Survey (USGS, http://earthexplorer.usgs.gov) were used to cover the 1987 Black Dragon fire to estimate aboveground biomass and burn severity. Only post-fire Landsat images were used for burn severity, given that NBR has been found to perform better than dNBR in my study area (Chang et al. 2016). The images were chosen primarily from June to August (growing season) shortly before and after the fire (June 26, 1986 and June 24, 1987 for path 121, row 23; June 12, 1986 and June 15, 1987 for path 122, row 23; August 6, 1986 for path 123, row 23; June 15, 1987 for path 122, row 24) to ensure the trees were in the same phenological phase. Because of a gap in the data, however, I chose April 26, 1989 and September 2, 1990 for path 123, row 23, and September 14, 1988 for path 121, row 24. The images were processed by the USGS to convert from DN (digital numbers) to surface reflectance using the LEDAPS algorithm (Landsat ecosystem disturbance adaptive processing system, Masek et al. 2006). Clouds, cloud shadows, and snow pixels were masked using the function of mask algorithm (FMASK; Zhu and Woodcock (2012)).

2.2.2 Pre-fire forest aboveground biomass density

Pre-fire forests in this area were primarily affected by historical harvesting, resulting in a homogenous species composition and an even-age distribution, with most trees between 40-60 years old. Zhang et al. (2018a) combined 2000s forest inventory data and remote sensing data to map species-level biomass in the boreal forests of China. The pre-fire aboveground biomass density maps by species in this study were produced using pre-fire Landsat data, according to the AGB estimation model developed by Zhang et al. (2018a). I calibrated and validated the results with post-fire forest inventory data (Figure

2-2). I subtracted biomass gained from succession based on stand-specific age-related increases in biomass estimated from 2000s (1997-2001) and 2010s (2010-2015) forest inventory data. I assumed that the forest species composition did not change within the 20-year period. The total aboveground biomass before fire was highly consistent between estimated results and forest inventory data (Figure 2-3), suggesting that my estimated species biomass could adequately represent the real pre-fire species biomass.

Aboveground biomass before the Black Dragon fire was generally homogeneous and averaged 63 Mg ha^{-1} (Figure 2-4a). Dahurian larch (*Larix gmelinii* Rupr. Kuzen, 34 Mg ha^{-1}, Figure 2-4b) and white birch (*Betula platyphylla* Suk, 24 Mg ha^{-1}, Figure 2-4c) were the most dominant species. Aspen (*Populus davidiana* Dode and *Populus suaveolens* Fischer, Figure 2-4d) and Mongolian Scots pine (*Pinus sylvestris* var. *mongolica* Litvinov, Figure 2-4e) were few, taking up less than 5% of total biomass.

2.3. Quantification of burn severity

Traditional methods of quantifying burn severity are based on field data (the difference between pre-fire and post-fire forest condition). However, historical pre- and post-fire inventories are not available for many regions of the world and collecting post-fire inventories is often not feasible for large fires. Therefore, the assessment of burn severity for a large area normally relies on remote sensing in conjunction with field-based indices (Loboda et al. 2007). The composite burn index (CBI) is the most commonly used index for burn severity characterization (Key and Benson 2005). It is calculated with field data to represent the magnitude of fire effects on a numeric scale between 0.0 and 3.0 (Table 2-1). Chang et al. (2016) explored relationships between remote sensing indices and CBI based on 85 CBI plots within 16 fires in this area. They found that

normalized burn ratio (NBR) was highly correlated with the field-based CBI (R^2=0.63, p<0.0001). Here, I used the developed relationship of CBI and NBR by Chang et al. (2016) to assess burn severity using the historical Landsat imagery for the Black Dragon fire, including four classes: no effect (unburned), low severity, moderate severity, and high severity. From the above relationship, I assigned tree mortality levels and consumed foliage rate based on the evaluation criterion of CBI (Table 2-2). The outermost fire perimeter was manually interpreted based on NBR values, because valleys and low-elevation areas in the south were not burned, but also characterized with low NBR values, which could be misclassified as low-severity burned areas using the NBR thresholds. My fire perimeter is highly consistent with the fire perimeter derived by Chen et al. (2016) using enhanced vegetation index with overall accuracy of 99.83% and kappa coefficient of 0.9946.

To validate the tree mortality levels assigned for each severity class, I used 612 recent (2010-2015) forest inventory plots in which tree species and diameter at breast height (DBH >5 cm) were recorded for each tree (Figure 2-2). I estimated the age for each tree using age-DBH relationships (Zhang et al. 2018b). I assumed that tree numbers from unburned forests were representative of tree numbers in this region prior to the 1987 fire, and that the trees older than the time gap between inventory year and 1987 represent the survived trees from the fire. I used the differences in tree number between the unburned forests and burned forests to estimate tree mortality due to the fire.

2.4. Calculation of aboveground biomass consumption and carbon emission

Total aboveground biomass consumed from the burned area was calculated with Equation (1), where $C_{t,c,s}$ is biomass consumption for species *t*, component *c*, and severity

s, A_i is the area of pixel *i*, $B_{t,c,i}$ is aboveground biomass density for species *t*, component *c*, pixel *i*, and $CE_{c,s,i}$ is combustion efficiency for component *c*, severity *s* and pixel *i*.

$$C_{t,c,s} = \sum_i A_i \times B_{t,c,i} \times CE_{c,s,i} \quad (2\text{-}1)$$

Stand-replacing fires rarely burn entire trees and instead leave many standing dead trees. Here, I defined combustion efficiency as the proportion of tree biomass consumed in a fire. In this study, the combustion efficiency (Table 2-3) of burned area was derived based on previously published results (Susott et al. 1991; Campbell et al. 2007; Hu et al. 2007; Garcia et al. 2017) and adjusted based on tree mortality levels and consumed foliage for different severity classes. To better estimate biomass consumed, I allowed combustion efficiency to vary among components (barks, branches, stems, and leaves). Since biomass allocation to different components varies among tree species, I compiled this information from published data for each of the four most common tree species in my study area (Wang et al. 2001; Hu et al. 2007; Poorter et al. 2015). For the remaining species in my area, I use the average biomass of components of all other tree species. Combining these data with the biomass by tree species within the burned area, I determined the distribution of combustion efficiency.

The equation for the emission of specific gases, $E_s = C_b \times f_c \times E_{fs}$, was based on the Seiler and Crutzen (1980) biomass combustion model, where E_s is the amount of specific gas released, C_b is consumed biomass, f_c is the fraction of carbon contained in the biomass, and E_{fs} is the emission factor for a specific gas. There are numerous experimental studies on the carbon content of different biomass components and species (Hu et al. 2012; Yu et al. 2012). Based on the results of this research, I determined the

fractional carbon content in different biomass components by tree species (Table 2-4). Emission factors of different gases are usually derived from laboratory or field experiments for different species or forest types (Susott et al. 1991; Kaufman et al. 1992). Many researchers have adopted the emission factors at the biome level. In this research, I further categorized the biome into more specific forest types based on dominant tree species, in contrast to the earlier approach where a single value was used for each biome. These emission factors for each emitted gas (Table 2-5) were based on previously published results from my study area (Hu et al. 2012).

3. Results

Burned and unburned areas were clearly distinguished from each other using an NBR value of 585 (Table 2-2, Figure 2-1), allowing for determining patterns of burned area affected by this megafire. The total burned area of the Black Dragon fire was approximately 1.3 million ha including four burn severity classes: unchanged\unburned, low severity, moderate severity, and high severity. High severity burned areas accounted for 52% (672,857 ha) of the total burned area; moderate severity burned areas accounted for 22% (288,483 ha), and low severity burned areas accounted for 26% (340,623 ha) (Table 2-6). Areas burned with high severity tended to be patchy with a few large and aggregated patches that fragmented the remaining area of the fire that had moderate and low severity (Figure 2-5). It was apparent that the fire crossed the rivers, and that the extreme conditions allowed for rapid fire spread over a large geographical area (Figure 2-5). Less affected areas were located mainly in high elevations (the mountain range blocked the path of fire spread) and close to the border of the burned area where fire suppression efforts were concentrated using the few fire breaks available in the area.

Combustion efficiency varied significantly among different severity classes with the highest value (0.67) in the high severity class, followed by 0.46 in the moderate severity class and 0.06 in the low severity class (Table 2-6). Total aboveground biomass consumption due to the Black Dragon fire was estimated to be 36.99 Tg. Most consumed biomass was in the high severity class, contributing to a total of 27.7 Tg, whereas the low and moderate severity classes only accounted for 4% and 22% of the total biomass consumed, respectively. The consumed biomass had very high spatial variability within and among burn severity classes because of the differences in tree species, pre-fire biomass and combustion efficiency, with extremely high values of biomass consumed primarily within the high severity burned areas (Figure 2-6). I assumed all biomass of the remaining live trees after the fire remained as live biomass because they can recovery relatively quickly. The remaining live biomass had an opposite trend compared to the consumed biomass. The high severity burned areas had fewer live trees and more standing dead trees (Table 2-6). Biomass consumed by fire was always less than the biomass lost to mortality, indicating that additional carbon will be lost through decomposition over time.

The Black Dragon fire in northern China emitted a total of 6.31×10^{10} kg CO_2e including 5.88×10^{10} kg CO_2, 3.71×10^{9} kg CO, 1.73×10^{8} kg CH_4, and 1.35×10^{8} kg NMHC (Table 2-7). High severity burned areas contributed the most to fire emissions. Low severity burned areas had lower emissions although they covered a larger area than moderate severity areas.

4. Discussion

4.1. Estimation of carbon emissions from the Black Dragon fire

The total burned area (1.3 million ha) of the Black Dragon fire mapped using NBR thresholds from remote sensing data was smaller than the official fire area (1.7 million ha). The fire burned over 20 days and generated large smoke plumes (Cahoon et al. 1994). Post-fire conditions and the remoteness of the area made it difficult to assess combustion efficiency across the entire megafire with a field inventory. The official fire area was derived from the maps of the outermost extent of the fire perimeter, whereas not all areas were burned within this perimeter. Thus, the estimates based on the outermost extent probably overestimate the total burned area and emissions. My estimates of burned area were derived from Landsat NBR values that highlighted areas with changes in vegetation biomass based on the change on visible-to-near-infrared surface reflectance and shortwave infrared reflectance (Trigg and Flasse 2000; Smith et al. 2005). The areal estimate from the remote sensing data was made using NBR thresholds consistently applied across the entire burned area, an approach that is more reproducible and is less error prone than field-based burned area mapping (Schepers et al. 2014).

The combustion efficiency varied depending on fuel type, soils, topography, and fire behavior within the megafire (Roy and Landmann 2005). Accounting for combustion efficiency using actual tree mortality estimated in different burn severity classes could reduce uncertainties in emission estimates compared to methods that use biome-wide combustion efficiencies. The average combustion efficiency (0.45) estimated in my study is relatively higher than the fixed values used by most studies (Table 2-8). However, my

high average combustion efficiency is reasonable given the extensive area within the fire that had high burn severity. The high average combustion efficiency is expected for such a megafire given the feedback loop between fire and fire weather: the increased air moving by heatwaves from the megafire and enhancement of dryness by radiative forcing of smoke particles further accelerated the fire, which exacerbates burn severity with high combustion efficiency (Liu et al. 2014; Coen et al. 2018). The estimates of combustion efficiency in high severity (0.67) and moderate severity (0.45) classes compare favorably with the estimates developed by De Santis et al. (2010) and reported by Chen et al. (2011).

The potential importance of the Black Dragon fire on the carbon cycle was first recognized by Cahoon et al. (1994), with an estimate of total 14.6 Tg C released. They used a bottom-up approach (the product of burned area, pre-fire biomass, combustion efficiency, and emission factors) with an average carbon consumption rate (1.125 kg C m^{-2}) derived from the prescribed burns in Canadian boreal forests. However, the Black Dragon fire was a megafire and the large area burned by megafires can create feedbacks with fire weather, which in turn leads to higher combustion efficiency, resulting in higher carbon emission than small-scale prescribed fires. Consequently, it is likely that the Cahoon et al. (1994) estimate of total carbon emissions is conservative. Wang et al. (2001) estimated that the Black Dragon fire released between 25 and 49 Tg C according to the live biomass difference between unburned forests and burned forests. They extrapolated the total carbon emission based on plot-scale inventories and scenarios of the percent of burned area for each burn severity without accounting for spatial variation. Also, Wang et al. (2001) assumed biomass for all live trees was consumed without

counting the standing dead trees, and thus, might overestimate the total carbon released. The total carbon loss (18.24 Tg C) estimated in this study is further constrained and more reasonable given that I accounted for fine-scale heterogeneity in fire combustion and post-fire residue. However, consumption of belowground biomass, and the understory and ground vegetation following the fire were not included in my estimates due to insufficient pre-fire data. Because these components were not included, my estimates are a conservative estimate of carbon loss.

4.2. Implications for understanding megafire impacts on fire emissions

The Black Dragon fire can be directly compared in terms of fire extent and carbon emissions to regional and global estimates as well as to other fires (Table 2-9). The fire burned an area larger than the annual area burned by all fires in China (0.9 Mha; 1950-2000), with a higher carbon loss and more emissions (13.2 Mg C ha^{-1}; Lu et al. 2006). Its carbon loss density was three times that of global biomass burning (Randerson et al. 2012; Van Der Werf et al. 2017). The 1997/1998 Kalimantan Complex was the largest fire (9.7 Mha) recorded in the fire history globally (Ferreira-Leite et al. 2015). The carbon loss density from the 1997/1998 Kalimantan Complex (96.3-112.4 Mg C ha^{-1}, Page et al.2002) was far greater than that of the Black Dragon fire (14 Mg C ha^{-1}). Because greater pre-fire biomass and more complete combustion were in peatlands than in boreal forests. That's especially true in the boreal forests of china where the forests have been highly affected by historical harvesting, resulting in low forest biomass with most trees between 40-60 years old. The 1988 Yellowstone Fire (1988) occurred at a similar time as the Black Dragon fire (1987) and was the largest and most intensive wildfire recorded in the world's first National Park (Ferreira-Leite et al. 2015). It burned

321,270 ha of which 31% burned by high severity fire and released 23.3 Mg C ha^{-1} (Turner et al. 1994; Zhao et al. 2018). The fire was quite patchy due to spotting behavior and variation in fuel conditions and topography (Christensen et al. 1989). Although the 1988 Yellowstone Fire was less severe than the Black Dragon fire, it had greater carbon loss density than the Black Dragon fire in part because of its high pre-fire biomass (175.4 Mg ha^{-1} C, Smithwick et al. (2009)). Russian boreal forests are comparable with the boreal forests of China based on the similar forest composition, structure and disturbance. The 1997 Taseevsky Fire in Russian boreal forests was a relatively low severity fire (2467.2 ha) and only released 6.5 Mg C ha^{-1} (Isaev et al. 2002). The comparisons between the Black Dragon fire and the 1997 Taseevsky Fire showed that the high percentage of high severity burned area in the Black Dragon fire resulted in higher carbon loss density.

National assessments of ecosystem carbon emissions are a critical component of documenting and fulfilling commitments to reduce overall carbon emissions. Wildfires are considered carbon neutral based on assumptions that forest regrowth will eventually recover carbon lost in the fire (Intergovernmental Panel on Climate Change 2015). However, regrowth may take much longer than the timeframe set for reductions in carbon emissions. Also, a great deal of uncertainty is involved in the recovery process especially under positive feedbacks between increased fire emissions and climate warming (Bowman et al. 2009). Hence, it is important to include and track emissions from wildfires in carbon accounting. Megafires have large effects on carbon emissions because of the large amount of carbon suddenly released into the atmosphere. For example, the Black Dragon fire released approximately 160% of China's mean annual carbon emissions from forest fires, and CO_2e emissions from the Black Dragon fire were

equivalent to 10% of China's annual CO_2 emissions from fossil fuel consumption (Table 2-9). This suggests that increases in megafires and their emissions may counteract efforts to reduce emissions from fossil fuel consumption. At present, estimation of carbon emissions in China has not included the potential impact of megafires. As a result, there is a large uncertainty in the national level of carbon emission estimates. Thus, this study of the Black Dragon fire provides an important step forward to accurately account for carbon emissions in China.

5. Conclusions

Significant amounts of carbon are emitted to the atmosphere due to large and catastrophic fires, affecting air quality and climate (Hurteau et al. 2008; Adams 2013). To better assess these effects of megafires, we improved estimates of satellite-based combustion efficiency for the Black Dragon fire using actual tree mortality estimates for different burn severity classes. This megafire burned 1.30 million ha, of which 52% was in high severity burned areas. Comparisons of combustion efficiency suggest that using fixed combustion efficiency values (usually the average combustion efficiency of forest fires that are primarily low-severity surface fires) may underestimate carbon emissions from megafires, and that the correlation between burn severity and combustion efficiency provides an alternative way to improve estimates of carbon emissions from megafires, especially historical megafires where pre- and post-fire field inventory data are lacking. Our approach can be used to constrain fire emission models and presents a methodology to estimate near-term emissions from fire and long-term emissions from dead biomass decay. The methodology can be applied on a continuous basis for forest fire monitoring and emissions accounting in different forested regions of the world. Furthermore, the

estimated fire emissions could be combined with estimates of forest regrowth biomass accumulation for including emissions from wildfire in a national carbon accounting and reporting framework. Hence, our study provides an important basis for considering the impacts of megafires on national-scale carbon accounting for China.

Figures

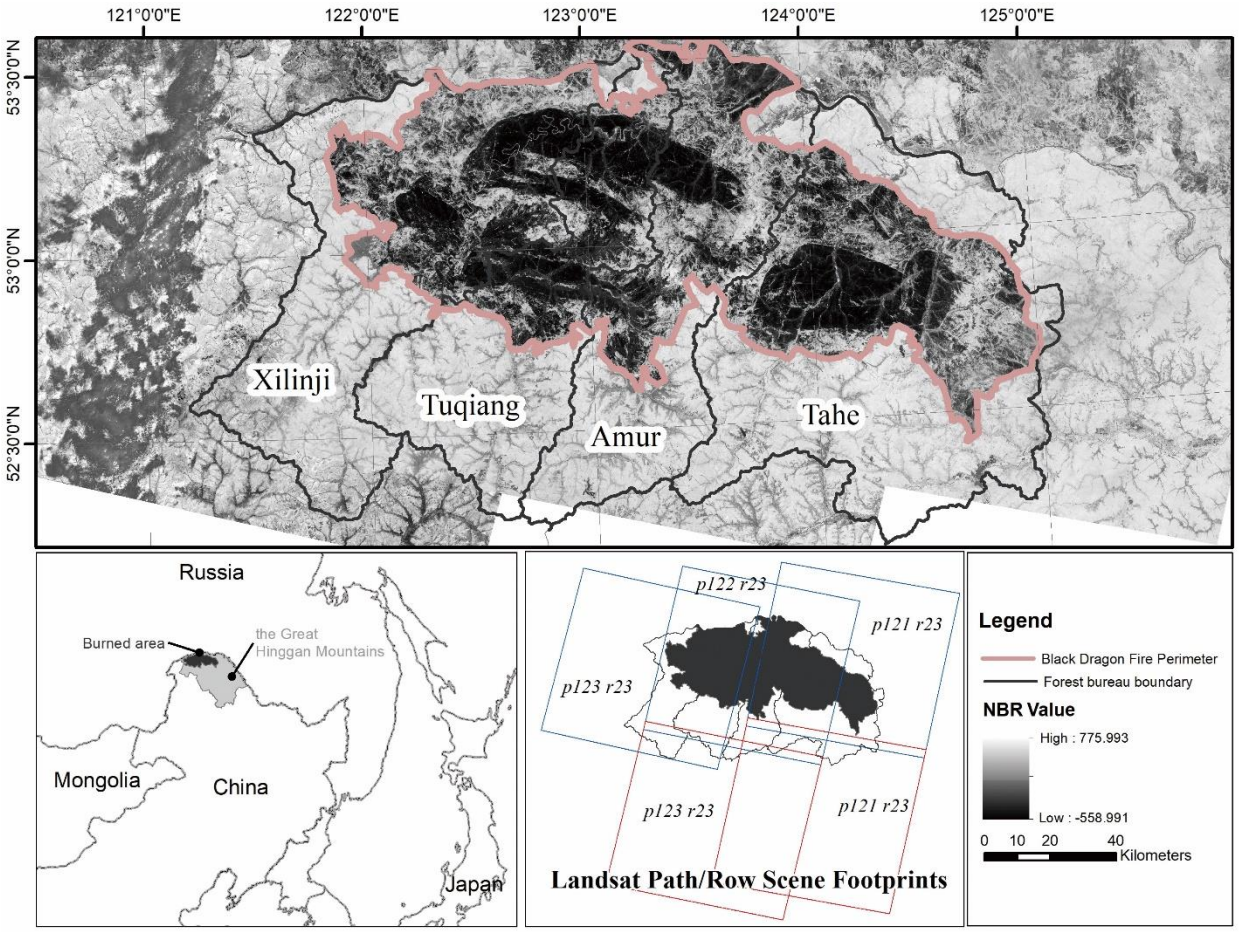

Figure 2-1. Location of the Black Dragon fire and the normalized burn ratio (NBR) value from Landsat Thematic Mapper data.

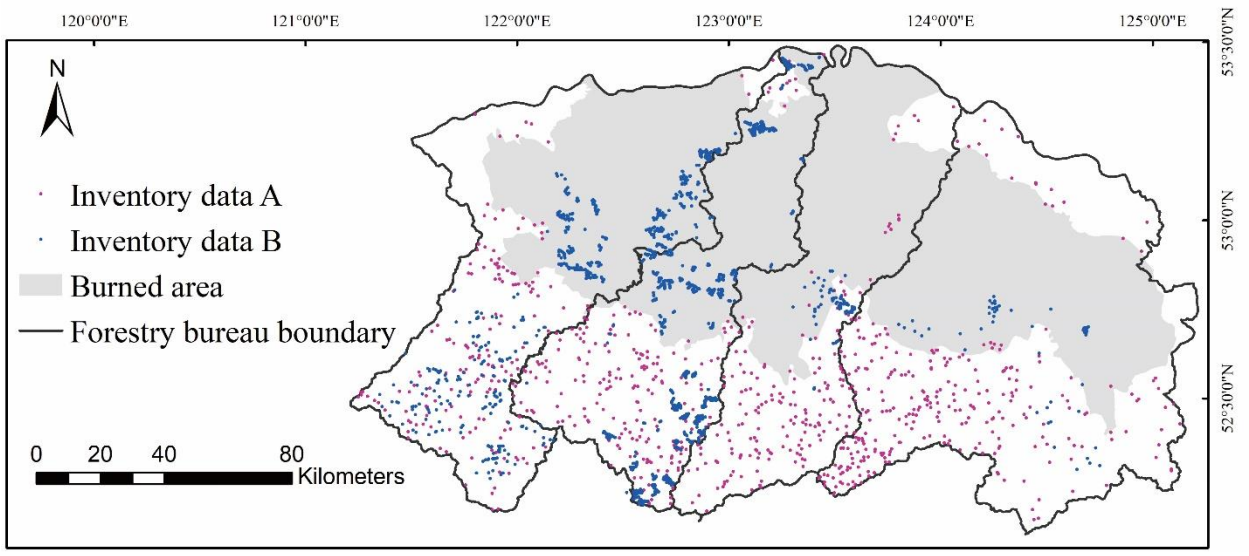

Figure 2-2. The location of the forest inventory data; Inventory data A includes 1426 natural succession forest inventory polygons with mean stand DBH, height, age, tree species composition (volume proportion), and stand volume density from 1997 to 2001; Inventory data B includes 612 plots with tree species and diameter at breast height (DBH >5 cm) for each tree from 2010 to 2015.

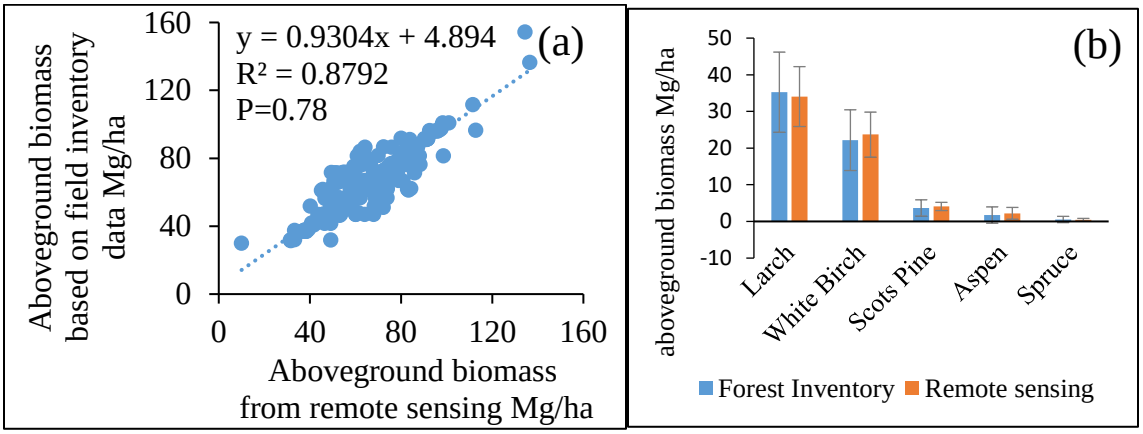

Figure 2-3. a) validation of pre-fire aboveground total biomass (single factor ANOVA p=0.78) and b) pre-fire species biomass composition (single factor ANOVA p>0.05 for each species). Error bars are marked as ± standard deviation.

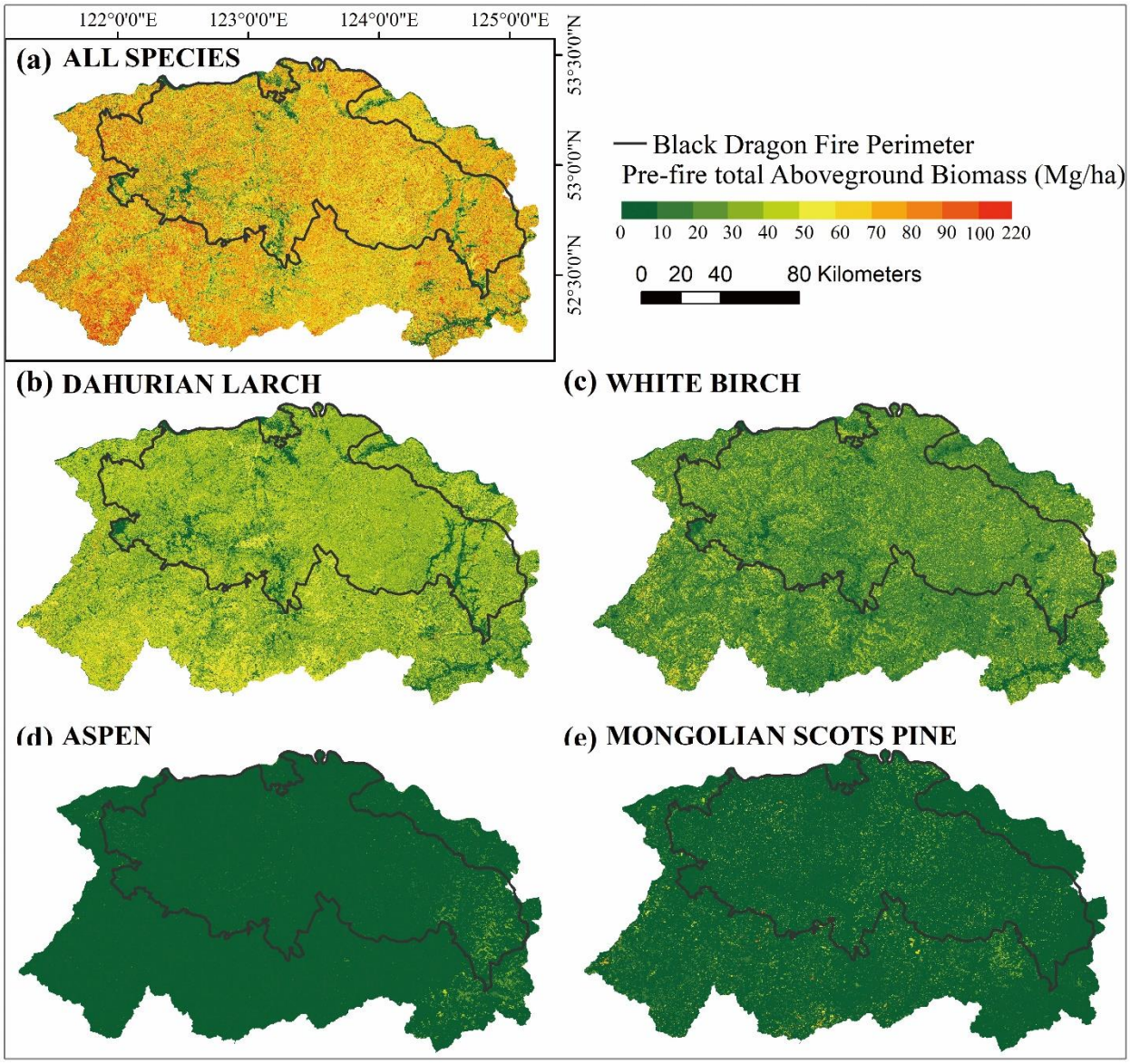

Figure 2-4. Maps of (a) total aboveground biomass and species-level biomass (b, Dahurian larch; c, white birch; d, aspen; e, Mongolian Scots pine) before the Black Dragon fire (1987).

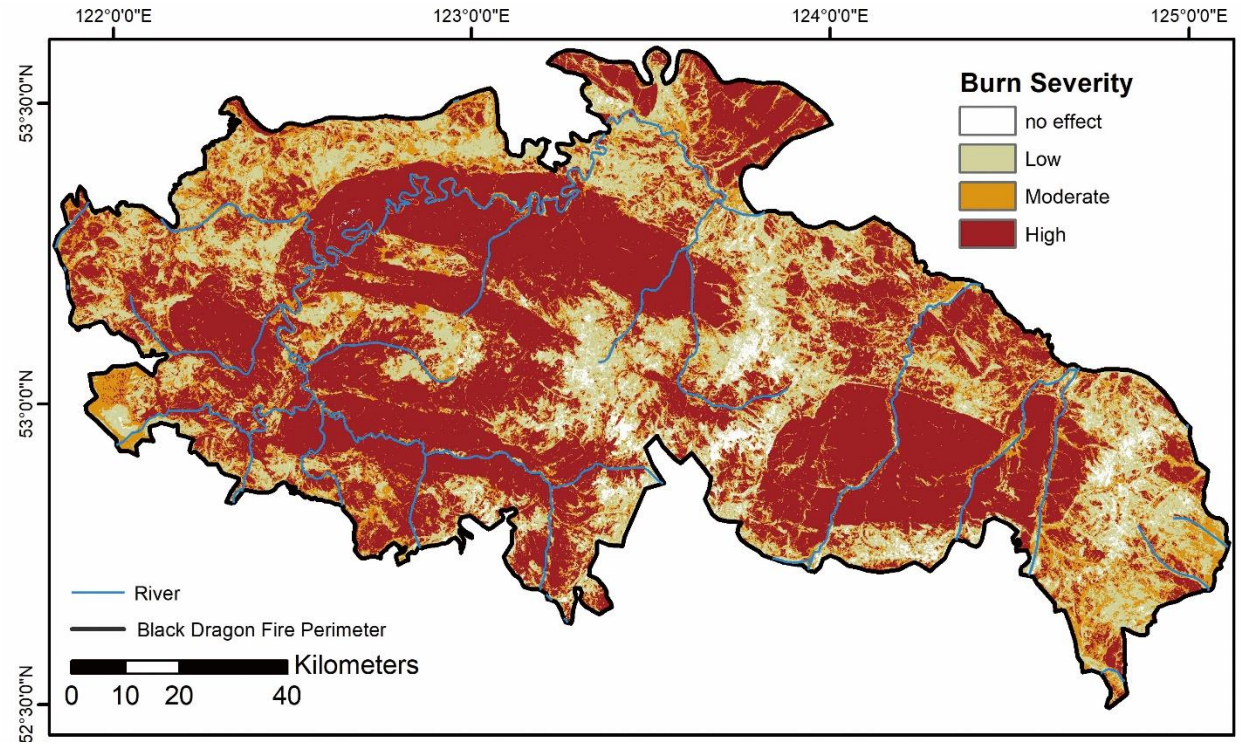

Figure 2-5. Map of burn severity classification produced from the normalized burn ratio thresholds.

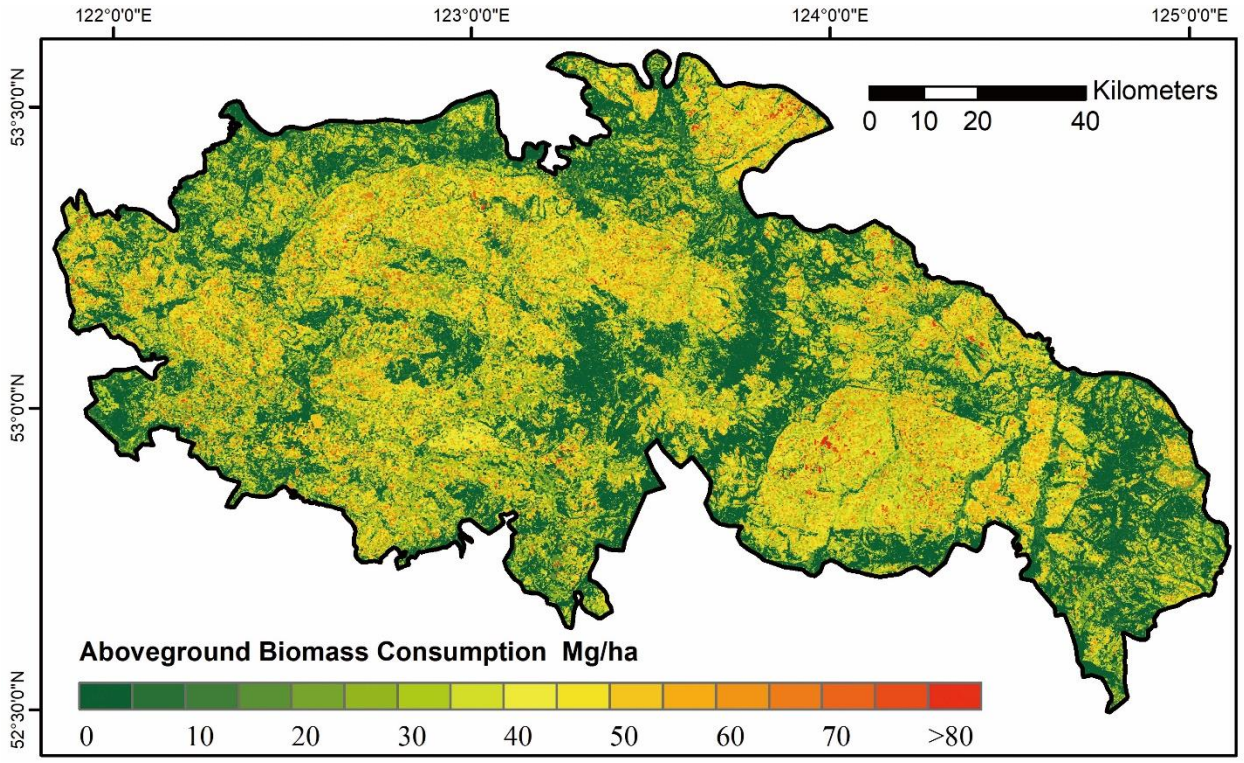

Figure 2-6. Maps of aboveground biomass consumption due to the Black Dragon fire in 1987.

Tables

Table 2-1. Investigated items and evaluation criterion of composite burn index (CBI).

Strata rating factors	Composite burn index					
	No effect	Low		Moderate		High
	0	0.5	1	1.5	2	2.5	3
Herbs, low shrubs and trees less than 1 m						
Foliage consumed (%)	0	30		80	95	100% branch loss
Mortality (%)	0	10		50	>80	100
Tall shrubs and small trees 1–5 m						
Foliage consumed (%)	0	20		60-90	>95	100
Mortality (%)	0	10		70	>85	100
Intermediate trees (sub-canopy, 5–15 m)						
Canopy consumed (%)	0	15		60	80	100
Mortality (%)	0	15		60	80	100
Big trees (upper-canopy, >15 m)						
Canopy consumed (%)	0	10		50	70	100
Mortality (%)	0	10		50	70	100

Table 2-2. Normalized burn ratio (NBR) thresholds, tree mortality, and foliage consumption by burn severity class.

Burn severity	NBR threshold	Tree mortality levels	Consumed foliage
Unchanged	> 585	0	0
Low	585 - 252	15%	20%
Moderate	252 - 53	65%	70%
High	≤ 53	90%	100%

Table 2-3. Combustion efficiency (CE) and tree species biomass distribution of different components.

Organs	CE

	High	Moderate	Low	Dahurian larch %	White birch %	Aspen %	Mongolian Scots pine %	Other species %
Leaves	1	0.7	0.2	2.7	5	5	3.2	4.9
Stems	0.62	0.41	0.03	80.3	73	70	86.5	75.8
Branch	0.79	0.57	0.13	9	12	12.5	6.3	10.1
Barks	0.85	0.62	0.16	8	10	12.5	4	9.2

Table 2-4. Carbon fraction (f_c) of organs by tree species (mg g^{-1})

Species	Stems	Branches	Leaves	Bark
White Birch	478.76	489.75	503.37	472.75
Dahurian larch	464.71	471.45	495.81	500.26
Mongolian Scots pine	473.26	475.45	499.87	471.93
Quaking aspen	463.87	458.39	460.72	471.4
Other species	465.6	473.21	475.91	470.56

Table 2-5. Carbon emission factors for each species, in g per kg carbon of dry biomass burned.

Forest type	Emission factors			
	CO_2	CO	CH_4	NMHC
Dahurian larch forests	3180	194	8.8	7
White birch forests	3256	206	10	6.5
Mongolian Scots pine forests	3032	239	10.5	8.4
Others	3250	202	9.8	7.6

Table 2-6. Estimates of consumed and remaining aboveground biomass and combustion efficiency (CE) in different burn severity classes.

Burn	Area (ha)	CE	Pre-fire Mg ha^{-1}	Consumed Mg ha^{-1}	Remaining live Mg ha^{-1}	Remaining dead biomass Mg ha^{-1}			Total Burned Carbon Tg
						stems	branches	barks	
Low	340,623	0.06	66	3.81	57.69	4.31	0.12	0.07	0.61
Moderate	288,483	0.46	60	27.69	19.44	12.2	0.51	0.16	3.81
High	672,857	0.67	61	41.17	4.96	14	0.62	0.25	13.82
Total	1,301,963	0.45	62.63	28.41	22.51	11.04	0.5	0.17	18.24

Table 2-7. Emissions of CO_2, CO, CH_4 and NMHC (kg) during the Black Dragon fire.

Burn severity	CO_2	CO	CH_4	NMHC
Low	3.5×10^{9}	2.17×10^{8}	1.02×10^{7}	7.91×10^{6}
Moderate	1.34×10^{10}	8.38×10^{8}	3.92×10^{7}	3.03×10^{7}
High	4.19×10^{10}	2.66×10^{9}	1.24×10^{8}	9.64×10^{7}
Total	5.88×10^{10}	3.71×10^{9}	1.73×10^{8}	1.35×10^{8}

Table 2-8. Combustion efficiency comparison (CBI: composite burn index, dNBR difference normalized burn ratio, NBR: normalized burn ratio).

Vegetation type	Combustion efficiency	Study area	References
Conifer	0.28	India	Prasad et al. (2001)
	0.25-low;0.47-moderate;0.65-high (spatial burn severity-GeoCBI)	California USA	De Santis et al. (2010)
	0.4	Northeast China	Yi and Bao (2016)
Deciduous	0.25-low; 0.40-moderate; 0.56-high (spatial burn severity-GeoCBI)	California USA	De Santis et al. (2010)
	0.3	India	Prasad et al. (2001)
	0.4	India	Prasad et al. (2001)
Mixed forest	0.2-low; 0.4-moderate; 0.6-high (spatial burn severity-dNBR)	Utah USA	Chen et al. (2011)
	0.4	Northeast China	Yi and Bao (2016)
Temperate	0.4	India	Prasad et al. (2001)
-	0.105	China	Lü et al. (2006)
	0.25	China	Lü et al. (2006)
Boreal forest	0.17-low; 0.37-moderate; 0.48-severe (the proportion of crown fires)	Alaska	Kasischke et al. (1995)
	0.06-low; 0.46-moderate; 0.67-severe (spatial burn severity-NBR)	Northeast China	This study

Table 2-9. Fire and carbon emissions comparison.

Carbon loss only included burned area.

Sources	Burned area	Burn severity	CO_2, g C	CO, g C	CH_4, g C	Carbon Mg C ha^{-1}
The Black Dragon	1.3 Mha	3% unburned; 25%, 22% and for low, moderate and high	1.6×10^{13}	1.6×10^{12}	1.3×10^{11}	14
China forest biomass burning (1950-2000)	0.9 Mha	--	1.1×10^{13}	1.2×10^{12}	8.4×10^{10}	13.2
Global biomass burning[b]	464 Mha	26% small fires	1.9×10^{15}	1.4×10^{14}	1.1×10^{13}	4.4
1997/1998 Complex[c]	9.7 Mha	--	--	--	--	96.3-112.4
The 1997 Taseevsky Fire of Russian forests	2467.2 ha	7% crown fire; 22%, 34% and for low, moderate and high ground fires	--	--	--	6.5
1988 Yellowstone Fire	0.32 Mha	28% unburned; 16%, 25% and for low, moderate and high in Wyoming	--	--	--	23.3
China fossil-fuels consumption[d]	--	--	1.64×10^{14} (1987	6- (2000s)	2.89×10^{1} (2000s)	--

[a] Annual average during 1950-2000 (Lü et al. 2006). [b] Agricultural residuals; annual average burned area during 2001-2010 (Randerson et al. 2012) and carbon emissions during 1997-2016 (Van Der Werf et al. 2017). [c] The carbon loss density of 1997/1998 Kalimantan Complex was calculated based on part of the burned area (the central of Kalimantan, page et al. 2002). [d] Annual average (Marland et al. 2006; Zhao et al. 2012; Peng et al. 2016)

Literature cited

Adams MA (2013) Mega-fires, tipping points and ecosystem services: Managing forests and woodlands in an uncertain future. *Forest Ecology and Management* **294**, 250-261.

Allen JL, Sorbel B (2008) Assessing the differenced Normalized Burn Ratio's ability to map burn severity in the boreal forest and tundra ecosystems of Alaska's national parks. *International Journal of Wildland Fire* **17**, 463-475.

Andreae MO, and Merlet P (2001) Emission of trace gases and aerosols from biomass burning. *Global biogeochemical cycles*, **15**(4), 955-966.

Boby LA, Schuur EA, Mack MC, Verbyla D, Johnstone JF (2010) Quantifying fire severity, carbon, and nitrogen emissions in Alaska's boreal forest. *Ecological Applications* **20**, 1633-1647.

Bowman DM, Balch JK, Artaxo P, Bond WJ, Carlson JM, Cochrane MA, D'Antonio CM, DeFries RS, Doyle JC, Harrison SP, Johnston FH et al. (2009) Fire in the Earth System. *Science* **324**, 481-484.

Cahoon DR, Jr, Stocks BJ, Levine JS, Cofer III WR, Pierson JM (1994) Satellite analysis of the severe 1987 forest fires in northern China and southeastern Siberia. *Journal of Geophysical Research: Atmospheres* **99**, 18627-18638.

Campbell J, Donato D, Azuma D, Law B (2007) Pyrogenic carbon emission from a large wildfire in Oregon, United States. *Journal of Geophysical Research: Biogeosciences* **112**, G04014.

Chang Y, He HS, Hu Y, Bu R, Li X (2008) Historic and current fire regimes in the Great Xing'an Mountains, northeastern China: Implications for long-term forest management. *Forest Ecology and Management* **254**, 445-453.

Chang Y, Zhu ZL, Feng YT, Li YH, Bu RC, Hu YM (2016) The spatial variation in forest burn severity in Heilongjiang Province, China. *Natural Hazards* **81**, 981-1001.

Chen W, Moriya K, Sakai T, Koyama L, Cao CX (2016) Mapping a burned forest area from Landsat TM data by multiple methods. *Geomatics Natural Hazards and Risk* **7**, 384-402.

Chen X, Liu S, Zhu Z, Vogelmann J, Li Z, Ohlen D (2011) Estimating aboveground forest biomass carbon and fire consumption in the US Utah High Plateaus using data from the Forest Inventory and Analysis Program, Landsat, and LANDFIRE. *Ecological Indicators* **11**, 140-148.

Christensen NL, Agee JK, Brussard PF, Hughes J, Knight DH, Minshall GW, Peek JM, Pyne SJ, Swanson FJ, Thomas JW (1989) Interpreting the Yellowstone fires of 1988. *BioScience* **39**, 678-685.

Coen JL, Stavros EN, Fites-Kaufman JA (2018) Deconstructing the King megafire. *Ecological Applications* **28**, 1565-1580.

De Santis A, Asner GP, Vaughan PJ, Knapp DE (2010) Mapping burn severity and burning efficiency in California using simulation models and Landsat imagery. *Remote Sensing of Environment* **114**, 1535-1545.

Epting J, Verbyla D, Sorbel B (2005) Evaluation of remotely sensed indices for assessing burn severity in interior Alaska using Landsat TM and ETM+. *Remote Sensing of Environment* **96**, 328-339.

Escuin S, Navarro R, and Fernandez P (2008) Fire severity assessment by using NBR (Normalized Burn Ratio) and NDVI (Normalized Difference Vegetation Index) derived from LANDSAT TM/ETM images. *International Journal of Remote Sensing* **29** (4), 1053-1073.

Fang JY, Chen AP, Peng CH, Zhao SQ, and Ci L (2001). Changes in forest biomass carbon storage in China between 1949 and 1998. *Science* **292** (5525):2320-2322.

Ferreira-Leite F, Bento-Gonçalves A, Vieira A, da Vinha L (2015) Mega-fires around the world: A literature review. In 'Wildland Fires: A Worldwide Reality'. (Eds Bento-Gonçalves A, Vieira A) pp. 15-34 (Nova Science Publishers: New York).

Flannigan MD, Krawchuk MA, deGroot WJ, Wotton BM, Gowman LM (2009) Implications of changing climate for global wildland fire. *International Journal of Wildland Fire*, **18**(5) 483- 507.

French NH, Goovaerts P, Kasischke ES (2004) Uncertainty in estimating carbon emissions from boreal forest fires. *Journal of Geophysical Research: Atmospheres* **109,** D14S08.

Fu H, Wei Y, Chen JJ (2013) Forest carbon storage and it's dynamics in the Great Xing'an Mountains Inner Mongolia (in Chinese). *J Arid Land Resour Environ* **27**:166–170.

Garcia M, Saatchi S, Casas A, Koltunov A, Ustin S, Ramirez C, Garcia-Gutierrez J, Balzter H (2017) Quantifying biomass consumption and carbon release from the

California Rim fire by integrating airborne LiDAR and Landsat OLI data. *Journal of Geophysical Research: Biogeosciences* **122**, 340-353.

Giglio L, Randerson JT, van der Werf GR (2013) Analysis of daily, monthly, and annual burned area using the fourth-generation global fire emissions database (GFED4). *Journal of Geophysical Research: Biogeosciences* **118**, 317-328.

Hu H, Sun L, Guo Q, Lu X (2007) Carbon emissions from forest fires on main arbor species in Daxing'an Mountains in Heilongjiang Province (in Chinese). *Scientia Silvae Sinicae* **11**, 016.

Hu H, Wei S, Sun L (2012) Estimation of carbon emissions due to forest fire in Daxing'an Mountain from 1965 to 2010 (in Chinese). *Chinese Journal of Plant Ecology* **36**, 629-644.

Hurteau MD, Koch GW, Hungate BA (2008) Carbon protection and fire risk reduction: Toward a full accounting of forest carbon offsets. *Frontiers in Ecology and the Environment* **6**, 493-498.

Intergovernmental Panel on Climate Change (2015) Climate change 2014: Mitigation of climate change. Cambridge University Press.

Isaev A, Korovin G, Bartalev S, Ershov D, Janetos A, Kasischke E, Shugart H, French N, Orlick BE, Murphy TL (2002) Using remote sensing to assess Russian forest fire carbon emissions. *Climatic Change* **55**, 235-249.

Ito A (2011) Mega fire emissions in Siberia: potential supply of bioavailable iron from forests to the ocean. *Biogeosciences* **8**, 1679-1697.

Ito A and Penner JE (2004) Global estimates of biomass burning emissions based on satellite imagery for the year 2000. *Journal of Geophysical Research: Atmospheres*, **109**(D14), 839:856.

Kaiser JW, Heil A, Andreae MO, Benedetti A, Chubarova N, Jones L, Van Der Werf GR (2012) Biomass burning emissions estimated with a global fire assimilation system based on observed fire radiative power.

Kasischke ES, French NH., Bourgeau-Chavez LL, and Christensen N, Jr (1995) Estimating release of carbon from 1990 and 1991 forest fires in Alaska. *Journal of Geophysical Research: Atmospheres* **100.D2**, 2941-2951.

Kasischke ES, Turetsky MR, Ottmar RD, French NHF, Hoy EE, Kane ES (2008) Evaluation of the composite burn index for assessing fire severity in Alaskan black spruce forests. *International Journal of Wildland Fire* **17**, 515-526.

Kaufman Y, Setzer A, Ward D, Tanre D, Holben B, Menzel P, Pereira M, Rasmussen R (1992) Biomass burning airborne and spaceborne experiment in the Amazonas (BASE-A). *Journal of Geophysical Research: Atmospheres* **97**, 14581-14599.

Kennedy RE, Andréfouët S, Cohen WB, Gómez C, Griffiths P, Hais M, Healey SP, Helmer EH, Hostert P, Lyons MB (2014) Bringing an ecological view of change to Landsat-based remote sensing. *Frontiers in Ecology and the Environment* **12**, 339-346.

Key, C. and N. Benson (2005). "Landscape assessment: ground measure of severity; the composite burn index, and remote sensing of severity, the normalized burn index and remote sensing of severity, the normalized burn ratio." FIREMON: Fire Effects Monitoring and Inventory System: 1-51.

Leistikow BN, Martin DC, Milano CE (2000) Fire injuries, disasters, and costs from cigarettes and cigarette lights: a global overview. *Preventive medicine* **31**, 91-99.

Liu Y, Goodrick S, Heilman W (2014) Wildland fire emissions, carbon, and climate: Wildfire–climate interactions. *Forest Ecology and Management* **317**, 80-96.

Liu ZH, Yang J, Chang Y, Weisberg PJ, He HS (2012) Spatial patterns and drivers of fire occurrence and its future trend under climate change in a boreal forest of Northeast China. *Global Change Biology* **18**, 2041-2056.

Loboda T, O'Neal KJ, Csiszar I (2007) Regionally adaptable dNBR-based algorithm for burned area mapping from MODIS data. *Remote Sensing of Environment* **109**, 429-442.

Lu A, Tian H, Liu M, Liu J, Melillo JM (2006) Spatial and temporal patterns of carbon emissions from forest fires in China from 1950 to 2000. *Journal of Geophysical Research: Atmospheres* **111**, D05313.

Luo J (2002). Influence of forest fire disaster on forest ecosystem in Great Xing'anling (in Chinese). *Journal of Beijing Forestry University*, **24**(5/6), 101-107.

[dataset] Marland, G., T. Boden, R. Andres, A. Brenkert and C. Johnston (2006). "Global, regional, and national fossil fuel CO2 emissions." Trends: A compendium of data on global change: 37. *http://cdiac.ess-dive.lbl.gov/trends/emis/tre_coun.html*

Masek, JG (2006) Landsat Ecosystem Disturbance Adaptive Processing System (LEDAPS).

Miller JD, Thode AE (2007) Quantifying burn severity in a heterogeneous landscape with a relative version of the delta Normalized Burn Ratio (dNBR). *Remote Sensing of Environment* **109**, 66-80.

Naficy CE (2017). A cross-scale assessment of historical fire severity patterns, landscape dynamics, and methodological challenges in mixed-severity fire regimes of the northern US Rockies. Ph.D. thesis, Department of Geography, University of Colorado, Boulder, Colo.

Page SE, Siegert F, Rieley JO, Boehm H-DV, Jaya A, Limin S (2002) The amount of carbon released from peat and forest fires in Indonesia during 1997. *Nature* **420**, 61-65.

Palacios-Orueta A, Chuvieco E, Parra A, Carmona-Moreno C (2005) Biomass burning emissions: A review of models using remote-sensing data. *Environmental Monitoring and Assessment* **104**, 189-209.

Peng S, Piao S, Bousquet P, Ciais P, Li B, Lin X, Tao S, Wang Z, Zhang Y, Zhou F (2016) Inventory of anthropogenic methane emissions in mainland China from 1980 to 2010. *Atmospheric Chemistry and Physics* **16**, 14545-14562.

Poorter H, Jagodzinski AM, Ruiz-Peinado R, Kuyah S, Luo Y, Oleksyn J, Usoltsev VA, Buckley TN, Reich PB, Sack L (2015) How does biomass distribution change with size and differ among species? An analysis for 1200 plant species from five continents. *New Phytologist* **208**, 736-749.

Prasad VK, Kant Y, Gupta PK, Sharma C, Mitra AA, Badarinath KVS (2001) Biomass and combustion characteristics of secondary mixed deciduous forests in Eastern Ghats of India. *Atmospheric Environment* **35**(18), 3085-3095.

Randerson J, Chen Y, Werf G, Rogers B, Morton D (2012) Global burned area and biomass burning emissions from small fires. *Journal of Geophysical Research: Biogeosciences* **117**, G04012.

Roy DP, Landmann T (2005) Characterizing the surface heterogeneity of fire effects using multi-temporal reflective wavelength data. *International Journal of Remote Sensing* **26**, 4197-4218.

Schepers L, Haest B, Veraverbeke S, Spanhove T, Vanden Borre J, Goossens R (2014) Burned area detection and burn severity assessment of a heathland fire in Belgium using airborne imaging spectroscopy (APEX). *Remote Sensing* **6**, 1803-1826.

Seiler W, Crutzen PJ (1980) Estimates of gross and net fluxes of carbon between the biosphere and the atmosphere from biomass burning. *Climatic Change* **2**, 207-247.

Smith AMS, Wooster MJ, Drake NA, Dipotso FM, Falkowski MJ, Hudak AT (2005) Testing the potential of multi-spectral remote sensing for retrospectively estimating fire severity in African Savannahs. *Remote Sensing of Environment* **97**, 92-115.

Smithwick E, Ryan M, Kashian D, Romme W, Tinker D, Turner M (2009) Modeling the effects of fire and climate change on carbon and nitrogen storage in lodgepole pine (Pinus contorta) stands. *Global Change Biology* **15**, 535-548.

Susott RA, Ward DE, Babbitt RE, Latham DJ (1991) The measurement of trace emissions and combustion characteristics for a mass fire [Chapter 32]. In 'Global biomass buring: Atmospheric, climatic, and biosphere implications'. (Eds Levine, JS) pp. 245-257. (Cambridge, MA: MIT Press).

Trigg S, Flasse S (2000) Characterizing the spectral-temporal response of burned savannah using in situ spectroradiometry and infrared thermometry. *International Journal of Remote Sensing* **21**, 3161-3168.

Turner MG, Hargrove WW, Gardner RH, Romme WH (1994) Effects of fire on landscape heterogeneity in Yellowstone National Park, Wyoming. *Journal of Vegetation Science* **5**, 731-742.

UNFCCC (2015) Adoption of the Paris Agreement. Report No. FCCC/CP/2015/L.9/Rev.1. New York: UNFCCC.

Urbanski, SP, Hao WM, and Baker S (2008) Chemical composition of wildland fire emissions. *Developments in Environmental Science* **8**, 79-107.

Van der Werf GR, Randerson JT, Giglio L, Collatz GJ, Kasibhatla PS, Arellano AF, Jr (2006) Interannual variability in global biomass burning emissions from 1997 to 2004. *Atmospheric Chemistry and Physics*, **6**(11), 3423-3441.

Van der Werf GR, Randerson JT, Giglio L, Collatz G, Mu M, Kasibhatla PS, Morton DC, DeFries R, Jin Yv, van Leeuwen TT (2010) Global fire emissions and the contribution of deforestation, savanna, forest, agricultural, and peat fires (1997–2009). *Atmospheric Chemistry and Physics* **10**, 11707-11735.

Van der Werf GR, Randerson JT, Giglio L, Van Leeuwen TT, Chen Y, Rogers BM, Mu M, Van Marle MJ, Morton DC, Collatz GJ (2017) Global fire emissions estimates during 1997-2016. *Earth System Science Data* **9**, 697-720.

Van Leeuwen TT, Van der Werf GR, Hoffmann AA, Detmers RG, Rücker G, French NH, Archibald S, Carvalho J, Jr, Cook GD, De Groot WJ (2014) Biomass burning

fuel consumption rates: a field measurement database. *Biogeosciences Discuss* **11**, 8115-8180.

Wang C, Gower ST, Wang Y, Zhao H, Yan P, Bond-Lamberty BP (2001) The influence of fire on carbon distribution and net primary production of boreal Larix gmelinii forests in north-eastern China. *Global Change Biology* **7**, 719-730.

Wiedinmyer C, Akagi SK, Yokelson RJ, Emmons LK, Al-Saadi JA, Orlando JJ, Soja AJ (2011) The Fire INventory from NCAR (FINN): A high resolution global model to estimate the emissions from open burning. *Geoscientific Model Development*, **4**(3), 625.

Williams J (2013) Exploring the onset of high-impact mega-fires through a forest land management prism. *Forest Ecology and Management* **294**, 4-10.

Williams J, Albright D, Hoffmann AA, Eritsov A, Moore P, Mendes de Morais J, Leonard M, San Miguel-Ayanz J, Xanthopoulos G, Van Lierop P (2011) Findings and implications from a coarse-scale global assessment of recent selected mega-fires. International Wildland Fire Conference (5th, 9-13 May 2011, Sun City, South Africa). FAO.

Wulder MA, Masek JG, Cohen WB, Loveland TR, Woodcock CE (2012) Opening the archive: How free data has enabled the science and monitoring promise of Landsat. *Remote Sensing of Environment* **122**, 2-10.

Wulder MA, White JC, Loveland TR, Woodcock CE, Belward AS, Cohen WB, Fosnight EA, Shaw J, Masek JG, Roy DP (2016) The global Landsat archive: Status, consolidation, and direction. *Remote Sensing of Environment* **185**, 271-283.

Xu H, Li Z, Qiu Y (1997) Fire disturbance history in virgin forest in northern region of Daxinganling Mountains (in Chinese). *Acta Ecologica Sinica* **17**, 337-343.

Yi K, Bao Y (2016) Estimates of wildfire emissions in boreal forests of China. *Forests* **7**(8), 158.

Yu Y, Fan W, Li M (2012) Forest carbon rates at different scales in Northeast China forest area (in Chinese). *The Journal of Applied Ecology* **23**, 341-346.

Zhang Q, He HS, Liang Y, Hawbaker TJ, Henne PD, Liu J, Huang S, Wu Z, Huang C (2018a) Integrating forest inventory data and MODIS data to map species-level biomass in Chinese boreal forests. *Canadian Journal of Forest Research* **48**, 1-19.

Zhang Q, Liang Y, He H (2018b). Tree-lists estimation for Chinese boreal forests by integrating weibull diameter distributions with MODIS-based forest attributes from kNN imputation. *Forests*, **9**(12), 758.

Zhao F, Healey SP, Huang C, McCarter JB, Garrard C, Goeking SA, Zhu Z (2018) Assessing the effects of fire disturbances and timber management on carbon storage in the Greater Yellowstone Ecosystem. *Environmental Management* **62**, 766-776.

Zhao Y, Nielsen CP, McElroy MB, Zhang L, Zhang J (2012) CO emissions in China: Uncertainties and implications of improved energy efficiency and emission control. *Atmospheric Environment* **49**, 103-113.

Zhu Z, Woodcock CE (2012) Object-based cloud and cloud shadow detection in Landsat imagery. *Remote Sensing of Environment* **118**, 83-94.

CHAPTER III. Spatially explicit reconstruction of post-megafire forest recovery through landscape modeling

1. Introduction

Forest fire is a primary disturbance in many forest ecosystems, influencing succession dynamics and carbon storage (Lecomte et al. 2006; Bowman et al. 2009). Fires that burned large areas with high intensity (areal extent > 100 km^2, often called megafires) can cause abrupt changes to ecosystems and have distinctly different ecological effects from other fires (Bradstock. 2008; Keane et al. 2008; Stephens et al. 2014). Post-fire recovery is an important variable for understanding fire effects on forest ecosystems, which is mainly determined by burn severity and species regeneration strategies (Johnstone et al. 2010; Halofsky et al. 2011). Megafires often result in a heterogeneous mosaic of burn severities across a wide range of environmental conditions; consequently, the vegetational response can be complex. Seedlings regenerated after the fire vary strongly among areas with contrasting burn severities due to species-specific differences in dispersal, seed size, shade tolerance and parent tree locations. Large-seeded species (e.g., *Pinus* spp.) have higher regeneration rates under partial shade, and thus have higher regeneration rates in areas with low or moderate severity burns, while fecund, light-seeded broadleaf species (e.g., *Betula* spp.) are wind dispersed and are more likely to colonize in areas with high severity burns (Greene et al. 2007; Johnstone et al. 2010). Megafires can also create large high-severity burn patches that could delay tree regeneration and prolong early seral conditions by limiting the reach of seed dispersal (Johnstone et al. 2016), which may even trigger a shift from forest to shrub- or grass-dominated cover types due to seed limitation

and climate-induced regeneration failure (Collins and Roller 2013; Savage et al. 2013; Harvey et al. 2016). Even with similar burn severity and sufficient seed availability, germination and establishment can be affected by tolerances to temperature and moisture that vary by species (Petrie et al. 2016; Davis et al. 2018) and microsite conditions, which can influence the success of tree establishment and regeneration, with fewer tree seedlings found on harsh sites (Broncano and Retana 2004; Bonnet et al. 2005; Kemp et al. 2019). The complex vegetation responses to megafires make assessments of post-fire recovery challenging.

Assessment of post-fire forest recovery is traditionally completed with plot-based field inventories. This method can provide relatively accurate and detailed measurements of post-fire plant communities, which can be used to quantify burn severity and recovery based on the time the plots were surveyed after the fire (e.g., Johnstone et al. 2004; Turner et al. 2016). However, field-based inventories generally cover small spatial extents and provide plot-based information on burn severity and recovery but not about the size and shape of burned patches (e.g., Crotteau et al. 2013). Since megafires burn large areas across a range of environmental gradients and a mix of burn severities, it is challenging to capture the heterogeneous burn severities and post-fire recovery patterns using field-based methods alone. In addition, forest inventories before and immediately after megafires, and the subsequent monitoring of vegetation recovery, are often lacking. These limitations hinder field-based approaches for assessing megafire effects and post-fire recovery.

Remote sensing is effective in capturing burn severity patterns and monitoring post-fire vegetation recovery for megafires (French et al. 2008; Gitas et al. 2012; Chu and

Guo 2014). Remote sensing-based vegetation indices such as the normalized burn ratio (NBR) (García and Caselles 1991; Epting et al. 2005) and its derivatives, differenced NBR (dNBR) and relative differenced NBR (RdNBR) (Key and Benson 2005; Miller and Thode 2007), have been widely used for detecting burn severity patterns (Eidenshink et al. 2007). The normalized difference vegetation index (NDVI), enhanced vegetation index (EVI) and soil adjusted vegetation index (SAVI) have been used for monitoring post-fire recovery (van Leeuwen et al. 2010; Gitas et al. 2012; Veraverbeke et al. 2012). However, a great deal of uncertainty exists when using these vegetation indices to assess post-fire recovery in terms of species composition and forest structure. Forest recovery assessments using vegetation indices can become complicated when different vegetation recovery states have similar vegetation index values (Glenn et al. 2008; Chu and Guo 2014). For instance, young (e.g., two years post-fire) broadleaf forest pixels may exhibit the same NDVI value as the unburned coniferous forest pixels that are on a very different successional stage (Idris et al. 2005; Cuevas-Gonzalez et al. 2009; Cai et al. 2018). The limited availability of cloud-free satellite images during the growing season can also impede continuous assessment of post-fire forest recovery (Ju and Roy 2008). In addition, remote sensing-based vegetation indices are limited in their ability to monitor demographic processes such as seed dispersal, tree establishment and mortality, species competition, and competition-caused mortality (self-thinning), which drive post-fire forest recovery.

Fire-succession models have been used to understand the interactions between vegetation response to forest fire, including post-fire forest structure, composition, and diversity (Boychuk et al., 1997; Millington et al., 2009; Miller and Ager, 2013).

However, most of these models lack demographic processes to capture the species regeneration traits. Alternatively, Forest landscape models (FLMs) spatially simulate forest dynamics (seed establishment, growth, competition, and succession) accounting for the processes not captured by remote sensing and fire-succession models, and have been effectively applied to spatially reconstructing historical post-disturbance forest conditions (He 2008; Seidl et al. 2014; Thrippleton et al. 2014). FLMs can also incorporate information from fire perimeters and the spatial patterns of burn severity derived from remote sensing as inputs (Wang et al. 2009). They can track the location and abundance of parent trees and seedlings when simulating the demographic processes that drive post-fire forest recovery (Wang et al. 2013; Wang et al. 2014a). Finally, FLMs can be calibrated and validated with forest inventory data (Seidl et al. 2012; Wang et al. 2014b; Luo et al. 2015).

The 1987 Black Dragon fire, which occurred in the boreal forest of China, stood out due to its size and severity. The fire burned 1.3×10^4 km^2, resulted in a high degree of tree mortality, and reset forest succession for most burned stands. It created opportunities to study post-fire forest dynamics at an unprecedented scale. In this study, my objectives were to (1) present a novel framework that integrates an FLM with field inventory and remote sensing data to spatially reconstruct the burn severity of the Black Dragon fire and the post-fire time series of forest conditions (i.e., forest composition, structure and aboveground biomass) and (2) evaluate whether the reconstructed forest conditions could realistically capture the post-fire recovery (e.g., density and basal area) at the level of individual tree species under different burn severities. Spatiotemporal reconstruction of the post-megafire forest condition provides a platform to investigate the recovery rate and

trajectories through model simulations and thus improve realism and reduce uncertainties.

2. Data and methods

2.1. Study area

My study area is located in the Great Xing 'an Mountains and encompasses approximately 8.46×10^4 km^2 (50°10’ N, 121°12’ E to 53°33’ N, 127°00’ E) in Northeast China. (Fig. 3-1). The area is hilly and mountainous (altitudes ranging from 134 to 1511 m) and falls within the continental cold temperate climate zone with long and severe winters but short summers. The average annual temperature is -3.9 °C with an average temperature of –33 °C in the coldest month (January), and an average temperature of 17.5 °C in the hottest month (July). The annual cumulative precipitation ranges from 400 to 500 mm. More than 60% of the annual precipitation occurs in the summer season from June to August (Zhou 1991; Xu 1998). Vegetation in this region is representative of cool boreal coniferous forests that cover 83% of the study area. The canopy species composition is relatively simple. Dahurian larch (*Larix gmelini*（Rupr.) Kuzen, hereafter “larch”), a deciduous conifer, and white birch (*Betula platyphylla* Suk.), a deciduous broadleaved species, are dominant, covering more than 80% of the study area. Other tree species include the evergreen conifers, Korean spruce (*Picea koriensis* Nakai, hereafter “spruce”) and Scots pine (*Pinus sylvestris* var. *mongolica* Litvinov, hereafter “pine”), and the deciduous broadleaved species, aspen (*Populus davidiana* Dole and *P. suaveolens* Fischer), willow (*Chosenia arbutifolia* (Pall.) A. Skv), Asian black birch (*Betula davurica* Pall., hereafter “black birch”), and Mongolian oak (*Quercus mongolica* Fisch.ex

Ledeb.). Black birch and Mongolian oak are mainly distributed in the southeastern low elevation part of the study area, whereas pine is distributed in the northern part.

Wildfire frequency and area burned in my study area are linked to human disturbances and annual variations in monsoonal strength (Liu et al. 2012). Low intensity surface fires (mean return interval ca. 30 yr) were historically frequent, occasionally mixed with infrequent stand-replacing fires (mean return interval ca. 120 yr) in the high elevation regions (Xu et al. 1997). However, long-term fire exclusion and timber harvest have altered the fire regime, where fires are infrequent but more intense (Chang et al. 2007). In my study area, fires burned 6.64×10^4 km^2 from 1967 to 2005 (Chang et al. 2008; Liu et al. 2012). One of the most noteworthy fires, known as the Black Dragon fire, ignited on 6 May 1987 and burned four forest bureaus (Xilinji, Tuqiang, Amuer, and Tahe). The Black Dragon fire resulted in over 200 deaths and 4 billion Yuan of losses at that time, causing the most forest fire damage in the history of China.

2.2. General approach

I first reconstructed forest stand conditions in my study area before the Black Dragon fire (i.e., in 1985) using remote sensing and forest inventory data (Fig.3-2). Since the remote sensing data could not provide detailed stand information at the pixel level across my entire landscape and pre-fire field inventory data were not available, I constructed the pre-fire forest conditions following the k-Nearest Neighbor (kNN) stand imputation approach of Zhang et al. (2018a, 2018b). I used Landsat data to delineate fire perimeters and derive burn severity classes associated with total tree mortalities (Xu et al. 2020). With the pre-fire landscape as a starting point, I 'burned in' the Black Dragon fire perimeter and severity in LANDIS PRO at the fire year 1987 and simulated the post-

megafire time series forest conditions using a forest landscape model (LANDIS PRO) (Fig. 3-2).

LANDIS PRO has been parameterized for numerous forest regions under different environmental settings (Huang et al. 2018; Wang et al. 2019). However, to ensure tree species parameters of the model (e.g., growth rate, available seeds, maximum stand density index, and maximum diameter) accurately captured the tree species in my study area, I used a data assimilation approach (Luo et al. 2011; Wang et al. 2014b) that iteratively calibrated the parameters by comparing the simulated results at years with the respective forest inventory data (Fig. 3-2a). The calibration process was followed by validation against field inventory data at a later stage (2015) to ensure that forest dynamics under no disturbance were correctly simulated (Fig. 3-2a). To ensure the response of tree species corresponded to various burn severities, I also applied the data assimilation approach to calibrate fire parameters (e.g., height of bark charring) in LANDIS PRO to precisely constrain post-fire tree species recovery processes (Fig. 3-2b). I used the year 2000 post-fire inventory data for the calibration and used the year 2015 post-fire inventory data for model validation since these were the only post-fire inventory data available in the burned area (Fig. 3-2b). Through the iterative calibration and validation processes, I was able to derive the continuous time-series forest conditions from which post-fire forest landscape recovery could be analyzed spatially and temporally (Fig. 3-2c).

2.3. Forest inventory data

The forest inventory data used for model initialization, calibration, and results validation in this study were collected from the China Forestry Science Data Center

(CFSDC, http://www.cfsdc.org), including forest plot inventory data from 2000, 2010, and 2015, and a forest stand map in polygons with relatively complete attributes from the early 2000s (Fig. 3-3). The plot inventory data includes 5752 unburned plots and 1305 burned plots following the Black Dragon fire. Each plot contained the number of trees and diameter at breast height (DBH >5 cm) class by species. The forest stand map comprised 276,273 stands with homogeneous forest attributes (e.g., dominant tree species, stand age, and site index) in each stand. The data contained stand area, mean DBH, stand height, stand age, stand volume, tree species composition (species percent volume), forest origin (natural regeneration vs. afforestation), and management and disturbances (harvest, plantation and forest fires) information in each stand polygon.

2.4 Remote sensing data

In this study, 20 pre- and post-fire Landsat TM (Thematic Mapper) images (Table 3-1) from the U.S. Geological Survey (USGS, http://earthexplorer.usgs.gov) were used to estimate pre-fire forest composition and burn severity of the 1987 Black Dragon fire. The images were processed by the USGS to convert from DN (digital numbers) to surface reflectance using the LEDAPS algorithm (Landsat Ecosystem Disturbance Adaptive Processing System, Masek et al. 2006). Clouds, cloud shadows, and snow pixels were masked using the function of mask algorithm (FMASK; Zhu and Woodcock 2012). The 1980s images were processed by radiometric normalization based on the images from the 2000s, using a histogram matching method to reduce radiometric differences among images caused by inconsistencies of acquisition conditions.

2.5. Pre-fire forest conditions

Forest inventory data before the Black Dragon fire were lacking. I combined 2000s forest inventory data with 1980s and 2000s Landsat TM data to map 1980s aboveground forest biomass and tree lists (i.e., lists of species and diameter for every tree), following the approaches of Zhang et al. (2018a, 2018b). I used 2000s forest inventory data and 2000s Landsat TM data as the training samples to fit a nonparametric random forest-based *k*NN model for biomass and *k*NN and Weibull parameter prediction models (WPPMs) for tree lists. Then I mapped species-level biomass and tree lists before the Black Dragon fire at 30-m resolution using 1980s Landsat TM data based on the developed biomass estimation model and tree-lists estimation model. Thus, the pre-fire forest composition (Figs. 3-4 and 3-5) represents the distribution and abundance of tree species before the 1987 Black Dragon fire.

My imputation results (Figs. 3-4 and 3-5) conformed to previous studies and field observations. The total tree density (ranging from 400 to 2500 trees/ha, Fig. 3-4) and aboveground biomass (62.4 ± 22.76 Mg/ha, Fig. 3-5) were close to the values reported by Zhai et al. (1990), Hu et al. (2015), and Fang et al. (2001) for northeastern China. Moreover, my estimates of the species distribution (Figs. 3-4 and 3-5) were consistent with the environmental niches of tree species. Larch, the representative Siberian boreal tree species, is distributed most widely since it can endure extremely cold winters and a short growing season, and it can grow in both well-drained and boggy sites due to its shallow roots (Xu 1998; Kajimoto et al. 2003; Yang et al. 2014). White birch is also distributed widely in the area but is less adaptable to shade and humid environments and typically has less biomass than larch (Xu. 1998). Aspen requires warmer temperatures

and higher soil fertility and is negatively correlated with elevation (Xu 1998). Scots pine has high tolerance of drought and low temperatures and consequently was mainly distributed on the sunny slopes and ridges of the northern part of my study area (Zhu et al. 2006). Mongolian oak and black birch were mainly distributed in the southeast of the area since they thrive in areas with higher temperatures (Xu 1998). Spruce grows under cold environments and therefore was mainly mapped in areas of relatively high elevation of the northern area. Willow requires sufficient humidity to survive and is therefore widespread along rivers, which are fed by water from the glaciers and snows of the high surrounding mountains. These evaluations ensured the subsequent reconstructions of forest recovery rate and trajectories bear high realism (Temperli et al. 2013).

2.6 Landscape model parameterization

I used the LANDIS PRO forest landscape model to simulate forest landscape changes and reconstruct tree species recovery trajectories after the Black Dragon fire. The model tracks the number (density) of each tree species by age cohort (size class) at the pixel level (i.e., 100 m resolution in this study) and simulates species-, stand-, and landscape-scale processes over large spatial and temporal extents (Wang et al. 2013; Wang et al. 2014a). I used the succession module in LANDIS PRO to simulate individual tree establishment, growth, resprouting, and mortality at the species level, resources competition, self-thinning and seedling establishment at stand level, and seed dispersal at the landscape level. Establishment success is determined by species-specific biological traits, such as shade tolerance, and suitability to establish under the other environmental conditions besides shade. Mortality is determined by longevity (i.e., maximum lifespans), competition, and disturbances. Other landscape-scale processes (i.e., natural and

anthropogenic disturbances) were simulated by independent modules (e.g., fire, harvesting, and fuel treatments are simulated using the fire, harvest, and fuel modules, respectively). Forest change is determined by the interactions of species-, stand-, and landscape-scale processes.

I modeled the eight most common tree species, which accounted for approximately 95% of stand volume in this study region. Tree species life history attributes included longevity, age of reproductive maturity, shade tolerance, fire tolerance, seed dispersal distance, maximum tree diameter, maximum stand density index, and number of potential germination seeds (Table 3-2). LANDIS PRO does not require climate and soil parameters; however, it requires species establishment probability (SEP) and maximum growing space occupied (MGSO) by land type, which delineates heterogeneous landscapes into smaller but relatively homogeneous land type units. Within each land type unit, resource availability represented by the MGSO and SEP is assumed to be homogeneous. For this study, SEP and MGSO were derived from an ecosystem process model LINKAGES 3.0 (Dijak et al. 2017) for each land type.

LINKAGES is a plot-based forest ecosystem process model that simulates seedling establishment, tree growth and competition for light, nutrients and soil moisture, carbon-nitrogen storage cycles, evapotranspiration, and soil hydrology (Dijak et al., 2017). I divided our study area into 166 land types based on the ecoregions (topography and climate; Xu, 1998), soil, land cover, and forest bureaus to reflect the variation of environment conditions (Fig. 3-6). Parameters for eight major tree species (Table 3-3) were derived from previous studies in northeastern China (He et al. 2005, Huang et al. 2018). Daily climate data (including daily minimum and maximum temperature, precipitation, average wind

speed, and total solar radiation) were derived from a China national meteorological monitoring dataset (http://data.cma.cn). I obtained soil parameters (thickness of soil layer, organic matter, nitrogen, rock fragment, clay, and sand content) from the China soil scientific database (http://www.soil.csdb.cn) and the China soil database (http://vdb3.soil.csdb.cn). Soil water-holding capacity and wilting point were estimated by rock fragment, clay, and sand content.

I estimated SEP on each land type by simulating species establishment and growth from bare ground over 30 years. I calculated SEPs from the maximum biomass reached by a species on each land type by converting biomass to a relative scale of 0–1 across species (He et al., 1999). I estimated MGSO as the maximum total biomass reached on each land type by simulating the establishment and growth of plots composed of the 8 mixed tree species over 300 years. Each simulation was replicated 20 times.

2.7 Black Dragon fire and its implementation in LANDIS PRO

The spatial pattern and variability of burn severity strongly influences vegetation response, forest structure, and post-fire successional trajectories (Halofsky et al. 2011). The burn severity map of the Black Dragon fire used in this study was extracted based on the remote sensing classification from a relationship between normalized burn ration (NBR) and composite burn index (CBI) (Xu et al. 2020). The burn severity explicitly accounted for different levels of tree mortality that are important for post-fire forest succession: unburned (no sign of fire effects, NBR > 585), low severity (252 < NBR < 585), moderate severity (53 < NBR < 252), and high severity (NBR < 53).

The simulation of fire is treated as a stochastic process in the LANDIS PRO Fire module. However, there was no guarantee that the Black Dragon fire would occur in

1987 in my simulation. Thus, I mimicked this specific fire event, and its effects using the LANDIS PRO Fuel module (He et al. 2004), which can deterministically specify how live fuel loads are reduced (corresponding to tree mortality detected for each burn severity class) in fuel reduction treatments. Post-fire live tree mortality was modeled using a logistic regression equation (Equation (1) where P is probability of mortality following fire, β_i are model coefficients determining fire tolerance, X_1 is tree diameter (cm), and X_2 is height of bark charring (m) analogously for burn severity) based on previous studies (Woolley et al. 2012; Fraser et al. 2019). I divided my study area into four fuel management areas based on the four fire severity classes (Xu et al. 2020). Initial model coefficients for each species were defined based on the species fire tolerance (Fraser et al 2019).

$$P = (1 + e^{-(\beta_0+\beta_1 X_1+\beta_2 X_2)})^{-1} \qquad \text{Equation (3-1)}$$

2.8 Model calibration and results validation

Forest inventory data in unburned area were available for years 2000, 2010, and 2015. The 2000 and 2010 data were used to calibrate tree species parameters while the 2015 data were used to validate the simulated results. Forest inventory data in burned areas were only available for years 2000 and 2015. The 2000 data were used to calibrate fire parameters and the 2015 data were used to validate the simulated fire effects (Fig. 3-2a, b). Only simulated trees with DBH > 5 cm and forest inventory data that were in the study areas with no evidence of disturbance (e.g., logging, insects, disease, and fire) after 1987 were used in the calibration and validation processes.

Model fit can be assessed using the difference between the simulated results and true values, while overfitting can result in deterioration in prediction accuracy (Lever et

al. 2016). In this study, to calibrate tree species parameters, I iteratively adjusted the age-DBH relationship and available seeds for each species by land types until the differences between simulated density and basal area by species and the forest inventory were not significant (no differences based on a one-way analysis of variance (ANOVA) test ($p > 0.05$)) at 2000 and 2010, to ensure that the these parameters realistically represented the actual forests in my study area. I validated the simulated results at the landscape scale by stratifying the simulation results and forest inventory data into subecoregions based on the ecoregion classification of Xu (1998) and soil types (Fig. 3-6), because resource availability and species assemblages were relatively homogeneous within a subecoregion and heterogeneous among subecoregions in LANDIS PRO for undisturbed forests. Specifically, I compared the simulated mean basal area and tree density of all cells to the observed mean values of all plots for each subecoregion in 2015 by using paired t-test to evaluate the overall accuracy, and the square of the Pearson correlation (R^2) and root mean square deviation (RMSD) for each species. RMSD was based on squared simulation errors and thus was sensitive to outliers.

To calibrate fire parameters, I iteratively adjusted fuel model coefficients for each species fire tolerance class and height of bark charring for each burn severity until the comparison between simulated density and basal area by species and the forest inventory data passed the significance test (no differences based on an ANOVA test ($p > 0.05$)) at 2000. I validated the simulation results for each burn severity class at site scale by extracting simulated results from raster cells corresponding to the forest inventory plot locations, because heterogeneous post-fire tree species recovery patterns overrode environmental heterogeneity delineated by subecoregion. Specifically, I compared basal

area and tree density within extracted raster cells with observed values in inventory plots for each burn severity class at 2015 by using two sample t-test to evaluate the accuracy of simulated post-fire recovery. All statistical analyses were performed using R statistical software (R Core Team, 2015).

2.9. Post-fire tree planting simulation

Large-scale tree plantings in the years immediately after the fire were implemented in each Forest Bureau. Thus, I simulated planting using the LANDIS PRO Harvest module (Fraser et al. 2013). The planting management units in this study were constructed based on the burn severity map of the 1987 Black Dragon fire, Forest Bureau boundaries, and harvest management units to capture the variation in planting practices across the region. I parameterized the percent area and number of trees planted every two years for each management unit based on forest management records from the China National Forest Inventory third tier data (http://www.cfsdc.org) and previous studies (Yang et al. 1998; Chen et al. 2014). Only coniferous species of larch and Scots pine were planted in the high burn severity area (70% larch + 30% pine) with a regular plant spacing (1.5 m×1.5 m or 1.5 m×2 m) according to field conditions (Chen et al. 2014). By the end of the 1990s, less than 10% of the burned forests were managed with planting (Yang et al. 1998).

3. Results

3.1. Results validation

Model simulations showed high agreement in the magnitude and time of observed basal area and density from unburned forests at the landscape scale (paired t-tests, $p > 0.05$). R^2 (> 0.8) is high and RMSD is low for both basal area and density for all species

(Fig. 3-7). The comparisons of different species demonstrated that dominant tree species (larch and white birch) had relatively higher accuracy than other species. The simulation accuracy for tree density was higher than for basal area because the density in the model was largely determined by a single parameter (available seeds), while the basal area was affected by the species age-DBH relationship that introduced additional uncertainties into estimation. Overall, my results indicated that the simulated forest development was consistent with the actual forest dynamics, and simulated density had higher accuracy than simulated basal area.

Comparison between simulated data and observed data showed that post-fire forest composition and structure closely represented the real forest composition and structure at different burn severity classes in 2015 (for all species and severities, two sample t-test, $p > 0.05$) (Fig. 3-8). My results indicated that the simulated post-fire forest development captured current forest composition and structure after the Black Dragon fire and thus the simulated fire-caused tree species mortality could be close to the real tree species mortality of the Black Dragon fire.

The observed and simulated density of conifer and broadleaf species in burned areas showed similar patterns in relation to distance to live-tree edges (trees mortality rate < 90% by the Black Dragon fire) (Fig. 3-9). Post-fire conifer density showed a decline with increasing distance to the live tree edge and was almost absent in the interior of high burn severity patches in 2015 (Fig. 3-9a). Post-fire broadleaf density was high across the whole high severity area and had an opposite trend of density versus distance relationship compared with conifer species (Fig. 3-9b). The self-thinning among competing trees led to a decrease in tree density near seed sources. The evaluation results increased my

confidence in the ability of the calibrated LANDIS PRO model to explore the long-term fire effects and post-fire forest recovery.

3.2. The Black Dragon fire effects and post-fire forest recovery trajectories

Tree mortality and post-fire recovery varied greatly among burn severities and tree species (Figs. 3-10 and 3-11). Mortalities of conifer and broadleaf species were both positively related to burn severity and were very high in areas with moderate and high burn severity (Fig. 3-10a and b). Approximately 50% - 90% of conifer and almost 100% of broadleaf stems died in areas of moderate and high burn severity. Nevertheless, recruitment of broadleaf trees was abundant in moderate and high severity burned areas. The post-fire density of broadleaf species gradually increased over the first 12 years, then sharply peaked between 2005 – 2010 (12,000 and 10,000 trees/ha), and finally decreased to 10,000 and 7,000 trees/ha by 2015 in high and moderate burn severity areas, respectively. The changes in density, basal area, and biomass over time in unburned and low severity areas were not significant (Fig. 3-10b). The post-fire density of conifer species showed a low rate of increase compared to broadleaf species (Fig. 3-10a). The post-fire basal areas of conifer and broadleaf species both showed increasing trends throughout the simulation years under all burn severities (Fig. 3-10c and d). For broadleaf species, the basal area has recovered to, and even exceeded pre-fire levels, although aboveground biomass always remained lower than pre-fire levels (Fig. 3-10c-f). For conifer species, both basal area and biomass remained below pre-fire levels, but the recovery rate in low burn severity was fastest (Fig. 3-10c and 3-10e). With time, the percentage of coniferous species decreased in high and moderate severity burned areas, but no significant changes occurred in low severity and unburned areas (Fig. 3-12a). The

percent of coniferous species in high and moderate severity burned areas was far less than the value in unburned forests at 2015, but the edges of these burned patches showed a composition recovery sign with larger conifer percentages than the interior (Fig. 3-12).

4. Discussion

I presented a spatially explicit framework to reconstruct post-megafire forest recovery through integrating a forest landscape model (FLM) and remote sensing and field inventory data. Reconstruction results showed that burn severity affected the relative dominance of broadleaf vs. conifer species in burned stands with probable effects on subsequent canopy dominance. In high severity burned areas, broadleaf species (e.g., white birch) rapidly emerged despite the large burn size, while regeneration of coniferous species (e.g., larch) was minimal in the interior of the burned patches. This pattern matches expectations because white birch can rapidly regenerate either by resprouting from stumps or roots that survived fires or by long distance seed dispersal (e.g., > 1000 m). However, the regeneration of larch depends on the seeds from surviving trees and a relatively short seed dispersal distance (<400 m) (Xu, 1998). Thirty years after the megafire, the broadleaf species fully recovered, and white birch stands went into the self-thinning stage in the interior of the high severity burned area as the newly established trees matured. However, coniferous species were still in the initial stand development stage. In contrast, more conifers than broadleaf species regrew in the low-severity burned areas, where canopies provided suitable conditions for the relatively more shade-tolerant conifers and where sufficient seeds from surviving trees had a higher chance to reach fire-released areas in the low-severity burned patches. The comparison of pre- and post-fire tree composition in the burned patches indicated that self-replacement succession was likely to occur in areas that

burned with low severity, whereas high severity burned areas are more likely to shift forest successional trajectories away from conifer self-replacement to pathways with greater broadleaf dominance, a finding that is reported in other post-fire studies (Johnstone and Chapin 2006; Johnstone et al. 2010; Cai et al. 2013). My reconstructed trajectories of post-megafire forest recovery were well supported by known data and empirical knowledge of forest stand development after large-scale disturbances (Oliver et al. 1996; Turner et al. 1998; Kurkowski et al. 2008), suggesting that my model framework is effective in spatially reconstructing post-megafire historical forest conditions.

Validating simulation results from FLMs is critical in quantifying the reliability and credibility of landscape reconstructions. My framework of reconstructing the spatiotemporal history of post-megafire forest conditions provided not only the spatial pattern and dynamics at the landscape scale, but also detailed stand attributes such as basal area, tree density, and age classes by species. I validated the simulated stand attributes with the contemporary inventory data. My simulated tree mortality rates were close to the estimates of tree mortality rates from field inventories within different burn severity classes of the Black Dragon fire (Luo 2002). The simulated post-fire density and biomass were comparable to the field observations reported by Wang et al. (2001), Wang et al. (2003), and Hu et al. (2016) for the same fire and other post-fire studies in boreal forests after similar recovery periods (Johnstone et al. 2004; Alexander et al. 2012; Cai et al. 2013). My validation results from current forest inventory data demonstrated the calibrated model performed well and ensured that the model was a reasonable and reliable platform for subsequent applications to quantify the effects of megafires on forest composition and landscape succession.

A notable benefit of my framework is that, once calibrated, the model is highly scalable and can be applied to filling the gaps where inventory data are not available to assess recovery trajectories across the whole landscape. This method offers an approach to augment traditional uses of forest inventory data in post-fire studies. My approach realistically captures the heterogeneity of post-fire recovery process in both time and space (Figs. 3-9, 3-10, 3-11). In contrast, forest inventories, when applied alone, have generally focused on fixed plots or time periods and on describing entire landscapes, which limit their ability to constrain the impacts of heterogeneity on timber volumes and carbon stocks (e.g., Kashian et al. 2005). Furthermore, inventory approaches can suffer from biased sampling design. For example, Wang et al. (2001) and Hu et al. (2016) conducted studies near the live-tree edges due to the logistical limitations, observed a higher biomass recovery than I did in this study, and thus overestimated the post-fire recovery status. They assumed that the mature forests were representative of the forests in this region prior to the 1987 fire. However, through historical forest conditions reconstruction, I found that pre-fire forests in this area were younger than Wang et al. (2001) and Hu et al. (2016) assumed, because forests in this region were affected by historical harvesting and fires, which resulted in relatively young stands with most trees between 40-60 years old. These studies may have overestimated pre-fire forest biomass and consequently biomass loss due to the Black Dragon fire, while my simulated biomass loss was closer to the estimated values from the traditional bottom-up method (Xu et al. 2020). This highlights the importance of my approach that reconstruction of the entire historical landscape reduced the biases from field sampling.

This framework can be applied to assess the legacy effects of a megafire over long time periods (i.e., decades to centuries). While previous empirical and field-based studies documented legacy effects (e.g., Downing et al. 2019), such effects can persist for decades to centuries (Seidl et al. 2012) and thus require long-term assessment. My framework can be further applied to projecting how forest landscapes respond to future megafires, which are expected to increase under warming climate and increased fuel accumulation from fire exclusion policies (Chang et al. 2007; Flannigan et al. 2009; Liu et al. 2012).

My framework can also be used to examine alternative management and disturbance scenarios. Managers could use the framework to evaluate forest resistance, rate of recovery, and the time to return to pre-disturbance states after megafires under various management and climate scenarios as well as to study the effect of alternative managements on mitigating future megafire risk. For example, reforestation is increasingly used to assist forest restoration and improve resilience, especially under warming climate as conifer forests will be increasingly regeneration limited with intensifying fire regimes (Hof et al. 2017; North et al. 2019). Different reforestation strategies (e.g., planting intensity and spatial assignment) can be evaluated with FLMs (Wang et al. 2006a; Wang et al. 2006b). Researchers can also use this framework to evaluate the response of forest landscapes to other forest disturbances such as drought, insect, and harvest under different environmental settings.

Figures

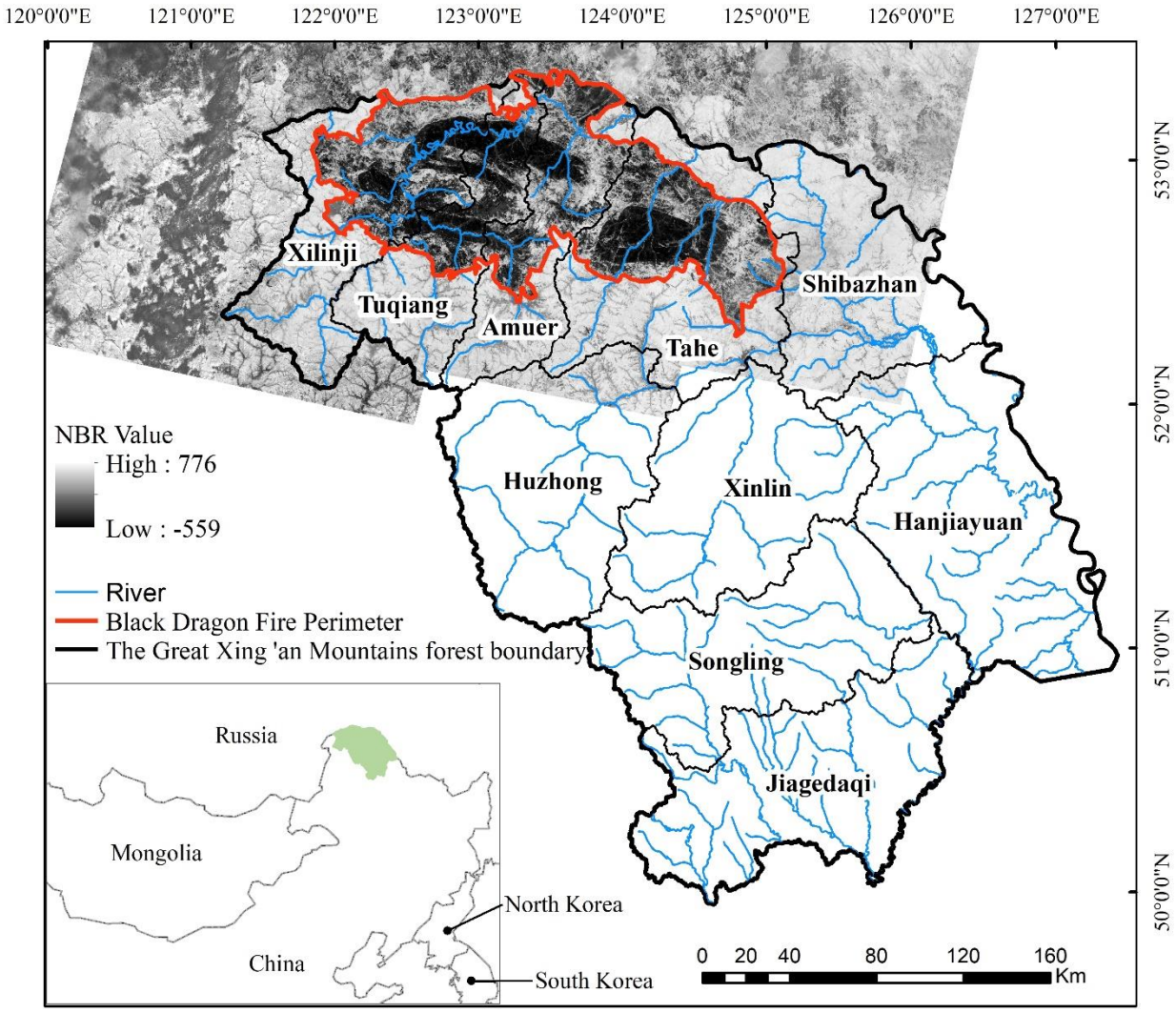

Fig. 3-1. The location of study area and the Black Dragon fire with Landsat 5 derived normalized burn ratio (NBR) values. The boundaries of the 10 forest bureaus are shown with thin black lines.

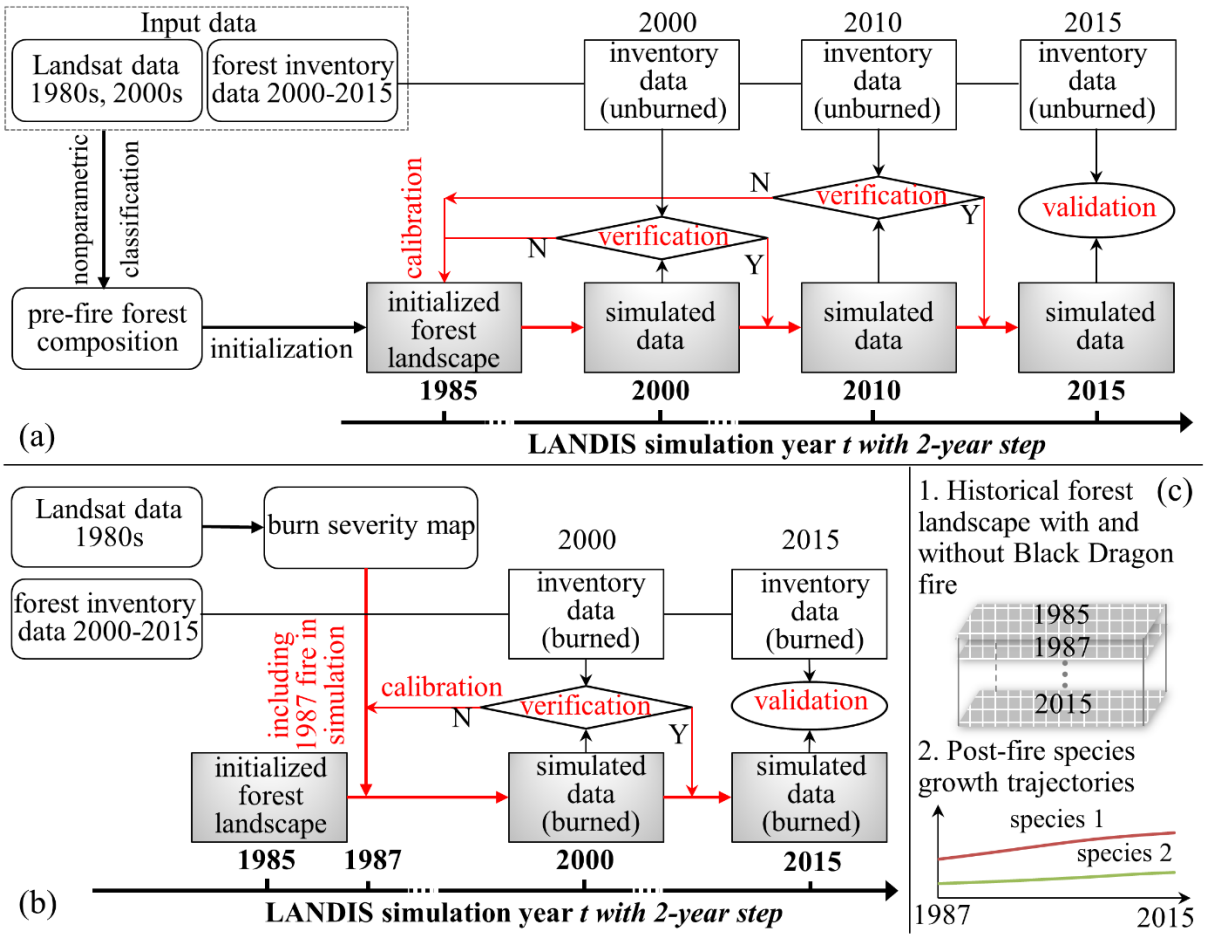

Fig. 3-2. The framework of reconstructing historical forest conditions and post-megafire recovery trajectories of density and basal area at species level. (a) Calibrating tree species parameters to constrain tree species growth strategies. (b) Calibrating fire parameters to constrain fire-caused mortality. (c) The outcome of the calibration and validation processes is the time-series post-fire forest conditions at species level.

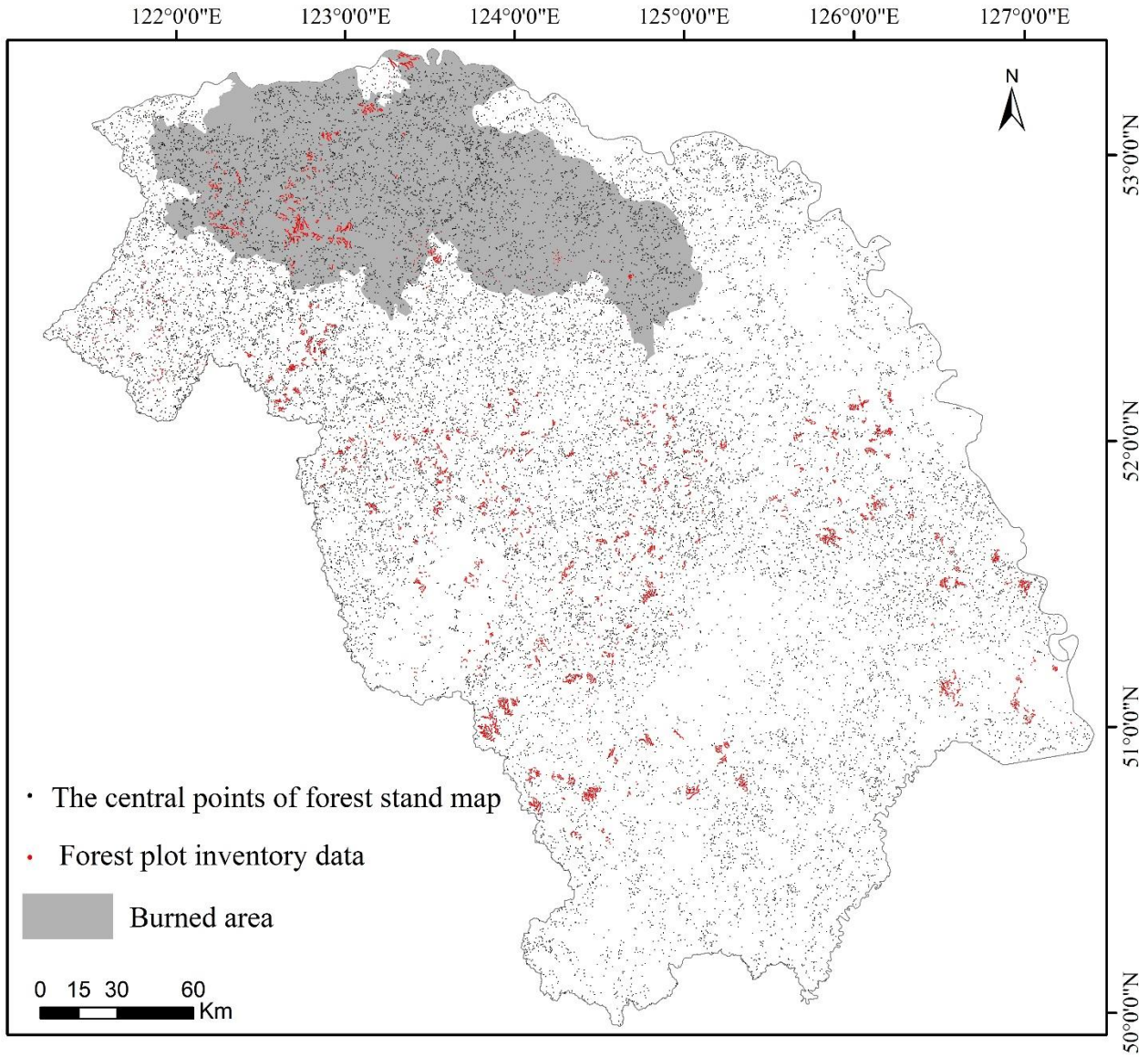

Fig. 3-3. The distribution map of forest inventory plots.

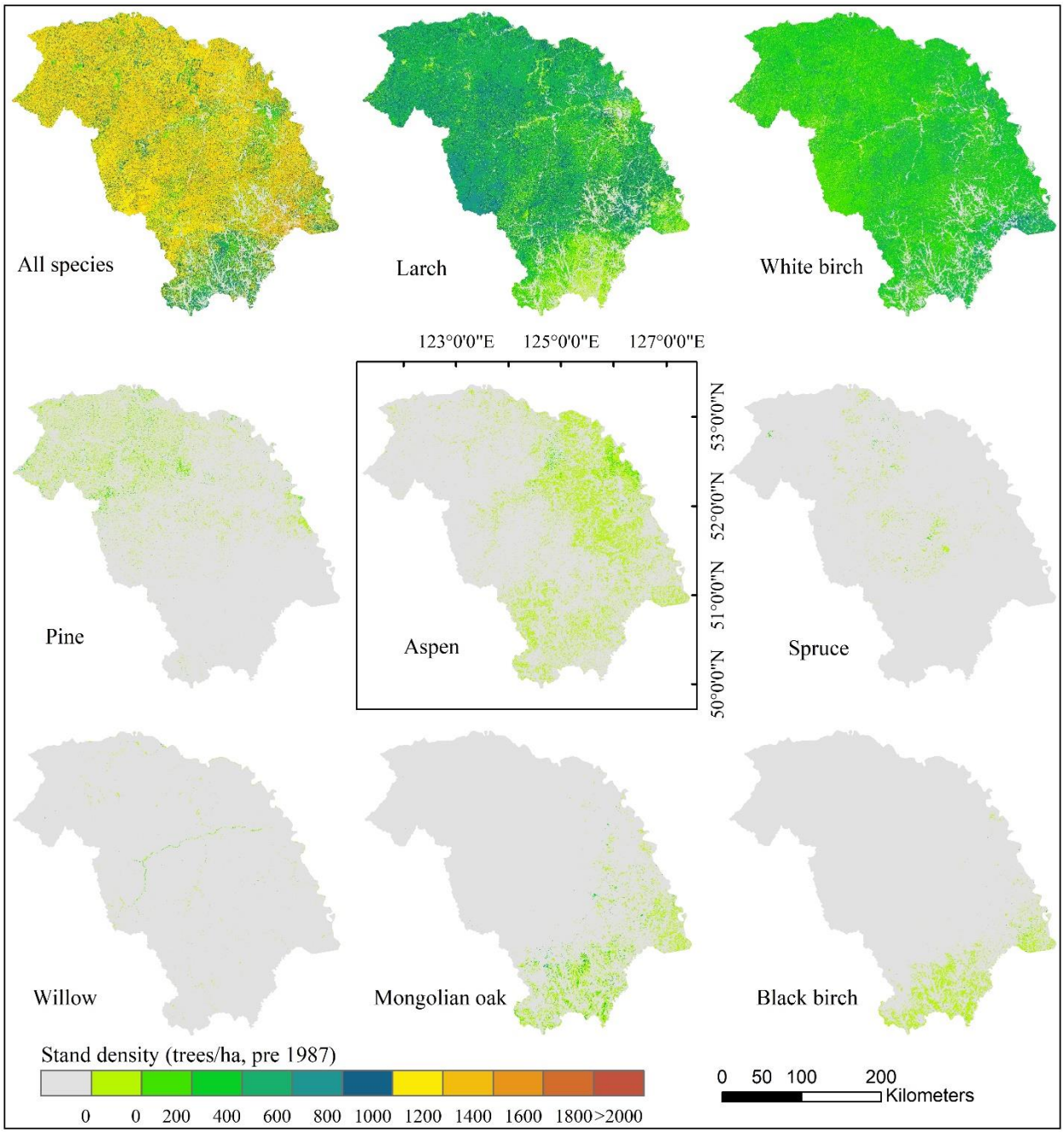

Fig. 3-4. Maps of total tree density and species-level density before the Black Dragon fire.

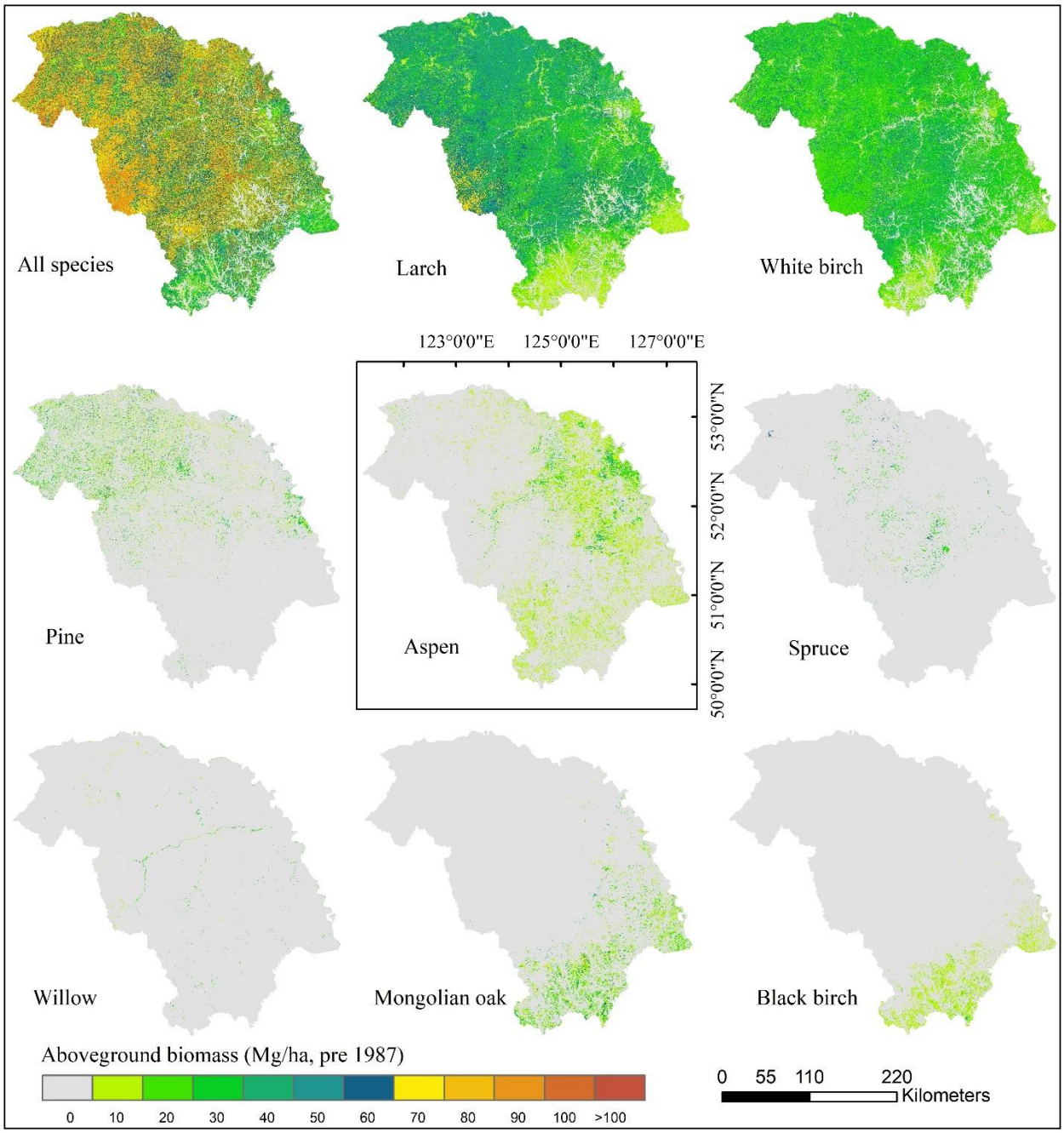

Fig. 3-5. Maps of total aboveground biomass and species-level biomass before the Black Dragon fire.

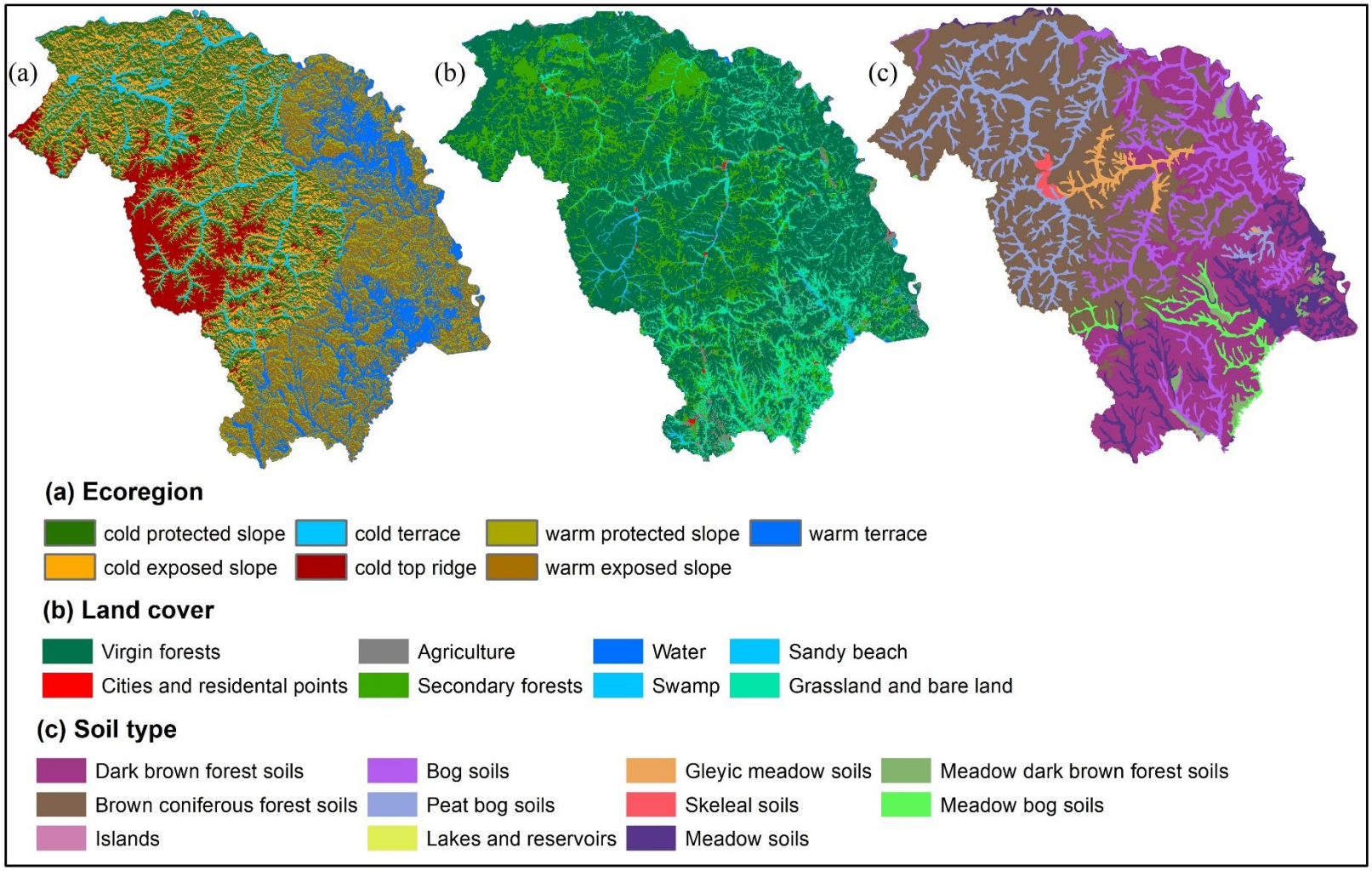

Fig. 3-6. Study area with a) 7 ecoregions divided by Xu et al. (1998), b) 8 land cover types, and c) 11 soil types.

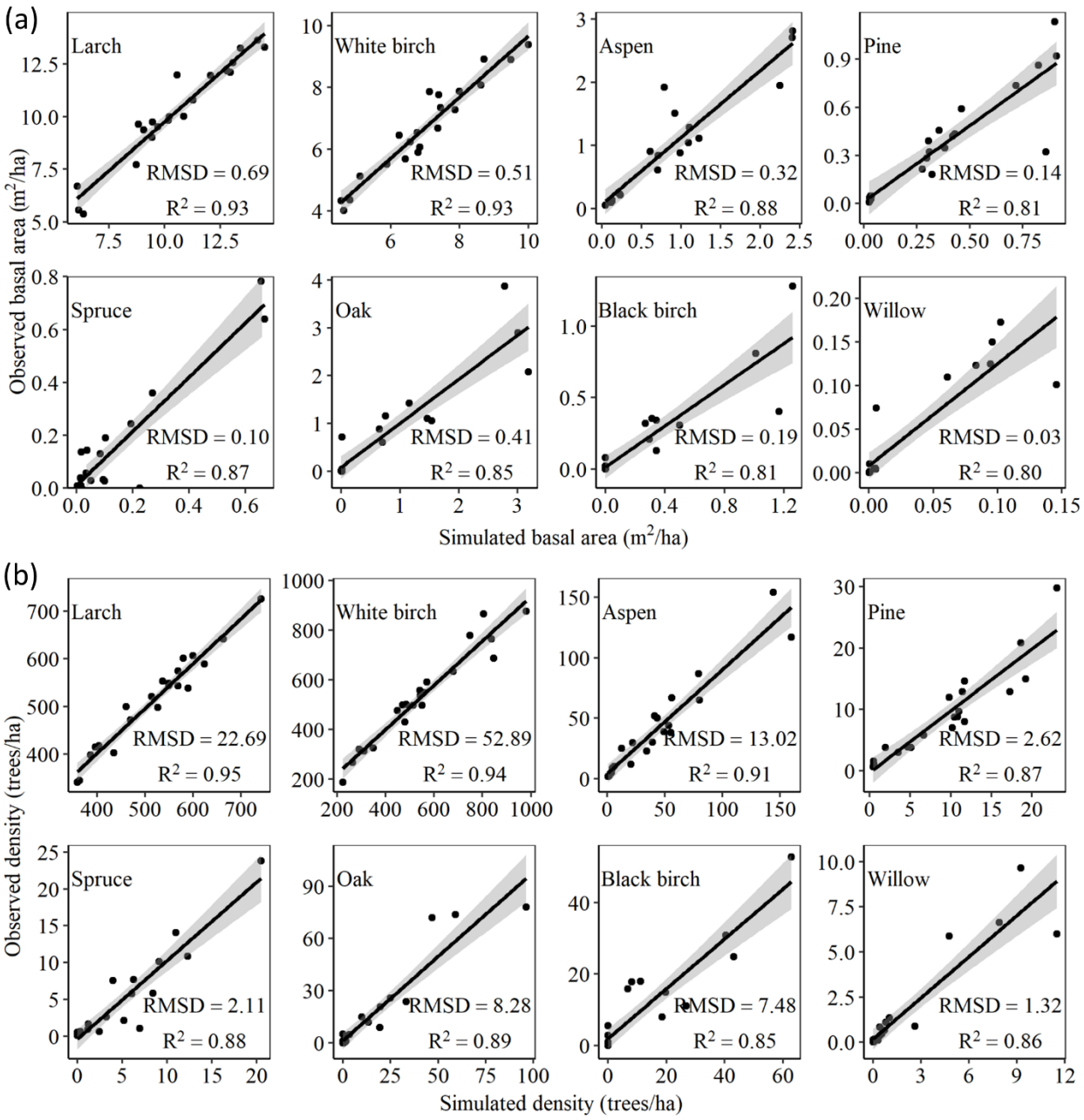

Fig. 3-7. Scatterplots of simulated versus forest inventory density (a) and basal area (b) of eight species at the landscape scale in 2015 (n=21). The black line is the regression line and the grey shaded area represents 95% confidence intervals. RMSD: root mean squared deviation.

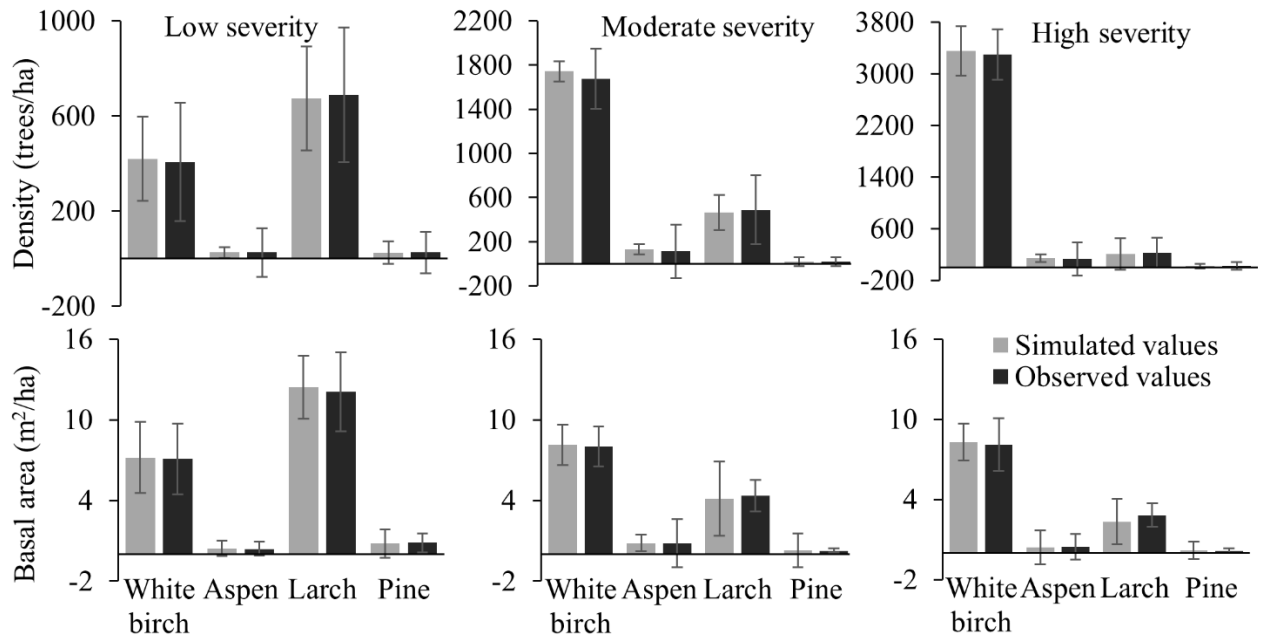

Fig. 3-8. Comparison of simulated tree species density (a) and basal area (b) with inventory data by burn severities of the Black Dragon fire at 2015. Error bars are marked as ± 1 standard deviation (n= 584, 366, and 355 for low, moderate, and high severity area, respectively).

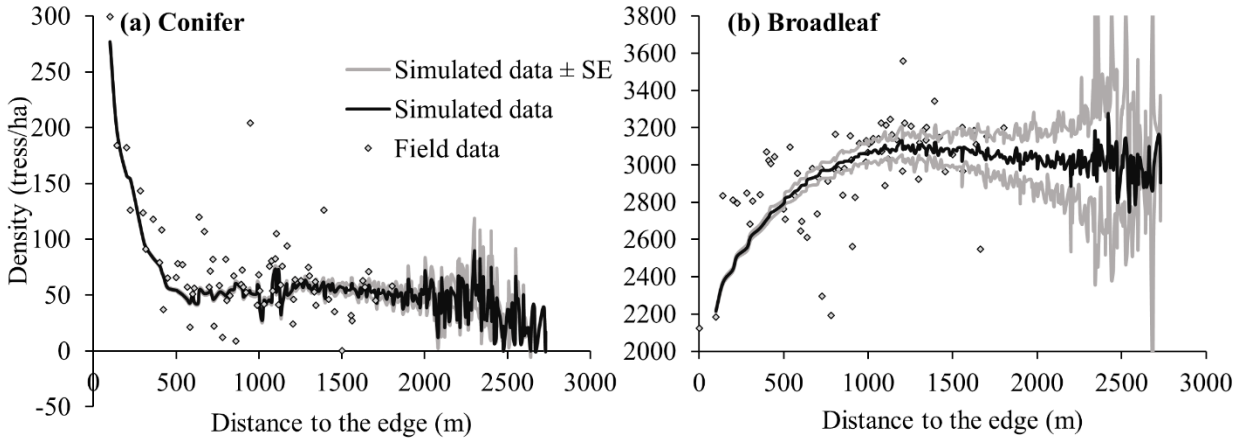

Fig. 3-9. Post-fire 28-year coniferous (a) and broadleaf (b) density in high burned area as a function of Euclidean distance to 1987 live-tree edge (trees mortality rate < 90%) after the Black Dragon fire. The black lines are simulated means and grey lines are ± 1 standard error (SE). The points are observed values from field inventory data.

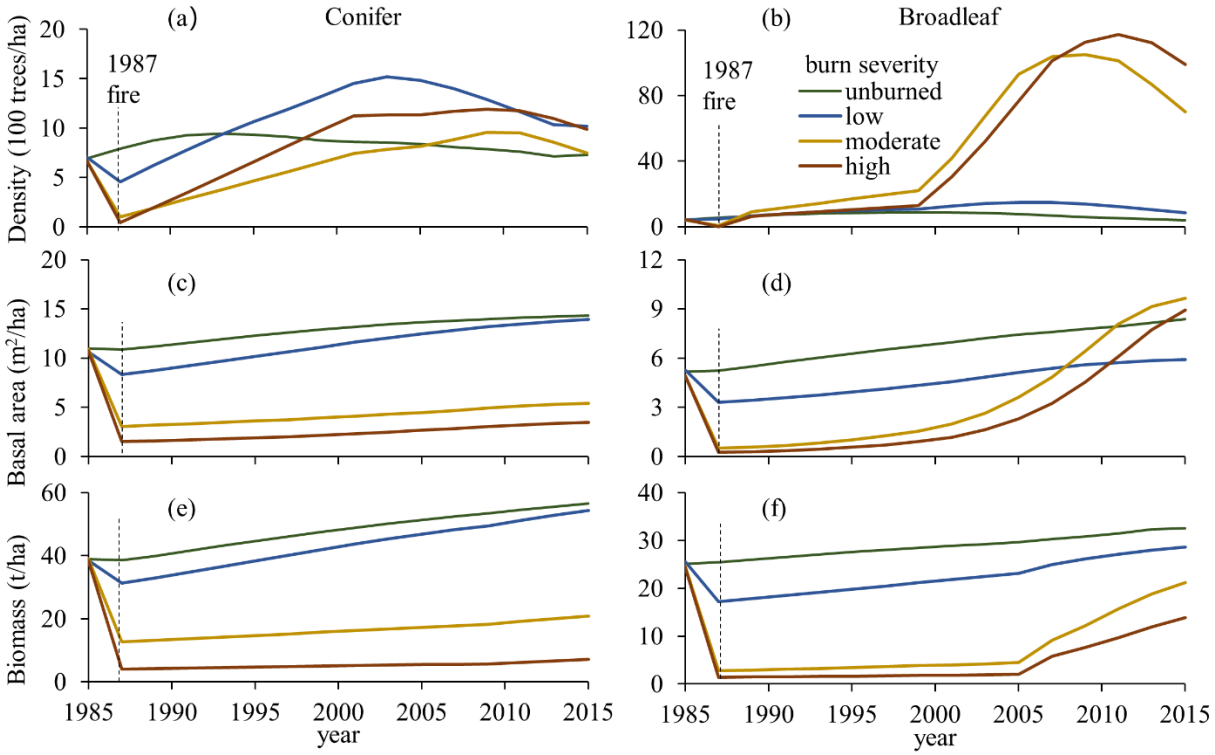

Fig. 3-10. Tree species recovery trajectories over time for each burn severity following the 1987 Black Dragon fire: the trajectories of conifer species recovery in density (a), basal area (c), and biomass (e), and broadleaf species recovery in density (b), basal area (d), and biomass (f) from 1985 to 2015.

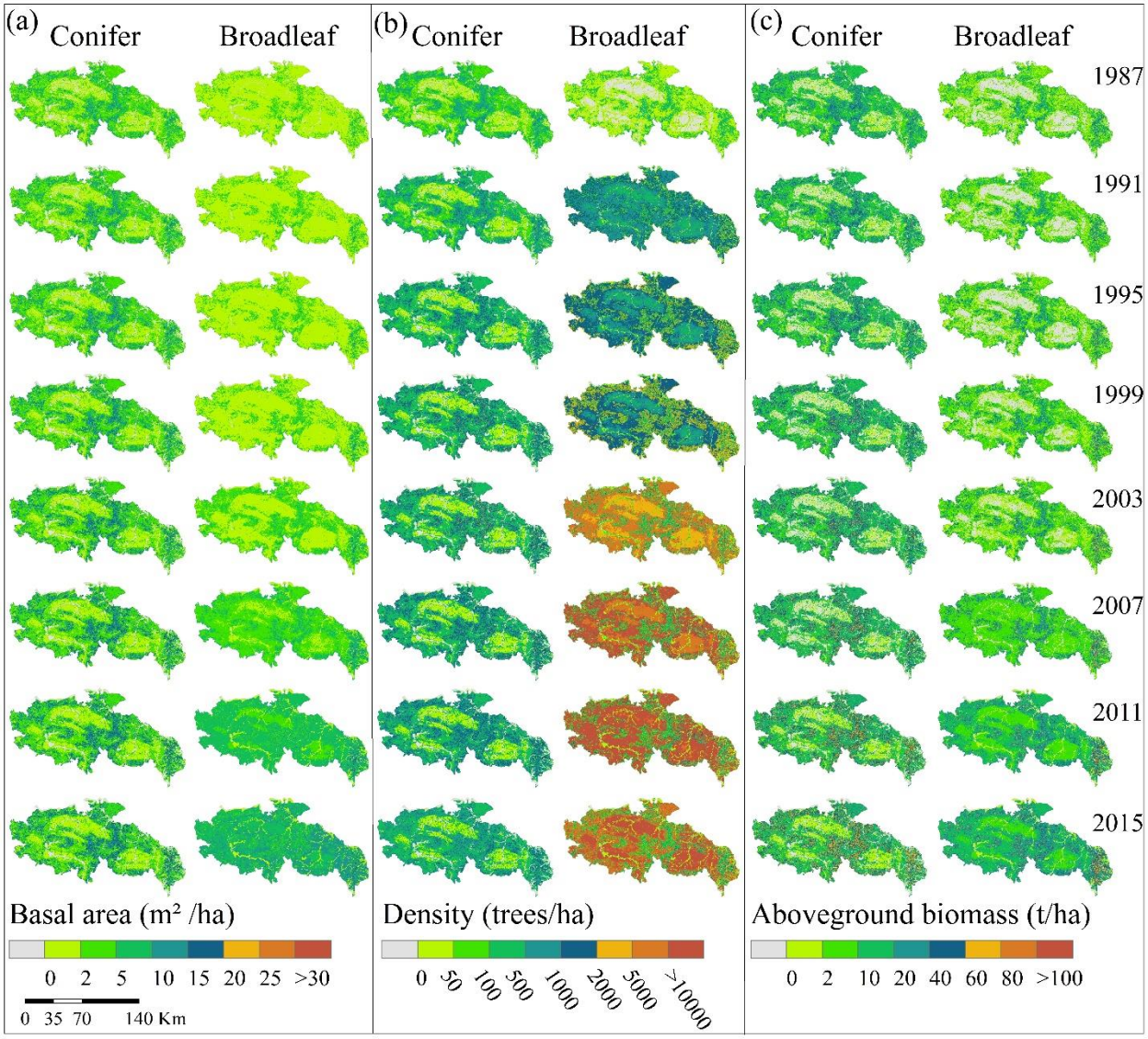

Fig. 3-11. Spatial pattern of post-fire coniferous and broadleaf recovery in basal area (a), density (b), and aboveground biomass (c) from 1987 to 2015 in the burned area of the Black Dragon fire.

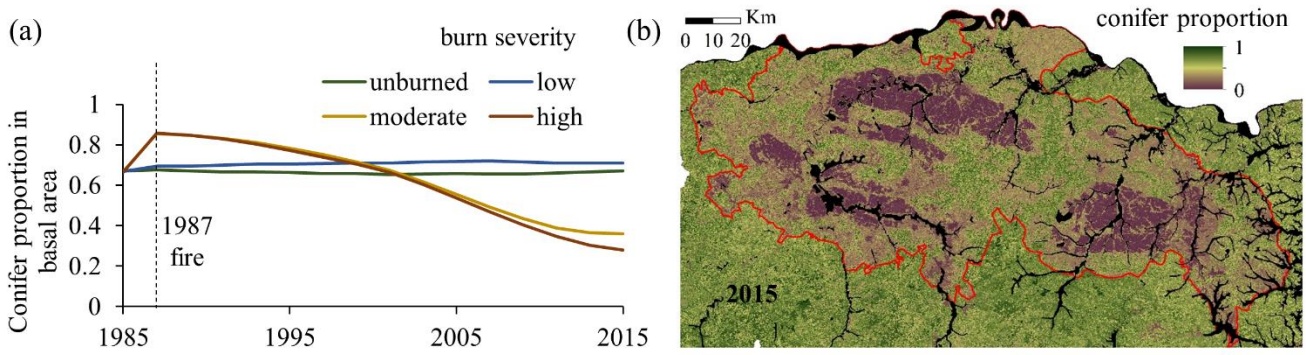

Fig. 3-12. Tracking changes in species composition. (a) Trajectories of conifer proportion in basal area for each burn severity from 1985 to 2015. (b) Map of conifer proportion in basal area in 2015. Red line denotes perimeter of Black Dragon fire.

Tables

Table 3-1. The acquired date, orbit number, and burning cover of Landsat.

Orbit number	Acquired data		The 1987 fire
	1980s	2000s	
119024	1985.06.04	2000.06.13	Unburned area
119025	1985.06.04	2000.06.13	Unburned area
120023	1988.09.23	2002.09.14	Unburned area
120024	1988.09.23	2002.09.14	Unburned area
120025	1987.09.05	2002.09.14	Unburned area
121023	1986.06.26	2000.05.26	Burned area
121024	1988.09.14	2000.09.15	Unburned area
122023	1986.06.12	2000.06.18	Burned area
122024	1987.06.15	2000.06.18	Unburned area
123023	1986.08.06	2000.08.12	Burned area

Table 3-2. Individual tree species biological traits used in LANDIS PRO in the boreal forests of China.

Major species	Longevity (years)	Maturity age (years)	Shade tolerance [a]	Fire tolerance [b]	Maximum seeding distance/m	Maximum DBH/cm	Maximum stand density (trees/ha)	Potential germination seeds [c]
Larch *(Larix gmelinii)*	300	20	2	4	150	55	600	10
Scots pine *(Pinus sylvestris)*	250	25	2	3	200	60	560	20
White birch *(Betula platyphylla)*	150	15	1	3	2000	30	690	30
Aspen (Populus davidiana)	120	10	1	4	2000	50	680	30
Spruce (Picea koraiensis)	300	30	4	3	150	60	520	10
Willow (*Chosenia arbutifolia*)	250	12	2	5	2000	50	780	20
Black birch (*Betula davurica)*	150	15	2	3	800	50	750	25
Mongolian oak *(Quercus mongolica)*	300	20	3	5	200	95	600	20

Species data were obtained from the Scientific Database of China Plant Species (http://db.kib.ac.cn) and previous studies (Li et al. 2013; Luo et al. 2015). [a, b] Shade/fire tolerance classes 1–5: 1 = least tolerant, 5 = most tolerant;

[c] Mean number of potential germinating seeds produced/mature tree/year.

Table 3-3. Individual tree species biological traits used in the ecosystem model LINKAGES 3.0 in the boreal forests of China.

Species name	DMAX	DMIN	B3	B2	SWITCH	D3	FROST	TL	FWT	SLTA	SLTB	RTST	FRT
Larch	1900	400	0.35	63.62	FFFFT	0.374	-45	12	440	0.804	0.069	1	1
Scots pine	1900	100	0.37	59.08	TTTFF	0.6	-58	12	440	0.804	0.069	1	2
Korean spruce	2500	600	0.35	63.62	FTFFF	0.18	-38	11	440	0.804	0.069	1	3
White birch	3167	600	0.94	94.52	FFFFT	0.412	-40	4	248	0.804	0.069	0.8	1
Aspen	3009	800	0.66	78.77	TTFFT	0.333	-32	7	248	0.804	0.069	0.5	1
Black birch	3169	1060	0.52	63.62	TTTFF	0.314	-30	4	248	0.804	0.069	0.8	1
Willow	1600	40	0.35	63.62	TTFFT	0.03	-35	7	248	0.804	0.069	0.5	1
Mongolian oak	3004	1010	0.37	59.08	TTTFF	0.514	-30	9	440	0.904	0.095	1	1

DMAX, degree day maximum for each species (degree).
DMIN, degree day minimum for each species (degree).
B2 and B3 are growth scaling parameters for each species.
SWITCH, reproduction switches.
D3, drought tolerance (maximum proportion of growing season that species can withstand drought).
FROST, Frost tolerance: minimum January temperature species can withstand (degree).
TL, leaf litter quality class (1-12; note: we assigned all root litter to class 13, fresh wood from trees < 10 cm to class 14, fresh wood from trees > 10 to class 15, twig litter to class 16, and well-decayed wood not contained in humus to class 17).
FWT, leaf weight per unit crown area ($100 g/m^2$).
SLTA and SLTB can be used to calculate crown area from diameter. SLTA and SLTB convert DBH to crown area ($100\ m^2$).
RTST, root-shoot ratio for each species.
FRT, foliage retention time (year).

Literature cited

Alexander HD, Mack MC, Goetz S, Loranty MM, Beck PSA, Earl K, Zimov S, Davydov S, Thompson CC (2012) Carbon accumulation patterns during post-fire succession in cajander larch (Larix cajanderi) forests of Siberia. *Ecosystems* **15**, 1065-1082.

Bonnet VH, Schoettle AW, Shepperd WD (2005) Postfire environmental conditions influence the spatial pattern of regeneration for Pinus ponderosa. *Canadian Journal of Forest Research* **35**, 37-47.

Bowman DMJS, et al. (2009) Fire in the earth system. *Science* **324**, 481-484.

Boychuk D, Perera AH, Ter-Mikaelian MT, Martell DL and Li C (1997) Modelling the effect of spatial scale and correlated fire disturbances on forest age distribution. *Ecological Modelling* **95**,145-164.

Bradstock RA (2008) Effects of large fires on biodiversity in southeastern Australia: disaster or template for diversity? *International Journal of Wildland Fire* **17**, 809–22

Broncano MJ, Retana J (2004) Topography and forest composition affecting the variability in fire severity and post-fire regeneration occurring after a large fire in the Mediterranean basin. *International Journal of Wildland Fire* **13**, 209-216.

Cai WH, Yang J, Liu Z, Hu Y, Weisberg PJ (2013) Post-fire tree recruitment of a boreal larch forest in Northeast China. *Forest Ecology and Management* **307**, 20-29.

Cai WH, Liu ZH, Yang YZ, Yang J (2018) Does environment filtering or seed limitation determine post-fire forest recovery patterns in boreal larch forests? *Frontiers in Plant Science* **9**, 1318.

Chang Y, He HS, Bishop I, Hu Y, Bu R, Xu C, Li X (2007) Long-term forest landscape responses to fire exclusion in the Great Xing'an Mountains, China. *International Journal of Wildland Fire* **16**, 34-44.

Chang Y, He HS, Hu Y, Bu R, Li X (2008) Historic and current fire regimes in the Great Xing'an Mountains, northeastern China: Implications for long-term forest management. *Forest Ecology and Management* **254**, 445-453.

Chen W, Moriya K, Sakai T, Koyama L, Cao CX (2014) Post-fire forest regeneration under different restoration treatments in the Greater Hinggan Mountain area of China. *Ecological Engineering* **70**, 304-311.

Chu TA, Guo XL (2014) Remote sensing techniques in monitoring post-fire effects and patterns of forest recovery in boreal forest regions: A review. *Remote Sensing* **6**, 470-520.

Collins BM, Roller GB (2013) Early forest dynamics in stand-replacing fire patches in the northern Sierra Nevada, California, USA. *Landscape Ecology* **28**, 1801-1813.

Crotteau JS, Varner JM, Ritchie MW (2013) Post-fire regeneration across a fire severity gradient in the southern Cascades. *Forest Ecology and Management* **287**, 103-112.

Cuevas-Gonzalez M, Gerard F, Balzter H, Riano D (2009) Analysing forest recovery after wildfire disturbance in boreal Siberia using remotely sensed vegetation indices. *Global Change Biology* **15**, 561-577.

Davis KT, Higuera PE, Sala A (2018) Anticipating fire-mediated impacts of climate change using a demographic framework. *Functional Ecology* **32**, 1729-1745.

Dijak WD, Hanberry BB, Fraser JS, He HS, Wang WJ, Thompson FR (2017) Revision and application of the LINKAGES model to simulate forest growth in central hardwood landscapes in response to climate change. *Landscape Ecology* **32**, 1365-1384.

Downing WM, Krawchuk MA, Meigs GW, Haire SL, Coop JD, Walker RB, Whitman E, Chong G, Miller C (2019) Influence of fire refugia spatial pattern on post-fire forest recovery in Oregon's Blue Mountains. *Landscape Ecology* **34**, 771-792.

Eidenshink J, Schwind B, Brewer K, Zhu Z-L, Quayle B, Howard S (2007) A project for monitoring trends in burn severity. *Fire ecology* **3**, 3-21.

Epting J, Verbyla D, Sorbel B (2005) Evaluation of remotely sensed indices for assessing burn severity in interior Alaska using Landsat TM and ETM+. *Remote Sensing of Environment* **96**, 328-339.

Fang JY, Chen AP, Peng CH, Zhao SQ, Ci L (2001) Changes in forest biomass carbon storage in China between 1949 and 1998. *Science* **292**, 2320-2322.

Flannigan MD, Krawchuk MA, de Groot WJ, Wotton BM, Gowman LM (2009) Implications of changing climate for global wildland fire. *International Journal of Wildland Fire* **18**, 483-507.

Fraser JS, He HS, Shifley SR, Wang WJ, Thompson III FR (2013) Simulating stand-level harvest prescriptions across landscapes: LANDIS PRO harvest module design. *Canadian Journal of Forest Research* **43**, 972-978.

Fraser JS, Wang WJ, He HS, Thompson FR (2019) Modeling post-fire tree mortality using a logistic regression method within a forest landscape model. *Forests* **10**.

French NHF, Kasischke ES, Hall RJ, Murphy KA, Verbyla DL, Hoy EE, Allen JL (2008) Using Landsat data to assess fire and burn severity in the North American boreal forest region: an overview and summary of results. *International Journal of Wildland Fire* **17**, 443-462.

García ML, Caselles V (1991) Mapping burns and natural reforestation using Thematic Mapper data. *Geocarto International* **6**, 31-37.

Gitas I, Mitri G, Veraverbeke S, Polychronaki A (2012) Advances in remote sensing of post-fire vegetation recovery monitoring—a review. *Remote Sensing of Biomass-Principles and Applications* **1**, 334.

Glenn EP, Huete AR, Nagler PL, Nelson SG (2008) Relationship between remotely-sensed vegetation indices, canopy attributes and plant physiological processes: What vegetation indices can and cannot tell us about the landscape. *Sensors* **8**, 2136-2160.

Greene DF, et al. (2007) The reduction of organic-layer depth by wildfire in the North American boreal forest and its effect on tree recruitment by seed. *Canadian Journal of Forest Research* **37**, 1012-1023.

Halofsky JE, et al. (2011) Mixed-severity fire regimes: lessons and hypotheses from the Klamath-Siskiyou Ecoregion. *Ecosphere* **2**.

Harvey BJ, Donato DC, Turner MG (2016) High and dry: post-fire tree seedling establishment in subalpine forests decreases with post-fire drought and large stand-replacing burn patches. *Global Ecology and Biogeography* **25**, 655-669.

He HS (2008) Forest landscape models: definitions, characterization, and classification. *Forest Ecology and Management* **254**, 484-498.

He HS, Hao ZQ, Mladenoff DJ, Shao GF, Hu YM, Chang Y (2005) Simulating forest ecosystem response to climate warming incorporating spatial effects in north-eastern China. *J Biogeogr* 32:2043-2056.

He HS, Mladenoff DJ, Crow TR (1999) Linking an ecosystem model and a landscape model to study forest species response to climate warming. *Ecological Modelling* 114, 213-233.

He HS, Shang BZ, Crow TR, Gustafson EJ, Shifley SR (2004) Simulating forest fuel and fire risk dynamics across landscapes - LANDIS fuel module design. *Ecological modelling* **180**, 135-151.

Hof AR, Dymond CC, Mladenoff DJ (2017). Climate change mitigation through adaptation: the effectiveness of forest diversification by novel tree planting regimes. *Ecosphere* **8**, e01981.

Hu H, Luo B, Wei S (2015) Estimating biological carbon storage of five typical forest types in the Daxing'anling Mountain, Heilongjia, China. *Acta Ecol Sin* **35**, 1-21.

Hu X, Zhu J, Wang C, Zheng T, Wu Q, Yao H and Fang J (2016) Impacts of fire severity and post-fire reforestation on carbon pools in boreal larch forests in Northeast China. *Journal of Plant Ecology* **9**, 1-9.

Huang C, He HS, Liang Y, Wu ZW, Hawbaker TJ, Gong P, Zhu ZL (2018) Long-term effects of fire and harvest on carbon stocks of boreal forests in northeastern China. *Annals of Forest Science* **75**.

Idris MH, Kuraji K, Suzuki M (2005) Evaluating vegetation recovery following large-scale forest fires in Borneo and northeastern China using multi-temporal NOAA/AVHRR images. *Journal of Forest Research* **10**, 101-111.

Johnstone JF, et al. (2016) Changing disturbance regimes, ecological memory, and forest resilience. *Frontiers in Ecology and the Environment* **14**, 369-378.

Johnstone JF, Chapin FS (2006) Effects of soil burn severity on post-fire tree recruitment in boreal forest. *Ecosystems* **9**, 14-31.

Johnstone JF, Chapin FS, Foote J, Kemmett S, Price K, Viereck L (2004) Decadal observations of tree regeneration following fire in boreal forests. *Canadian Journal of Forest Research* **34**, 267-273.

Johnstone JF, Hollingsworth TN, Chapin FS, Mack MC (2010) Changes in fire regime break the legacy lock on successional trajectories in Alaskan boreal forest. *Global Change Biology* **16**, 1281-1295.

Ju JC, Roy DP (2008) The availability of cloud-free Landsat ETM plus data over the conterminous United States and globally. *Remote Sensing of Environment* **112**, 1196-1211.

Kajimoto T, Matsuura Y, Osawa A, Prokushkin AS, Sofronov MA, Abaimov AP (2003) Root system development of Larix gmelinii trees affected by micro-scale conditions of permafrost soils in central Siberia. *Plant and Soil* **255**, 281-292.

Kashian DM, Turner MG, Romme WH, Lorimer CG (2005) Variability and convergence in stand structural development on a fire-dominated subalpine landscape. *Ecology* **86**, 643-654.

Keane RE, Agee JK, Fule P, Keeley JE, Key C, Kitchen SG, Miller R, Schulte LA (2008) Ecological effects of large fires on US landscapes: benefit or catastrophe? *International Journal of Wildland Fire* **17**, 696-712.

Kemp KB, Higuera PE, Morgan P, Abatzoglou JT (2019) Climate will increasingly determine post-fire tree regeneration success in low-elevation forests, Northern Rockies, USA. *Ecosphere* **10**, e02568**.**

Key C, Benson N (2005) Landscape assessment: ground measure of severity; the composite burn index, and remote sensing of severity, the normalized burn index and remote sensing of severity, the normalized burn ratio. *FIREMON: Fire Effects Monitoring and Inventory System*. USDA Forest Service, Rocky Mountain Research Station, Ogden, UT, 1-51.

Kurkowski TA, Mann DH, Rupp TS, Verbyla DL (2008) Relative importance of different secondary successional pathways in an Alaskan boreal forest. *Canadian Journal of Forest Research-Revue Canadienne De Recherche Forestiere* **38**, 1911-1923.

Lecomte N, Simard M, Fenton N, Bergeron Y (2006) Fire severity and long-term ecosystem biomass dynamics in coniferous boreal forests of eastern Canada. *Ecosystems* **9**, 1215-1230.

Lever J, Krzywinski M, Altman N (2016). Points of significance: model selection and overfitting. *Nature Methods* **13**, 703.

Li X, He HS, Wu Z, Liang Y, Schneiderman JE (2013) Comparing effects of climate warming, fire, and timber harvesting on a boreal forest landscape in northeastern China. *PLoS One* **8**, e59747.

Liu ZH, Yang J, Chang Y, Weisberg PJ, He HS (2012) Spatial patterns and drivers of fire occurrence and its future trend under climate change in a boreal forest of Northeast China. *Global Change Biology* **18**, 2041-2056.

Luo J (2002) Influence of forest fire disaster on forest ecosystem in Great Xing'anling (in Chinese). *Journal of Beijing Forestry University* **24**, 101-107.

Luo X, He HS, Liang Y, Wu Z (2015) Evaluating simulated effects of succession, fire, and harvest for LANDIS PRO forest landscape model. *Ecological modelling* **297**, 1-10.

Luo YQ, Ogle K, Tucker C, Fei SF, Gao C, LaDeau S, Clark JS, Schimel DS (2011) Ecological forecasting and data assimilation in a data-rich era. *Ecological Applications* **21**, 1429-1442.

Masek JG, Vermote EF, Saleous NE, Wolfe R, Hall FG, Huemmrich KF, Gao F, Kutler J, Lim TK (2006) A Landsat surface reflectance dataset for North America, 1990-2000. *Ieee Geoscience and Remote Sensing Letters* **3**, 68-72.

Miller JD, Thode AE (2007) Quantifying burn severity in a heterogeneous landscape with a relative version of the delta Normalized Burn Ratio (dNBR). *Remote Sensing of Environment* **109**, 66-80.

Miller C, Ager AA (2013) A review of recent advances in risk analysis for wildfire management. *International Journal of Wildland Fire* **22**, 1-14.

Millington JD, Wainwright J, Perry GL, Romero-Calcerrada R, Malamud BD (2009) Modelling Mediterranean landscape succession-disturbance dynamics: a landscape fire-succession model. *Environmental Modelling & Software*, **24**, 1196-1208.

North MP, Stevens JT, Greene DF, Coppoletta M, Knapp EE, Latimer AM, Restaino CM, Tompkins RE, Welch KR, York RA, Young DJ (2019) Tamm Review:

Reforestation for resilience in dry western US forests. *Forest Ecology and Management* **432**, 209-224.

Oliver CD, Larson BC, Oliver C (1996) Forest stand dynamics. Wiley New York.

Petrie MD, Wildeman AM, Bradford JB, Hubbard RM, Lauenroth WK (2016) A review of precipitation and temperature control on seedling emergence and establishment for ponderosa and lodgepole pine forest regeneration. *Forest Ecology and Management* **361**, 328-338.

R Core Team. (2015). R: A Language and Environment for Statistical Computing (Version 3.2.2). Vienna, Austria: R Foundation for Statistical Computing. Retrieved from http://www.R-project.org/.

Savage M, Mast JN, Feddema JJ (2013) Double whammy: high-severity fire and drought in ponderosa pine forests of the Southwest. *Canadian Journal of Forest Research-Revue Canadienne De Recherche Forestiere* **43**, 570-583.

Seidl R, Rammer W, Scheller RM, Spies TA (2012) An individual-based process model to simulate landscape-scale forest ecosystem dynamics. *Ecological Modelling* **231**, 87-100.

Seidl R, Rammer W, Spies TA (2014) Disturbance legacies increase the resilience of forest ecosystem structure, composition, and functioning. *Ecological Applications* **24**, 2063-2077.

Stephens SL, Burrows N, Buyantuyev A, Gray RW, Keane RE, Kubian R, Liu S, Seijo F, Shu L, Tolhurst KG (2014) Temperate and boreal forest mega-fires: characteristics and challenges. *Frontiers in Ecology and the Environment* **12**, 115-122.

Temperli C, Zell J, Bugmann H, Elkin C (2013) Sensitivity of ecosystem goods and services projections of a forest landscape model to initialization data. *Landscape Ecology* **28**, 1337-1352.

Thrippleton T, Dolos K, Perry GLW, Groeneveld J, Reineking B (2014) Simulating long-term vegetation dynamics using a forest landscape model: the post-Taupo succession on Mt Hauhungatahi, North Island, New Zealand. *New Zealand Journal of Ecology* **38**, 26-U43.

Turner MG, Baker WL, Peterson CJ, Peet RK (1998) Factors influencing succession: Lessons from large, infrequent natural disturbances. *Ecosystems* **1**, 511-523.

Turner MG, Whitby TG, Tinker DB, Romme WH (2016) Twenty-four years after the Yellowstone Fires: Are postfire lodgepole pine stands converging in structure and function? *Ecology* **97**, 1260-1273.

van Leeuwen WJD, Casady GM, Neary DG, Bautista S, Alloza JA, Carmel Y, Wittenberg L, Malkinson D, Orr BJ (2010) Monitoring post-wildfire vegetation response with remotely sensed time-series data in Spain, USA and Israel. *International Journal of Wildland Fire* **19**, 75-93.

Veraverbeke S, Gitas I, Katagis T, Polychronaki A, Somers B, Goossens R (2012) Assessing post-fire vegetation recovery using red-near infrared vegetation indices: Accounting for background and vegetation variability. *Isprs Journal of Photogrammetry and Remote Sensing* **68**, 28-39.

Wang C, Gower ST, Wang Y, Zhao H, Yan P, Bond-Lamberty BP (2001) The influence of fire on carbon distribution and net primary production of boreal Larix gmelinii forests in north-eastern China. *Global Change Biology* **7**, 719-730.

Wang WJ, He HS, Fraser JS, Thompson FR, Shifley SR, Spetich MA (2014a) LANDIS PRO: a landscape model that predicts forest composition and structure changes at regional scales. *Ecography* **37**, 225-229.

Wang WJ, He HS, Spetich MA, Shifley SR, Thompson FR, Dijak WD, Wang Q (2014b) A framework for evaluating forest landscape model predictions using empirical data and knowledge. *Environmental Modelling & Software* **62**, 230-239.

Wang WJ, He HS, Spetich MA, Shifley SR, Thompson FR, Larsen DR, Fraser JS, Yang J (2013) A large-scale forest landscape model incorporating multi-scale processes and utilizing forest inventory data. *Ecosphere* **4**, 1-22.

Wang WJ, Thompson FR, He HS, Fraser JS, Dijak WD, Jones-Farrand T (2019) Climate change and tree harvest interact to affect future tree species distribution changes. *Journal of Ecology* **107**, 1901-1917.

Wang X, Li X, Kong F, Li Y, Shi B, Gao Z (2003) Model of vegetation restoration under natural regeneration and human interference in the burned area of northern Daxinganling. *Chinese Journal of Ecology* **22**, 30-34.

Wang XG, He HS, Li XZ, Chang Y, Hu YM, Xu CG, Bu RC, Xie FJ (2006a) Simulating the effects of reforestation on a large catastrophic fire burned landscape in northeastern China. *Forest Ecology and Management* **225**, 82-93.

Wang XG, He HS, Li XZ, Hu YM (2006b) Assessing the cumulative effects of postfire management on forest landscape dynamics in northeastern China. *Canadian Journal of Forest Research* **36**, 1992-2002.

Wang Y, Zhou Y, Yang J, He H, Zhu Z, Ohlen D (2009) Simulation of short-term post-fire vegetation recovery by integration of LANDFIRE data products, DNBR data and LANDIS modeling. *Annals of GIS* **15**, 47-59.

Woolley T, Shaw DC, Ganio LM, Fitzgerald S (2012) A review of logistic regression models used to predict post-fire tree mortality of western North American conifers. *International Journal of Wildland Fire* **21**, 1-35.

Xu H (1998) Forest in Great Xing'an mountains of China (in Chinese). *Beijing: Science Press* **1**, 231.

Xu H, Li Z, Qiu Y (1997) Fire disturbance history in virgin forest in northern region of Daxinganling Mountains (in Chinese). *Acta Ecologica Sinica* **17**, 337-343.

Xu W, He HS, Hawbaker TJ, Zhu Z, Henne PD (2020) Estimating burn severity and carbon emissions from a historic megafire in boreal forests of China. *Science of The Total Environment* **716**, 136534.

Yang S, Liu X, Cao H, Guo B (1998) Vegetation change on burn blank in Daxing'anling forest area (in Chinese). *Journal of Northeast Forestry University* **26**, 19-22.

Yang Z, Zhou G, Yin X, Jia B (2014) Geographic distribution of Larix gmelinii natural forest in China and its climatic suitability (in Chinese). *Chinese Journal of Ecology* **33**, 1429-1436.

Zhai M, Yi W, Ja L, Ma L, Sun Y, Liu Z, Wang Y (1990) Investigation and study on mixed forest of Hingan larch and white birch in Xilinji (in Chinese). *Northeast. For. Univ.* **12**, 78-85.

Zhang QL, He HS, Liang Y, Hawbaker TJ, Henne PD, Liu JX, Huang S, Wu ZW, Huang C (2018a) Integrating forest inventory data and MODIS data to map species-level biomass in Chinese boreal forests. *Canadian Journal of Forest Research* **48**, 1-19.

Zhang QL, Liang Y, He HS (2018b) Tree-lists estimation for chinese boreal forests by integrating Weibull diameter distributions with MODIS-based forest attributes from kNN imputation. *Forests* **9**.

Zhou Y (1991) Vegetation in Great Xing'an mountains of China (in Chinese). Beijing: Science Press.

Zhu JJ, Kang HZ, Tan H, Xu ML (2006) Effects of drought stresses induced by polyethylene glycol on germination of Pinus sylvestris var. mongolica seeds from natural and plantation forests on sandy land. *Journal of Forest Research* **11**, 319-328.

Zhu Z, Woodcock CE (2012) Object-based cloud and cloud shadow detection in Landsat imagery. *Remote Sensing of Environment* **118**, 83-94.

CHAPTER IV. Large fires or small fires, will they differ in affecting shifts in species composition and distribution under climate warming?

1. Introduction

Global warming has led to tree species migrating toward higher latitudes and elevations (Parmesan et al. 2003; Chen et al. 2011), resulting in shifts in species composition and distribution in local systems. Increasing evidence suggests tree species may fail to keep pace with the rate of climate change due to demographic constraints, resulting in a migration lag (Woodall et al. 2013; Sittaro et al. 2017; Wang et al. 2018; Román-Palacios et al. 2020). Indeed, trees are long-lived species, have limited dispersal capacity, and need time (10–40 years) to reach reproductive maturity. Thus, colonization and extinction events in response to environmental changes are often delayed (Loehle 2000; Boulangeat et al. 2012; Bertrand et al. 2016). Accordingly, tree species shifts in composition and distribution following natural succession pathways are expected to be slow (Davis et al. 2001; Mcgill 2012; Vanderwel et al. 2014; Zhu et al. 2012) because they are limited by the persistence of resident tree species (Loehle 2000; Bouchard et al. 2019) and the dispersal and establishment of migrating tree species (Wang et al. 2018).

Many studies showed that disturbances can catalyze climate-induced shifts in species composition and distribution, because they can remove resident trees that could otherwise persist in novel climate conditions no longer suitable for seedling establishment, and thus increase the turnover of resident tree species to provide establishment opportunities for migrating tree species (Turner 2010; Boulanger et al.

2019; Brice et al. 2020). However, some studies have predicted that disturbances are unlikely to promote extensive species shifts in the next century because they would favor mainly the rapid recovery of resident species (Liang et al. 2018) or the expansion of pioneer species (Vanderwel et al. 2014). Since size, heterogeneity, frequency, and severity of the disturbances may interact with tree species with varied life history attributes differently, often resulting in multiple succession pathways, forest dynamics may respond to climate warming in different ways. For example, low severity disturbances create canopy gaps, often favoring shade-tolerance species, whereas high severity disturbances could create large open areas, often benefiting pioneer species (Landhäusser et al. 2010; Grondin et al. 2018). Larger severe disturbance patches could delay tree regeneration and prolong early seral conditions by limiting the reach of seed dispersal (Johnstone et al. 2016), which may even trigger climate-induced regeneration failure (Savage et al. 2013; Harvey et al. 2016).

Fire is the major disturbance agent, and the ongoing climate warming and human activities are altering fire regimes relative to their historic range of variability. Both the fire occurrence probability and burned area have been projected to increase in the next century due to climate warming, extreme weather, increased anthropogenic ignitions, and fuel accumulation from fire exclusion policies (Arno et al. 2000; Flannigan et al. 2009; Liu et al. 2012; Stephens et al. 2014). However, there is considerable controversy over the future fire sizes even if return interval and the total area burned may be similar (the total area burned in a region could be from many small fires or a few large fires with the same return interval and total area burned) (Cui et al. 2008; Thonicke et al. 2010). Some studies showed that future fire regimes could be characterized by large fires because

warmer temperatures and drier conditions leading to dryer fuels that favor fire spread while fire suppression could lead to increased fuel accumulation that favors large fires (Parsons et al. 1979; Stavros et al. 2014). Yet other studies predicted that future fire regimes could be characterized by frequent small fires because increased fire suppression efficiency and landscape fragmentation could impede large fires even under very dry weather conditions (Loepfe et al. 2014; Hantson et al. 2015). Furthermore, active fuel management increasingly using prescribed fires and naturally ignited managed small fires as a tool to reduce fuels (Collins et al. 2010; Parks et al. 2014; Meyer 2015). Large and small fires are distinctively different in creating larger and more regular and aggregated patterns of high-severity patches (Romme et al. 1998; Bradstock 2008; Keane et al. 2008; Miller et al. 2012). They may lead to different tree species response to climate warming.

Boreal forests of China, the southern extension of the eastern Siberian boreal forests, have experienced considerable temperature increases, and are predicted to warm further over the 21st century (IPCC 2013). Warming improves recruitment, survival, and growth of temperate tree species (e.g. Mongolian oak, *Quercus mongolica* Fisch.ex Ledeb.) at their northern limits, whereas boreal tree species (e.g. Dahurian larch, *Larix gmelini*（Rupr.) Kuzen) are competitively disadvantaged by slower growth and a larger increase in mortality associated with heat and drought stress (Kharuk et al. 2007; Leng et al. 2008; Peng et al. 2011). Thus, climate warming will promote colonization by temperate species into boreal forests and competitive exclusion of boreal species, causing an increase in the proportion of temperate species. Meanwhile, fire is the primary disturbance and has a significant impact on the forest dynamics in the flammable boreal forest ecosystems (Bowman et al. 2009). Historically, fire regime in this area is

characterized by small frequent fires (Xu et al. 1997). With effective fire suppression and warming climate, future fire regimes are predicted to be either large infrequent fires or small frequent fires (Chang et al. 2008; Hu et al. 2014). The boreal forests will have different responses to these fire regimes.

In this study, I investigated how the boreal forests of China are influenced by future fires under warming climate in the next 100 years. In particular, I asked the following questions: 1) how fires interact with climate warming to affect the species composition and distribution; 2) whether the climate-induced composition and distribution shifts will respond differently between small and large fires; and 3) to what extent could the small or large fires enhance or hinder the shifts in species composition and distribution under a warming climate? I hypotheses that fires may provoke shifts to pioneer species and favor temperate species shifts, but large fires should have less effect on the temperate species distribution shifts than small fires because the larger burn patches may hinder the mitigation of temperate species at their northern limits due to low sprouting from pre-fire trees and the limitation of dispersed tree seeds from unburned edges. I answer these questions through a simulation approach using a species-specific, forest landscape model, LANDIS PRO. Forest landscape models have been considered the effective tool for spatially studying forest dynamics in response to disturbances and climate change (Seidl et al. 2011, He et al. 2017; Wang et al. 2019). They are designed to spatially simulate demographic processes (seed establishment, growth, competition, and succession) that drive the shifts of tree species composition and distribution interacted with disturbances. The models also have the ability to examine alternative disturbance and climate scenarios, disentangling compounding impacts of climate and disturbances

by studying the effect of different scenarios separately as well as in combination (Temperli et al. 2013; Seidl et al. 2014).

2. Materials and methods

2.1 Study area

My study area is located on the Great Xing'an Mountains of northeast China (Fig. 4-1), encompassing approximately 8.46×10^4 km^2 (from 50°10’ N, 121°12’ E to 53°33’ N, 127°00’ E) and ranging in elevation from 134 to 1511 m. The Great Xing'an Mountains forests lie in the southern extension of eastern Siberian boreal forests, where vegetation is representative of cool-temperate coniferous forests. The forests mainly comprise of Dahurian Larch (*Larix gmelini*（Rupr.) Kuzen), with a few other locally abundant species, such as white birch (*Betula platyphylla* Suk.), Korean spruce (*Picea koriensis* Nakai) and Scots pine (*Pinus sylvestris* var. *mongolica* Litvinov), aspen (*Populus davidiana* Dole and *P. suaveolens* Fischer) and willow (*Chosenia arbutifolia* (Pall.) A. Skv). Few Asian black birch (Betula davurica Pall., hereafter “black birch”) and Mongolian oak (Quercus mongolica Fisch.ex Ledeb.) are only distributed in the southeastern low-elevation part of the forests. Since the temperate species have the potential to migrate northward in response to climate warming (approximately 50 km per 100 years), I extended my study area southward by 100 km (the extended area was treated as the seed buffer) to reflect the impact of species shifts on the species composition and distribution of the Great Xing’an Mountains.

2.2 Model simulation and parameterization

I used the forest landscape model, LANDIS PRO, to simulate forest dynamics in response to fire and climate change (Wang et al. 2013, 2014). The model tracks the

density and size by species age cohort at pixel level (100 m resolution in this study) and simulates changes to each pixel over time. I used the succession module in LANDIS to simulate tree establishment, growth, resprouting, mortality, and seed dispersal. Mortality is determined by longevity (i.e., maximum lifespans) and competition (i.e., self-thinning). Seed dispersal is simulated by accounting for seed source location, abundance, and dispersal distance (dispersal kernel) (Wang et al. 2013).

I simulated forest fires using the LANDIS PRO fire module under each fire scenario (Yang et al. 2004; Fraser et al. 2019). Fire regimes in the LANDIS PRO fire module are defined by ignition probability, fire return interval, and fire size distribution. Post-fire mortality is modeled as a function of model coefficients (correspond to species fire tolerance classes), tree diameter, and height of bark charring (Fraser et al. 2019). The height of bark charring is used analogously for fire intensity level which is determined by the quantity and quality of fuel in the site (He et al. 2004). These parameters for the post-fire mortality rate used in this study have been well calibrated using forest inventory data in my previous study (Xu et al. 2020).

I used the forest ecosystem process model, LINKAGES III, to encapsulate the climate change effects. Novel climates affected maximum growing space occupied (MGSO) and species demography by modifying species establishment probability (SEP). I divided my study area into 166 land types to account for environmental heterogeneity in vegetation, topography, soil, temperature, and precipitation (Dijak et al. 2017). Within each land type unit, resource availability represented by the MGSO and SEP is assumed to be homogeneous. I estimated SEP on each land type by simulating species establishment and growth from bare ground over 30 years. I calculated SEPs from the maximum biomass

reached by a species on each land type by converting biomass to a relative scale of 0–1 across species (He et al. 1999). I estimated MGSO as the maximum total biomass reached on each land type by simulating the establishment and growth of plots composed of the 8 mixed tree species over 300 years. Each simulation was replicated 20 times. The SEPs and MGSO for each land type under two climate scenarios were inputted into LANDIS PRO as model parameters.

2.3 Climate scenarios

I included the current climate as a baseline climate scenario and a climate warming scenario based on the GFDL-CM3 general circulation models (GCMs) under the representative concentration pathway (RCP) 8.5. The GFDL-CM3 model that was developed by the NOAA Geophysical Fluid Dynamics Laboratory, effectively represented the warming tendency and inter-annual variation of precipitation in northeastern China (Sun et al. 2015). The RCP 8.5 emission scenario is the highest emission scenario used in the IPCC Fifth Assessment Report and is close to current emission trajectories.

Current daily climate data (including daily minimum and maximum temperature, precipitation, average wind speed, and total solar radiation) were derived from a China national meteorological monitoring dataset (1980-2009; http://data.cma.cn). Future daily GFDL-CM3 data were obtained from the Coupled Model Inter-Comparison Project Phase five (CMIP5; 2005-2100; https://esgf-node.ipsl.upmc.fr/search/cmip5-ipsl/). I interpolated current climate data to 0.25˚ × 0.25˚ grids using an R package ‘meteoland’ (De Caceres et al. 2018). I downscaled future climate data based on the interpolated finer-scale current climate data (Wang and Chen 2014).

2.4 Fire scenarios

To investigate the effect of future fire regimes (large infrequent fires or small frequent fires) on tree species in response to climate change, I developed two future fire scenarios, and a baseline fire scenario. The baseline fire scenario corresponds to the fire-size distribution, ignition probability, and return interval from the historical fire dataset from 1965 to 2009 (http://www.cfsdc.org/). A "long-tailed" distribution is needed to accurately depict fire size distributions where most fires are small, but rare extreme events account for most area burned. Therefore, I fitted lognormal fire-size distributions. The future fire scenarios included a small fires scenario and a large fires scenario by fitting different fire-size distributions with the same return interval and total area burned. The future fire return interval in my study region under the climate warming scenario (projected by the GFDL-CM3, RCP8.5) was derived by integrating a forest ecosystem model LINKAGES, a forest landscape model LANDIS, and a spatial point pattern analysis model SPP (Huang et al. 2020). Fire occurrences would increase by 138% compared to historical fire regimes by the year 2100.

2.5 Simulation design and model validation

I designed five simulation scenarios: (1) baseline climate scenario (current climate without fire); (2) baseline fire scenario (current climate and current fire regime) (3) climate warming scenario (future climate without fire); (4) small fires scenario (future climate and future small fires); and (5) large fires scenario (future climate and future large fires). For each scenario, I ran five replicate simulations in LANDIS PRO for 115 years at 5-year time steps starting in the year 1985. Baseline parameters were used for the

1985-2100 period for all simulations except for the climate-sensitive parameters (fire regime, SEP, and MGSO).

Validation of natural succession results was assessed under the baseline climate scenario by comparing simulated species-specific basal area and density with the actual basal area and density from forest inventory data in 2015 (Xu et al. 2020). Validation of the burned area was assessed under the baseline fire scenario by comparing simulated mean burned area/year with the actual mean burned area/year from the historical fire dataset.

2.6 Data analysis

I combined the tree species in my study area into three groups based on their ecological and successional states, namely boreal (Dahurian larch, Scots pine, Korean spruce, and willow), temperate (black birch and Mongolian oak), and pioneer species (white birch and aspen, early successional species which can be found any disturbed habitats across the study area). I calculated importance value (IV) for each species group IV = ([individual group density]/total density] + [individual group basal area]/total basal area]/2). Differences in species composition among scenarios and across time (initial conditions and year 2100) was evaluated using the Bray-Curtis (BC) dissimilarity index (Faith et al. 1987) based on IVs. I used non-parametric Wilcoxon test to test if there was a significant difference in species composition shifts between large fires and small fires scenarios. All statistical analyses were performed using R statistical software (R Core Team, 2015).

3. Results

3.1 Model validation

My simulated results showed that the simulations reasonably captured the forest composition and species distribution in the year 2015. Simulated basal area and tree species density from LANDIS PRO were in high agreement with forest inventory data. ((paired t-tests, df = 6, $p > 0.05$ for each species, Fig. 4-2). Larch and white birch were the most dominant species in all ecoregions and widely distributed in the study area, while larch is more abundant than white birch. Aspen and willow were mainly distributed on terraces. Scots pine was mainly distributed on exposed slopes in the northern area. Mongolian oak and Black birch were mainly found in the southeastern area.

My simulated burned area under the base fire scenario was similar to the observed burned area and the simulated post-fire recovery in tree density and basal area dynamics closely followed the observed data (Fig. 4-3). High values in tree density were observed within10 years after fires due to the release of growing space that provided for the establishment of seedlings. The tree density then decreased in the following years because of the mortality from self-thinning after post-fire stands reaching the stem exclusion stage (Fig. 4-3a). The post-fire basal area increased steadily throughout the first 30 years (Fig. 4-3b).

3.2 Shifts in species composition and distribution

Changes in forest species composition relative to baseline climate were highly variable among scenarios and temperate zones, with the most dramatic (Bray-Curtis dissimilarity 0.4) occurring in the medium temperate zone under the small fires scenario (Fig. 4-4). The medium temperate zone appeared to be more vulnerable to changes in

composition with the particularly swift and large increases in Bray-Curtis dissimilarity. The changes in species composition were strongly driven by a shift in dominance from boreal to pioneer, disturbance-adapted species (Table 4-1, Fig. 4-5). Boreal tree species experienced an overall decrease in IV, and a large decrease occurred in the southern low-elevation part (medium temperate zone). Pioneer species showed an opposite trend of changes in IV compared with boreal species with great increases in the southern low-elevation part and small increases in the northern part of the region. In the southern low-elevation region, the shift in species composition resulted partially from an increase in the IV of temperate, warm-adapted species (Fig.4-5). Temperate tree species were limited in the southern low elevation region since they thrive in areas with higher temperatures, but were more abundant under a warming climate (Table 4-1, Fig.4-5). These changes were rather small under climate warming scenario but became more pronounced under fires scenarios (Table 4-1, Figs. 4-4, 4-5). Both small and large fires favored climate-reduced shifts from boreal to pioneer and temperate species. The IVs of pioneer species and temperate species surged almost 4 and 2 times higher respectively under fires scenarios compared to climate warming scenario. However, the magnitude of shifts in species composition and distribution was different between small and large fires scenarios. Based on the non-parametric Wilcoxon test, there was a significant difference ($P < 0.05$) in overall species composition (Bray-Curtis dissimilarity relative to initial conditions) between large fires and small fires scenarios. Frequent small fires exert stronger effects on the species composition shifts than infrequent large fires (Table 4-1, Figs. 4-4, 4-5). The increases of IVs in pioneer and temperate species from the small fires scenario were 13% and 23% higher than those from the large fires scenario, respectively (Table 4-1).

4. Discussion

My study reveals that climate warming and future fire regimes strongly affect tree species composition in the boreal forests of China. Many studies have shown that boreal tree species growing at their southern limits of present-day distribution are vulnerable to warmer temperatures (Pedlar et al. 2017; Huang et al. 2013; Reich et al. 2018). My results demonstrate a widespread decline of boreal tree species under warming climate due to warming-induced potential decreases in regeneration and growth, and thus confirmed the findings from these studies. In contrast, warming climate improves recruitment, survival, and growth of pioneer and temperate tree species in the boreal forests (Bolte et al. 2014; Fisichelli et al. 2014; Boisvert-Marsh et al. 2019), thus providing a competitive advantage to these species over the boreal species. Overall, my results support the work that showed climate warming promoted transitions from boreal coniferous species to broadleaf species (pioneer and temperate species in this study) (Wu et al. 2017; Boulanger et al. 2019). In my study, fires were projected to catalyze the transitions under climate warming, in line with the work of others (Turner, 2010; Johnstone et al., 2016). Fires caused widespread mortality of dominant boreal species, while climate warming likely increased the growth of pioneer and temperate species in the newly opened canopy gaps, thus altering post-disturbance successional trajectories and catalyzing regional composition transitions (Johnstone et al., 2016). The combined effects of climate warming and fire on the shifts in species composition will accumulate through time and space and can induce a complete transition of forest type, and alter forest dynamics and functions.

My study highlights that frequent small fires exerted stronger effects on the species composition shifts than infrequent large fires, although both fire regimes had equivalent burned areas and interacted with trees at stand-level similarly. Many researchers believed that large fires could cause major shifts in structure and composition through the creation of large, high-severity patches (Bradstock 2008; Keane et al. 2008; Miller et al. 2012). They showed that the large opened areas were colonized swiftly by pioneer species because these species have long dispersal distances, high resprouting probabilities, and fast growth rates (Boucher et al. 2017; Grondin et al., 2018), whereas boreal coniferous species were slower to come back following large fires because of their dispersal limitations (e.g. maximums of 200 m dispersal distance for Dahurian larch compared to 2,000 m for white birch) and restricted abundance of seed sources (Xu, 1998). However, my results exhibited a greater composition shift under the small fires scenario where more boreal species shifted to pioneer and temperate species. This can be explained by the relatively small percent of pioneer species that were directly killed from small fires. Most of fires occurred in boreal coniferous species dominated stands due to higher flammability of surface fuels than broadleaf forests (Hély et al. 2000; Krawchuk et al. 2006). Large fires are more likely to burn into broadleaf stands, resulting in higher mortality of broadleaf species (e.g. white birch), and consequently more boreal coniferous species than small fires at the landscape scale. Moreover, temperate species have a slower migration rate under large fire scenarios because of the dispersal limitations and the competition with the swiftly colonized pioneer species that can persist for a long time after large fires. Therefore, the forests with infrequent large fires likely

maintain a higher percentage of boreal coniferous species, and thus exhibited less shift in species composition than that with frequent small fires.

Although climate warming and fires significantly influenced species' importance (promoting an increase in the proportion of pioneer and temperate species), species' range distribution (represented by absence/presence) exhibited little change in the year 2100. For example, temperate species were still mostly confined in the southern low-elevation area of the study area. The reason for this may be from the competition of the resident species. Tree species may take decades to centuries to respond to changing climates due to inherent demographic inertia that enables adult trees to resist extinction during unfavorable climatic conditions, and thus may wield a strong competition to newcomers (Sittaro et al. 2017; Wang et al. 2019). Furthermore, temperate species in their northern limits have limited dispersal and establishment capabilities and long generation times that result in very slow rates of migration even with the competitive advantage (Hanski et al. 1993). As a result, my 100-year simulation may not be long enough for the effects of climate warming and fires to manifest. However, over longer time scales (e.g. 200-300 years), fires may accelerate boreal tree species extinctions in the southern portion of their range, and thus the northward shift of temperate species ranges through accelerated species turnover under warming climates.

As forests are increasingly affected by intensifying fire regimes and a greater degree of climatic variability, forest management faces new challenges. In forests where managers seek to maintain the composition and structure of the historic forest conditions, prescribed burning and harvesting have been used to mimic historic disturbance regimes and reduce structural and compositional dissimilarities with historical forests (Stanturf et

al. 2014). However, Boulanger et al. (2019) showed that these methods would fail to restore historic forest conditions under future climate because the novel climate conditions would not favor the regeneration of resident species but bring in new migrating species to fill in the gaps. Moreover, my results from the frequent small fire scenario indicate that prescribed burn and stand-level harvest could trigger more rapid transitions in forest composition than large-scale harvest and natural disturbances. Since maintaining historic forest conditions is likely impractical under future climate, some studies suggested adaptive management strategy- replacing declining species (e.g. boreal species) with advancing species (e.g. temperate species) in response to climate warming (McLachlan et al. 2007; Pedlar et al. 2012; Stanturf et al. 2014). My study suggests that natural recruitment of temperate trees might not be sufficient due to seed source and dispersal limitation. Thus, assisted migration may be necessary to facilitate temperate trees range expansion to improve forest adaptation to future climate warming (Duveneck et al. 2016).

Figures

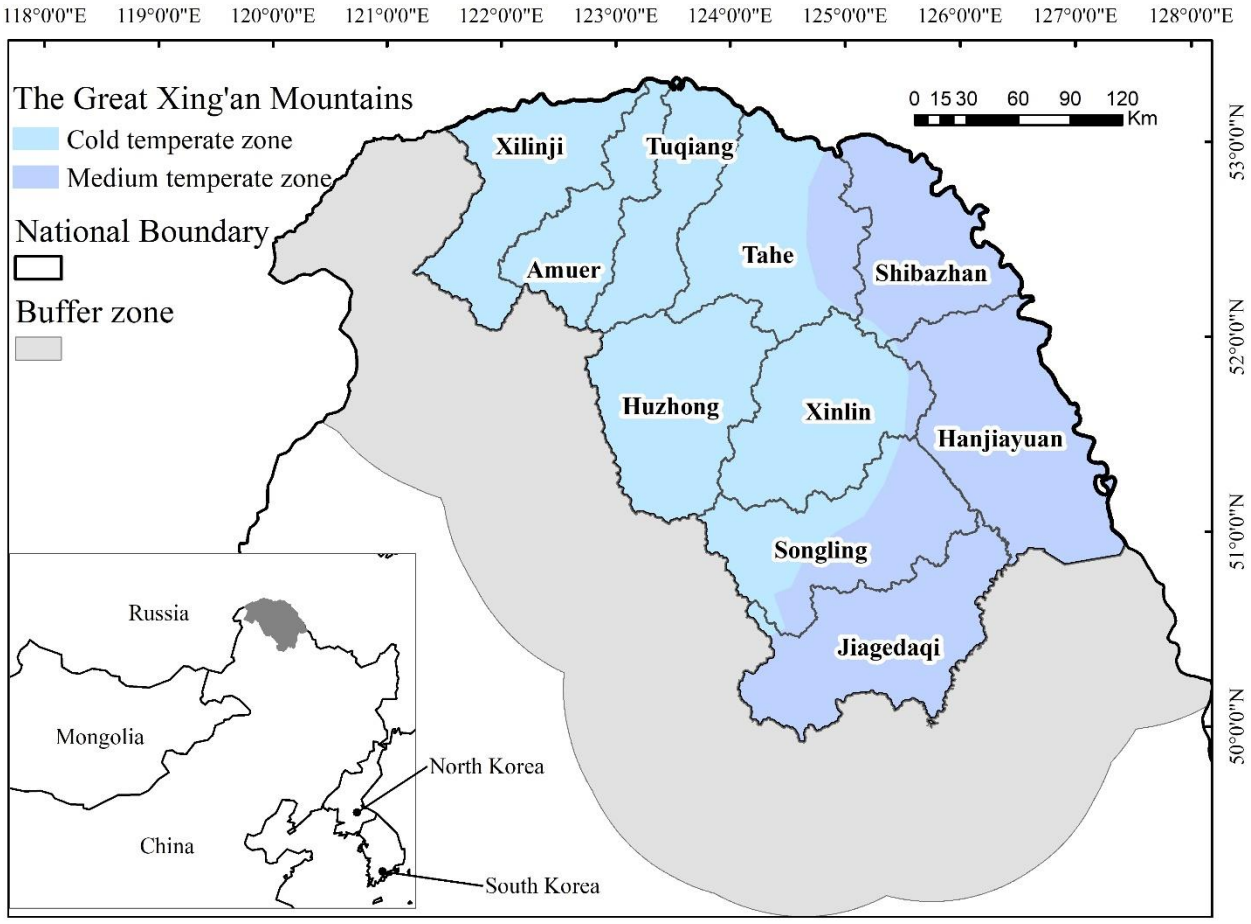

Fig. 4-1. The location of the study area with 10 forest bureaus and a seed buffer zone. I only buffered the boundaries in China because they include the transition between temperate forests and boreal forests.

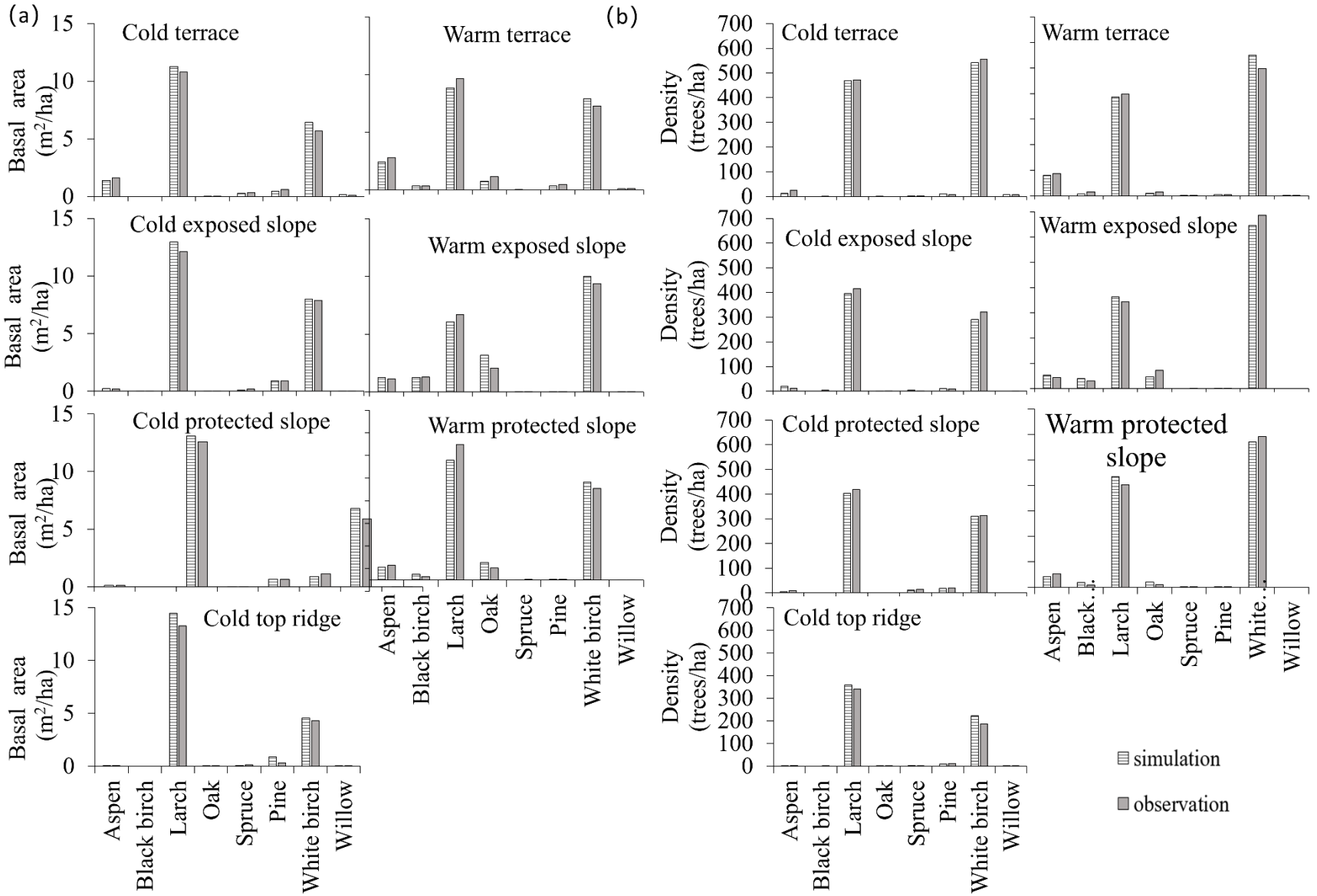

Fig. 4-2 Comparison of simulated basal area (a) and tree species density (b) with inventory data by ecoregions in 2015

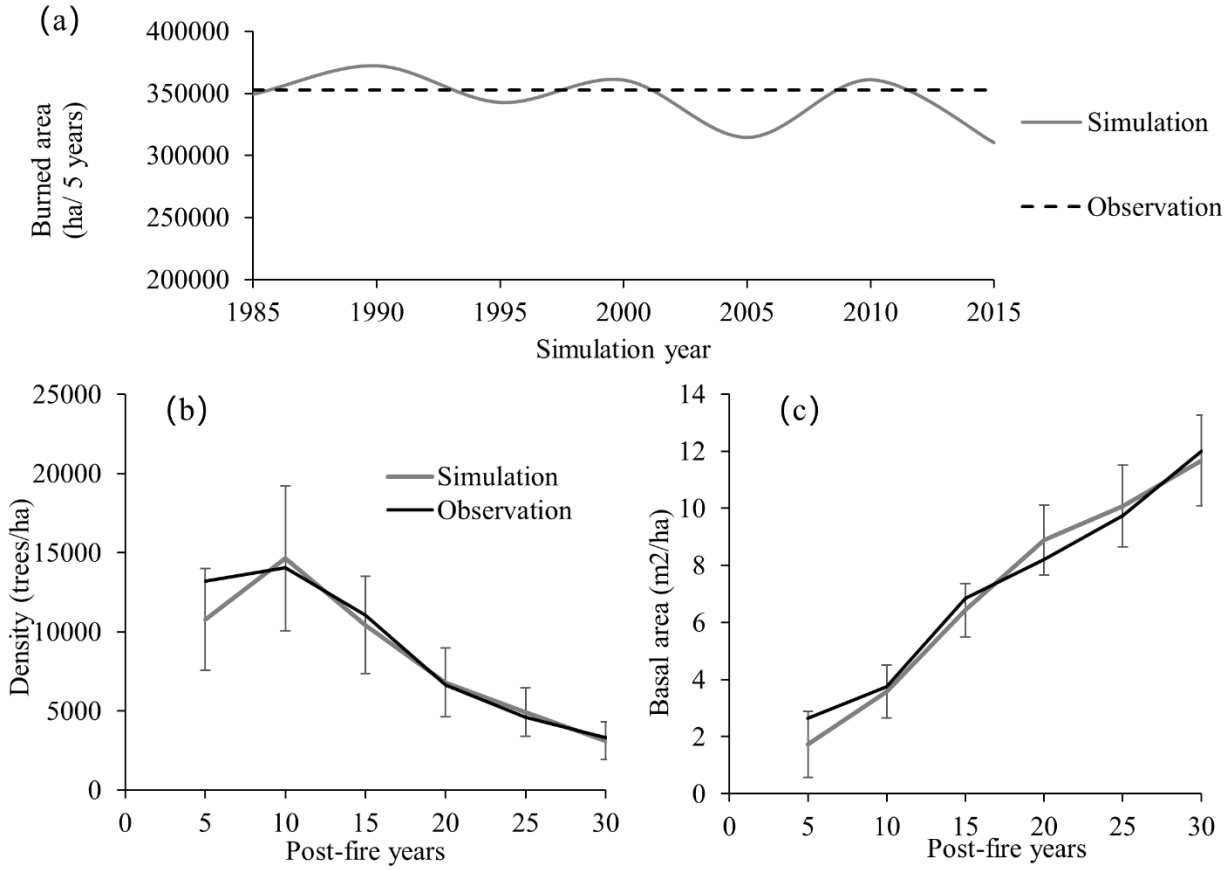

Fig. 4-3. Comparison between simulated and observed values for total burned area (a), post-fire density (b) and basal area (c). The observed burned area represents the mean burned area/5 years from historic fire spanning 1965-2009. Error bars of simulated post-fire density and basal area are marked as ± 1 standard deviation (n= 100 for each timestep).

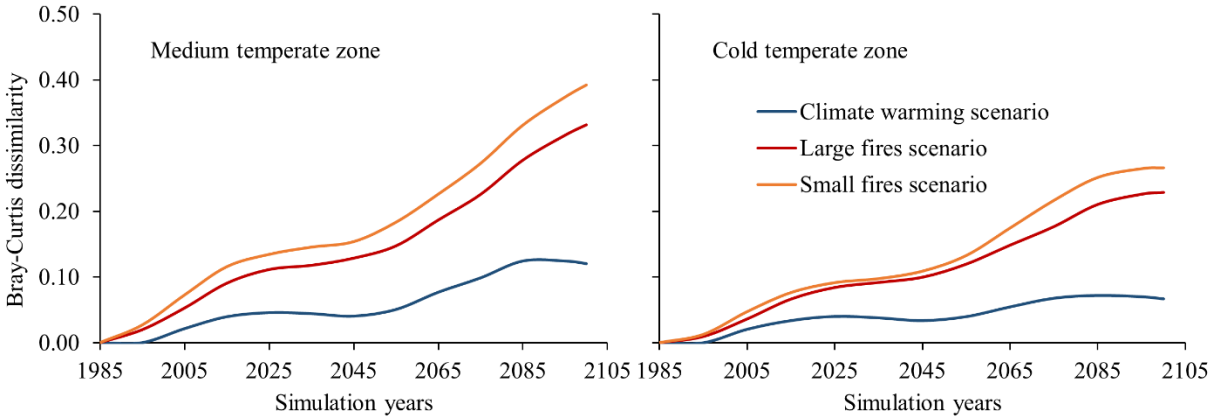

Fig. 4-4. Bray-Curtis dissimilarity indices for simulated forest communities projected under climate warming, large fires and small fires scenarios compared with those simulated under baseline climate at the same timestep by temperate zones.

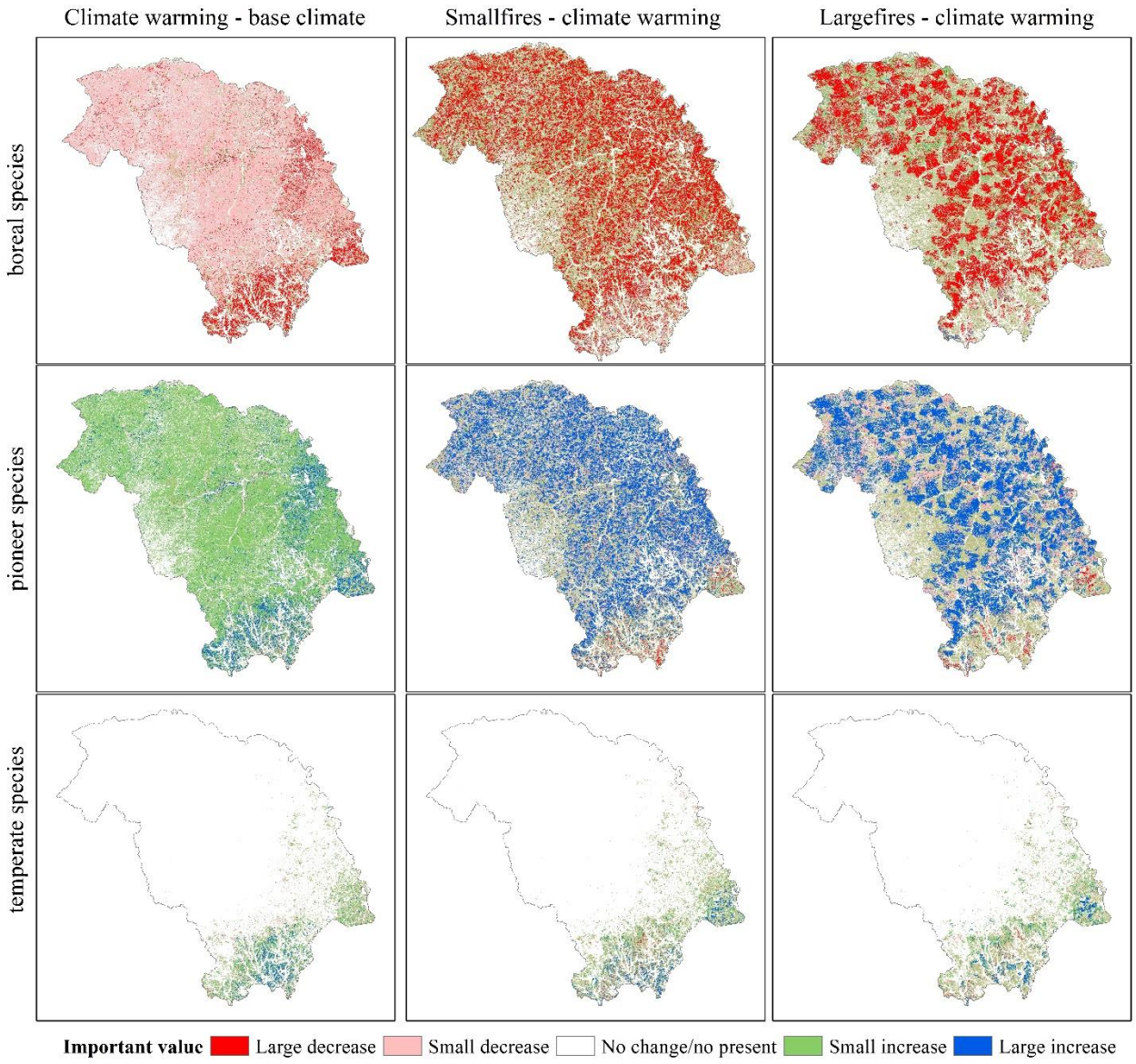

Fig. 4-5. Predicted differences in important value for boreal, pioneer, and temperate tree species between climate warming vs base climate, small fires vs climate warming, and large fires vs climate warming scenarios in 2100.

Tables

Table 4-1. Changes (%) of tree species important values under climate warming, large fires, and small fires scenarios relative to baseline climate scenario by the year 2100.

Species group	Climate warming scenario	Large fires scenario	Small fires scenario
Boreal species	-8.18	-29.24	-32.90
Pioneer species	63.15	232.38	261.92
Temperate species	23.23	44.50	54.90

Literature cited

Arno SF, Parsons DJ, Keane, R.E. (2000) Mixed-severity fire regimes in the northern Rocky Mountains: consequences of fire exclusion and options for the future. *Proceedings of the wilderness science in a time of change conference* **5**, 225-232.

Bertrand R, Riofrio-Dillon G, Lenoir J, Drapier J, De Ruffray P, Gégout JC, Loreau M (2016) Ecological constraints increase the climatic debt in forests. *Nature communications* **7**, 1-10.

Boisvert-Marsh L, Périé C, de Blois S (2019) Divergent responses to climate change and disturbance drive recruitment patterns underlying latitudinal shifts of tree species. *Journal of Ecology* **107**,1956–1969.

Bolte A, Hilbrig L, Grundmann BM, Roloff A (2014) Understory dynamics after disturbance accelerate succession from spruce to beech-dominated forest—The Siggaboda case study. *Annals of Forest Science* **71**, 139–147.

Boucher Y, Auger I, Noël J, Grondin P, Arseneault D (2017) Fire is a stronger driver of forest composition than logging in the boreal forest of eastern Canada. *Journal of Vegetation Science* **28**, 57-68.

Boulangeat I, Gravel D, Thuiller W (2012) Accounting for dispersal and biotic interactions to disentangle the drivers of species distributions and their abundances. *Ecology Letters* **15**, 584–593.

Boulanger Y, Arseneault D, Boucher Y, Gauthier S, Cyr D, Taylor AR, Dupuis S (2019) Climate change will affect the ability of forest management to reduce gaps between current and presettlement forest composition in southeastern Canada. *Landscape Ecology* **34**, 159–174.

Bowman DM, Balch JK, Artaxo P, Bond WJ, Carlson JM, Cochrane MA, D'Antonio CM, DeFries RS, Doyle JC, Harrison SP, Johnston FH et al. (2009) Fire in the Earth System. *Science* **324**, 481-484.

Bradstock RA (2008) Effects of large fires on biodiversity in southeastern Australia: disaster or template for diversity? *International Journal of Wildland Fire* **17**, 809–22

Brice MH, Vissault S, Vieira W, Gravel D, Legendre P, Fortin MJ (2020) Moderate disturbances accelerate forest transition dynamics under climate change in the temperate-boreal ecotone of eastern North America. *Global Change Biology* **00**,1–18

Chen IC, Hill JK, Ohlemüller R, Roy DB, Thomas CD (2011). Rapid range shifts of species associated with high levels of climate warming. *Science* **333**, 6045.

Collins BM, Stephens ST, Moghaddas JJ, Battles J (2010) Challenges and approaches in planning fuel treatments across fire-excluded forested landscapes. *Journal of Forestry* **108**, 24-31.

Cui W, Perera AH (2008) What do we know about forest fire size distribution, and why is this knowledge useful for forest management?. *International Journal of Wildland Fire* **17**, 234-244.

Davis MB, Shaw RG (2001) Range shifts and adaptive responses to quaternary climate change. *Science* **292**, 673–678.

De Caceres M, Martin-StPaul N, Turco M, Cabon A, Granda V (2018) Estimating daily meteorological data and downscaling climate models over landscapes. *Environmental Modelling & Software* **108**, 186-196.

Dijak WD, Hanberry BB, Fraser JS, He HS, Wang WJ, Thompson FR (2017) Revision and application of the LINKAGES model to simulate forest growth in central hardwood landscapes in response to climate change. *Landscape Ecology* **32**, 1365-1384.

Duveneck MJ, Scheller RM (2016) Measuring and managing resistance and resilience under climate change in northern Great Lake forests (USA). *Landscape Ecology* **31**, 669–686.

Faith DP, Minchin PR, Belbin L (1987) Compositional dissimilarity as a robust measure of ecological distance. *Plant Ecology* **69**,57–68.

Fisichelli NA, Frelich LE, Reich PB (2014) Temperate tree expansion into adjacent boreal forest patches facilitated by warmer temperatures. *Ecography* **37**, 152–161.

Flannigan MD, Krawchuk MA, deGroot WJ, Wotton BM, Gowman LM (2009) Implications of changing climate for global wildland fire. *International Journal of Wildland Fire*, **18**(5) 483- 507.

Fraser JS, Wang WJ, He HS, Thompson FR (2019) Modeling post-fire tree mortality using a logistic regression method within a forest landscape model. *Forests* **10**.

Grondin P, Gauthier S, Poirier V, Tardif P, Boucher Y, Bergeron Y (2018) Have some landscapes in the eastern Canadian boreal forest moved beyond their natural range of variability? *Forest Ecosystems* **5**(1), 5–30.

Hanski I, Gyllenberg M (1993) Two general metapopulation models and the core-satellite species hypothesis. *The American Naturalist* **142**, 17–41.

Hantson S, Lasslop G, Kloster S, Chuvieco E (2015) Anthropogenic effects on global mean fire size. *International Journal of Wildland Fire* **24**(5), 589-596.

Harvey BJ, Donato DC, Turner MG (2016) High and dry: post-fire tree seedling establishment in subalpine forests decreases with post-fire drought and large stand-replacing burn patches. *Global Ecology and Biogeography* **25**, 655-669.

He HS, Gustafson EJ, Lischke H (2017) Modeling forest landscapes in a changing climate: theory and application.

He HS, Mladenoff DJ, Crow TR (1999) Linking an ecosystem model and a landscape model to study forest species response to climate warming. *Ecological Modelling* 114, 213-233

He HS, Shang BZ, Crow TR, Gustafson EJ, Shifley SR (2004) Simulating forest fuel and fire risk dynamics across landscapes—LANDIS fuel module design. *Ecological Modelling* **180**(1), 135-151.

Hély C, Bergeron Y, Flannigan MD (2000) Effects of stand composition on fire hazard in mixed-wood Canadian boreal forest. *Journal of Vegetation Science* **11**(6), 813-824.

Huang, J.G., Bergeron, Y., Berninger, F., Zhai, L., Tardif, J.C. and Denneler, B., 2013. Impact of future climate on radial growth of four major boreal tree species in the eastern Canadian boreal forest. PloS one, 8(2), p.e56758.

Huang C, He HS, Liang Y, Hawbaker TJ, Henne PD, Xu WR, Gong P, Zhu ZL (2020) Vegetation feedback mediates the direct effects of climate change on future fire regimes of boreal forests in northeastern China. *Journal of Applied Ecology* (Accepted).

IPCC (2013) Summary for policymakers. In: Climate Change 2013: The Physical Science Basis. Contribution of Working Group I to the Fifth Assessment Report of the

Intergovern-mental Panel on Climate Change (eds Stocker TF, Qin D, Plattener GK et al.), 4–19. Cambridge University Press, Cambridge, UK and New York, NY, USA.

Johnstone JF, et al. (2016) Changing disturbance regimes, ecological memory, and forest resilience. *Frontiers in Ecology and the Environment* **14**, 369-378.

Keane RE, Agee JK, Fule P, Keeley JE, Key C, Kitchen SG, Miller R, Schulte LA (2008) Ecological effects of large fires on US landscapes: benefit or catastrophe? *International Journal of Wildland Fire* **17**, 696-712.

Kharuk V, Ranson K, Dvinskaya M (2007) Evidence of evergreen conifer invasion into larch dominated forests during recent decades in central Siberia. *Eurasian Journal of Forest Research* **10**(2), 163-171.

Krawchuk MA, Cumming SG, Flannigan MD (2009) Predicted changes in fire weather suggest increases in lightning fire initiation and future area burned in the mixedwood boreal forest. Climatic Change, 92, 83–97.

Landhäusser SM, Deshaies D, Lieffers VJ (2010) Disturbance facilitates rapid range expansion of aspen into higher elevations of the Rocky Mountains under a warming climate. *Journal of Biogeography* **37**(1), 68–76.

Leng W, He HS, Bu R, Dai L, Hu Y, Wang X (2008) Predicting the distributions of suitable habitat for three larch species under climate warming in Northeastern China. *Forest Ecology and Management* **254**(3), 420-428.

Liang Y, Duveneck MJ, Gustafson EJ, Serra-Diaz JM, Thompson JR (2018) How disturbance, competition, and dispersal interact to prevent tree range boundaries

from keeping pace with climate change. *Global Change Biology* **24**(1), e335–e351.

Liu ZH, Yang J, Chang Y, Weisberg PJ, He HS (2012) Spatial patterns and drivers of fire occurrence and its future trend under climate change in a boreal forest of Northeast China. *Global Change Biology* **18**, 2041-2056.

Loehle C (2000) Forest ecotone response to climate change: Sensitivity to temperature response functional forms. *Canadian Journal of Forest Research* **30**, 1632–1645.

Loepfe L, Rodrigo A, Lloret F (2014) Two thresholds determine climatic control of forest fire size in Europe and northern Africa. *Regional environmental change* **14**(4), 1395-1404.

Mcgill BJ (2012) Trees are rarely most abundant where they grow best. *Journal of Plant Ecology* **5**, 46–51.

McLachlan JS, Hellmann JJ, Schwartz MW (2007) A framework for debate of assisted migration in an era of climate change. *Conservation Biology* **21**, 297-302

Meyer MD, Roberts SL, Wills R, Brooks M, Winford EM (2015) Principles of effective USA federal fire management plans. *Fire Ecology* **11**(2), 59-83.

Miller JD, Skinner CN, Safford HD, Knapp EE and Ramirez CM (2012) Trends and causes of severity, size, and number of fires in northwestern California, USA. *Ecological Applications* **22**, 184-203.

Parks SA, Miller C, Nelson CR, Holden ZA (2014) Previous fires moderate burn severity of subsequent wildland fires in two large western US wilderness areas. *Ecosystems* **17**:29–42.

Parmesan C, Yohe G (2003) A globally coherent fingerprint of climate change impacts across natural systems. *Nature* **421**(6918), 37–42.

Parsons DJ, DeBenedetti SH (1979) Impact of fire suppression on a mixed-conifer forest. *Forest Ecology and Management* **2**, 21-33.

Pedlar JH, McKenney DW, Aubin I, Beardmore T, Beaulieu J, Iverson L, O'Neill GA, Winder RS, Ste-Marie C (2012) Placing forestry in the assisted migration debate *BioScience* **62**, 835-842.

Pedlar JH, McKenney DW (2017) Assessing the anticipated growth response of northern conifer populations to a warming climate. *Scientific Reports* **7**(1), 1-10.

Peng C, Ma Z, Lei X, Zhu Q, Chen H, Wang W, Zhou X (2011) A drought-induced pervasive increase in tree mortality across Canada's boreal forests. *Nature Climate Change*, **1**(9), 467–471.

Román-Palacios C, Wiens JJ, 2020. Recent responses to climate change reveal the drivers of species extinction and survival. *Proceedings of the National Academy of Sciences* **117**(8), 4211-4217.

R Core Team. (2015). R: A Language and Environment for Statistical Computing (Version 3.2.2). Vienna, Austria: R Foundation for Statistical Computing. Retrieved from http://www.R-project.org/.

Reich PB, Sendall KM, Stefanski A, Rich RL, Hobbie SE, Montgomery RA (2018) Effects of climate warming on photosynthesis in boreal tree species depend on soil moisture. *Nature* **562**(7726), 263-267.

Romme WH, Everham EH, Frelich LE, Moritz MA, Sparks RE (1998) Are large, infrequent disturbances qualitatively different from small, frequent disturbances? *Ecosystems* **1**, 524–534.

Savage M, Mast JN, Feddema JJ (2013) Double whammy: high-severity fire and drought in ponderosa pine forests of the Southwest. *Canadian Journal of Forest Research-Revue Canadienne De Recherche Forestiere* **43**, 570-583.

Seidl R, Fernandes PM, Fonseca TF, Gillet F, Jönsson AM, Merganičová K, Netherer S, Arpaci A, Bontemps JD, Bugmann H, González-Olabarria JR (2011) Modelling natural disturbances in forest ecosystems: a review. *Ecological Modelling*, **222**(4), 903-924.

Seidl R, Rammer W, Spies TA (2014) Disturbance legacies increase the resilience of forest ecosystem structure, composition, and functioning. *Ecological Applications* **24**, 2063-2077.

Sittaro F, Paquette A, Messier C, Nock CA (2017) Tree range expansion in eastern North America fails to keep pace with climate warming at northern range limits. *Global Change Biology* **23**, 3292–3301.

Stanturf JA, Palik BJ, Dumroese RK (2014) Contemporary forest restoration: a review emphasizing function. *Forest Ecology and Management* **331**, 292-323.

Stavros EN, Abatzoglou J, Larkin NK, McKenzie D, Steel EA (2014) Climate and very large wildland fires in the contiguous western USA. *International Journal of Wildland Fire* **23**(7), 899-914.

Stephens SL, Burrows N, Buyantuyev A, Gray RW, Keane RE, Kubian R, Liu S, Seijo F, Shu L, Tolhurst KG (2014) Temperate and boreal forest mega-fires:

characteristics and challenges. *Frontiers in Ecology and the Environment* **12**, 115-122.

Sun Q, Miao C, Duan Q (2015) Comparative analysis of CMIP3 and CMIP5 global climate models for simulating the daily mean, maximum, and minimum temperatures and daily precipitation over China. *Journal of Geophysical Research: Atmospheres* **120**, 4806-4824.

Temperli C, Zell J, Bugmann H, Elkin C (2013) Sensitivity of ecosystem goods and services projections of a forest landscape model to initialization data. *Landscape Ecology* **28**, 1337-1352.

Thonicke K, Spessa A, Prentice IC, Harrison SP, Dong L, Carmona-Moreno C (2010) The influence of vegetation, fire spread and fire behaviour on biomass burning and trace gas emissions: results from a process-based model. *Biogeosciences* **7**, 1991–2011.

Turner MG (2010) Disturbance and landscape dynamics in a changing world. *Ecology* **91**(10), 2833–2849.

Vanderwel MC, Purves DW (2014) How do disturbances and environmental heterogeneity affect the pace of forest distribution shifts under climate change? *Ecography* **37**, 10–20.

Wang Lin, Chen Wen (2014) A CMIP5 multimodel projection of future temperature, precipitation, and climatological drought in China. *International Journal of Climatology* **34**, 2059-2078.

Wang WJ, He HS, Fraser JS, Thompson FR, Shifley SR, Spetich MA (2014) LANDIS PRO: a landscape model that predicts forest composition and structure changes at regional scales. *Ecography* **37**, 225-229.

Wang WJ, He HS, Spetich MA, Shifley SR, Thompson FR, Larsen DR, Fraser JS, Yang J (2013) A large-scale forest landscape model incorporating multi-scale processes and utilizing forest inventory data. *Ecosphere* **4**, 1-22.

Wang WJ, He HS, Thompson III FR, Spetich MA, Fraser JS (2018) Effects of species biological traits and environmental heterogeneity on simulated tree species distribution shifts under climate change. *Science of the Total Environment* **634**, 1214-1221.

Wang WJ, Thompson III FR, He HS, Fraser JS, Dijak WD, Jones-Farrand T (2019) Climate change and tree harvest interact to affect future tree species distribution changes. *Journal of Ecology* **107**(4), 1901-1917.

Woodall CW, Zhu K, Westfall JA, Oswalt CM, D'amato AW, Walters BF, Lintz HE (2013) Assessing the stability of tree ranges and influence of disturbance in eastern US forests. *Forest Ecology and Management* **291**, 172–180.

Wu C, Venevsky S, Sitch S, Yang Y, Wang M, Wang L, Gao Y (2017) Present-day and future contribution of climate and fires to vegetation composition in the boreal forest of China. *Ecosphere* **8**(8), e01917.

Xu H (1998) Forest in Great Xing'an mountains of China (in Chinese). *Beijing: Science Press* **1**, 231.

Xu H, Li Z, Qiu Y (1997) Fire disturbance history in virgin forest in northern region of Daxinganling Mountains (in Chinese). *Acta Ecologica Sinica* **17**, 337-343.

Xu WR, He HS, Fraser JS, Hawbaker TJ, Henne PD, Duan SW, Zhu ZL (2020) Spatially explicit reconstruction of post-megafire forest recovery through landscape modeling. *Environmental Modelling and Software* **134**, 104884.

Yang J, He HS, Gustafson EJ (2004) A hierarchical statistical approach to simulate the temporal patterns of forest fire disturbance in LANDIS model. *Ecological. Modelling* **180**, 119-133.

Zhu K, Woodall CW, Clark JS (2012) Failure to migrate: Lack of tree range expansion in response to climate change. *Global Change Biology* **18**, 1042–105.

CHAPTER V. CONCLUSIONS

The dissertation focused on the effects of large fires on the boreal forests of China. Specifically, I estimated the burn severity and carbon emissions from a large fire, investigated post-fire forest recovery, and examine the effects of future fire regimes on forest dynamics under a warming climate. Key findings and insights gained from this study are listed below.

The Black Dragon fire released significant amounts of carbon into the atmosphere. The emitted carbon dioxide equivalents (CO2e) from the Black Dragon fire, accounted for approximately 10% of total fossil fuel emissions from China in 1987, along with CO (2% - 3% of annual anthropogenic CO emissions from China) and non-methane hydrocarbons (NMHC) contributing to the atmospheric pollutants. The estimates of carbon emissions were improved by using burn severity related combustion efficiency that was calculated using actual tree mortality estimates for different burn severity classes. The methodology can be applied on a continuous basis for forest fire monitoring and emissions accounting in different forested regions of the world. Furthermore, the estimated fire emissions could be combined with estimates of forest regrowth biomass accumulation for including emissions from wildfire in a national carbon accounting and reporting framework. My study provides an important basis for considering the impacts of megafires on national-scale carbon accounting for China.

I developed a framework to spatially reconstruct the post-fire time-series of forest conditions (i.e., forest composition, structure, and aboveground biomass) after the 1987

Black Dragon fire. This framework provided not only the spatial pattern and dynamics at the landscape scale, but also detailed stand attributes such as basal area, tree density, and age classes by species that can be validated against the contemporary inventory data. The framework can be applied to filling the gaps where inventory data are not available to assess recovery trajectories across the whole landscape and capture the heterogeneity of the post-fire recovery process in both time and space. The framework can be used to assess the legacy effects of a megafire over long time periods (i.e., decades to centuries) and examine alternative management and disturbance scenarios.

I investigated the effects of two possible future fire regimes (frequent small fires and infrequent large fires) on forest dynamics in the boreal forests of China under a warming climate. Climate warming and fires strongly affected tree species composition and distribution in the boreal forests of China. Climate warming promoted transitions from boreal species to pioneer and temperate species. Fires were projected to catalyze the transitions under climate warming, whereas frequent small fires exerted stronger effects on the species composition shifts than infrequent large fires. The combined effects of climate warming and fire on the shifts in species composition will accumulate through time and space and can induce a complete transition of forest type, and alter forest dynamics and functions.

My study brings insights into the role of large fires in national and global carbon balance and forest dynamics, and provide reference for other large fires. For example, the large fires often result in large and aggregated high severity patches that can jump over the terrain limitation. The large burn patches could delay vegetation recovery processes by limiting the reach of seed, and thus the forest recovery after large fires is a long-lasting

process. Reasonable human help to natural recovery to pre-fire forests is necessary for severe burns with a large patch size. This study also provides important implications for developing adaptive management plans under future climate.

VITA

Wenru Xu was born and grew up in the city of Suihua, Heilongjiang Province, China. She graduated from Northeast Normal University in 2015 with a bachelor's degree in Geographical Information System. Because of her outstanding academic performance, she was recommended and recruited by the graduate school of the same university in 2015 and graduated with a master’s degree in Physical Geography. Holding a desire of applying his geospatial skills into the field of natural resources, she joined the graduate program of the University of Missouri in 2017, pursuing a doctorate in Natural Resource (Forestry) and she received her doctoral degree in 2020. During this period, her research involved using field inventory and remote sensing data, and forest landscape modeling approaches to address the environmental issues and provide alternative management practices under changing climate.